CHEMICAL REVIEWS

Review

pubs.acs.org/CR

Stabilizing and Modulating Color by Copigmentation: Insights from Theory and Experiment

Patrick Trouillas,[*,†,‡] Juan C. Sancho-García,[§] Victor De Freitas,[∥] Johannes Gierschner,[⊥] Michal Otyepka,[*,‡] and Olivier Dangles[@]

[†]INSERM UMR 850, Univ. Limoges, Faculty of Pharmacy, 2 rue du Dr. Marcland, F-87025 Limoges, France

[‡]Regional Centre of Advanced Technologies and Materials, Department of Physical Chemistry, Faculty of Science, Palacký University Olomouc, tr. 17. listopadu 12, 771 46 Olomouc, Czech Republic

[§]Departamento de Química Física, Universidad de Alicante, Apartado de Correos 99, E-03080 Alicante, Spain

[∥]REQUIMTE/LAQV − Research Unit, Faculty of Science, Porto University, Rua do Campo Alegre, 4169-007 Porto, Portugal

[⊥]Madrid Institute for Advanced Studies - IMDEA Nanoscience, C/Faraday 9, Ciudad Universitaria de Cantoblanco, E-28049 Madrid, Spain

[@]University of Avignon, INRA, UMR408 SQPOV, F-84000 Avignon, France

ABSTRACT: Natural anthocyanin pigments/dyes and phenolic copigments/co-dyes form noncovalent complexes, which stabilize and modulate (in particular blue, violet, and red) colors in flowers, berries, and food products derived from them (including wines, jams, purees, and syrups). This noncovalent association and their electronic and optical implications constitute the copigmentation phenomenon. Over the past decade, experimental and theoretical studies have enabled a molecular understanding of copigmentation. This review revisits this phenomenon to provide a comprehensive description of the nature of binding (the dispersion and electrostatic components of $\pi-\pi$ stacking, the hydrophobic effect, and possible hydrogen-bonding between pigment and copigment) and of spectral modifications occurring in copigmentation complexes, in which charge transfer plays an important role. Particular attention is paid to applications of copigmentation in food chemistry.

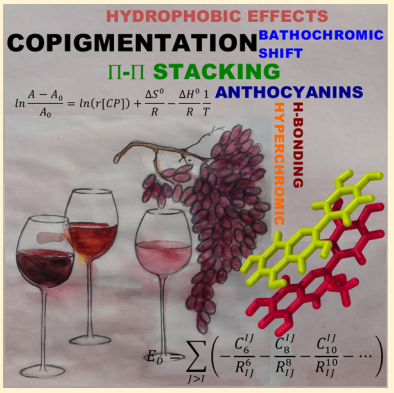

CONTENTS

Special Issue: Noncovalent Interactions

Received: August 30, 2015
Published: March 9, 2016

DOI: 10.1021/acs.chemrev.5b00507
Chem. Rev. 2016, 116, 4937−4982

1. INTRODUCTION

Copigmentation is a fascinating natural process based on noncovalent (supramolecular) complexation. It has been shown to be the main mechanism by which certain colors, particularly blue, violet, and red, are stabilized and modulated in flowers,[1] vegetables, and fruit (in particular, berries), as well as food products derived from them (in particular, wine,[2] but also jams, purees, and syrups). The term "copigmentation" is commonly reserved for anthocyanins, a large class of phenolic derivatives spread over the plant kingdom. Because of their extended π-conjugated systems, they absorb in the visible range and can readily form supramolecular assemblies with other pigments and cofactors (so-called, in this case, copigments), mainly phenolic acids and flavonoids (Scheme 1). Other pigments/dyes are also known to form supramolecular assemblies, for example, carotenoid aggregates.[3] However, this aggregation is usually not termed "copigmentation" because this process is primarily driven by self-association governed by dispersion interactions.[4]

The definition of copigmentation has been refined over time, and recently by complementing experimental investigations with accurate computational studies. The atomistic understanding of copigmentation is inevitable to better understand, on the one hand, the diversity of color in nature,[5] but on the other hand, the process of color stabilization. Indeed, there has been growing interest for the latter issue in the food industry, which aims at using and controlling copigmentation by addition of copigments in food products to enhance the color palette, in direct relation with consumers' perception. Here, modern food engineering requires a precise (computer-aided) control of the noncovalent supramolecular pigment-copigment assemblies.

This review links experimental and theoretical chemistry approaches to a coherent interdisciplinary understanding of copigmentation, which has been enabled by the recent developments in computational methodology. We aim at providing a comprehensive picture of the current knowledge in copigmentation, mainly concerning driving forces and structure-affinity relationships between pigments and copigments. With reference to several examples (including blue flowers, wine, and other food products), sections 2 and 3 describe the families of pigments and copigments that are most likely to exhibit copigmentation. Section 4 describes the experimental tools to study copigmentation, mainly based on UV−vis absorption spectroscopy, NMR (nuclear magnetic resonance), CD (circular dichroism), and X-ray crystallography. Stability of inter- and intramolecular copigmentation complexes is discussed in sections 5 and 6, respectively, based on experimental data. Section 7 then details all possible driving forces that are involved in the copigmentation process. Section 8 introduces molecular mechanics (MM) and molecular dynamics (MD) methods that can be used to sample the conformational space of supramolecular pigment-copigment assemblies. The use of MD-based methods to estimate enthalpies and Gibbs energies of association is also discussed. Section 9 describes the quantum mechanics (QM)-based methods that can be used to accurately describe the noncovalent interactions involved in copigmentation. Section 10 rationalizes the UV−vis spectral shifts upon copigmentation based on time-dependent density functional theory (TD-DFT) calculations and excited state description, allowing elucidation of the electronic origin through Molecular Orbital (MO) analysis. Finally, a summary and outlook are given in Section 11.

2. PIGMENTS AND COPIGMENTS

2.1. Pigments

Anthocyanins are intriguing natural compounds that are responsible for the color of many plants. Their study was pioneered by the German chemist R. Willstätter, who conducted extensive investigations into their properties, as reported in his "Untersuchungen über die Anthocyane" monograph.[6] Anthocyanins were subsequently shown to be a subclass of the flavonoids present in numerous flowers, leaves, fruit, and vegetables as well as beverages made from fruit, notably red wine but also some fruit juices and even some pink ciders. Anthocyanins are commonly referred to as pigments (i.e., a coloring agent plants). It should be remarked however that different to the use in biology, "pigment" in strict terms is used for nonsoluble colorants, whereas soluble colorants are named "dyes". Although anthocyanin-based crystals have been observed in plants,[7] these compounds are mainly water-soluble and exist in solution, in the vacuoles of plant cells.

2.1.1. (Proto)typical Pigments. As of the time of writing, almost 1000 plant-derived anthocyanins have been identified. An exhaustive list of these pigments is beyond the scope of this review; partial lists can be found in various books and other review papers.[8,9]

Twenty-three anthocyanidins that mainly differ in terms of their B-ring hydroxyl and methoxyl substitution patterns have been identified in fruit and vegetables.[8] Six of these 23 compounds are particularly abundant, namely cyanidin, delphinidin, malvidin, pelargonidin, peonidin, and petunidin (see Figure 1). Most anthocyanins are 3-*O*-glycosides. Approximately 50% of the known anthocyanins feature the cyanidin moiety. Compared to those derived from fruit and vegetables, anthocyanins from flowers tend to have a higher degree of glycosylation and acylation. The most common sugar moiety is D-glucose, but anthocyanidins are also often conjugated to L-rhamnose, D-xylose, D-galactose, arabinose, and fructose as well as rutinose (6-*O*-α-L-rhamnosyl-D-glucose), sophorose (2-*O*-β-D-xylosyl-D-glucose), gentiobiose (6-*O*-β-D-glucosyl-D-glucose), sambubiose (2-*O*-β-D-xylosyl-D-glucose), xylosylrutinose, and glycosylrutinose.

Most detailed studies on anthocyanins are found for red wine driven by the need for understanding and control of wine color.

DOI: 10.1021/acs.chemrev.5b00507
Chem. Rev. 2016, 116, 4937−4982

Scheme 1. Prototypical Copigmentation Complexes[a]

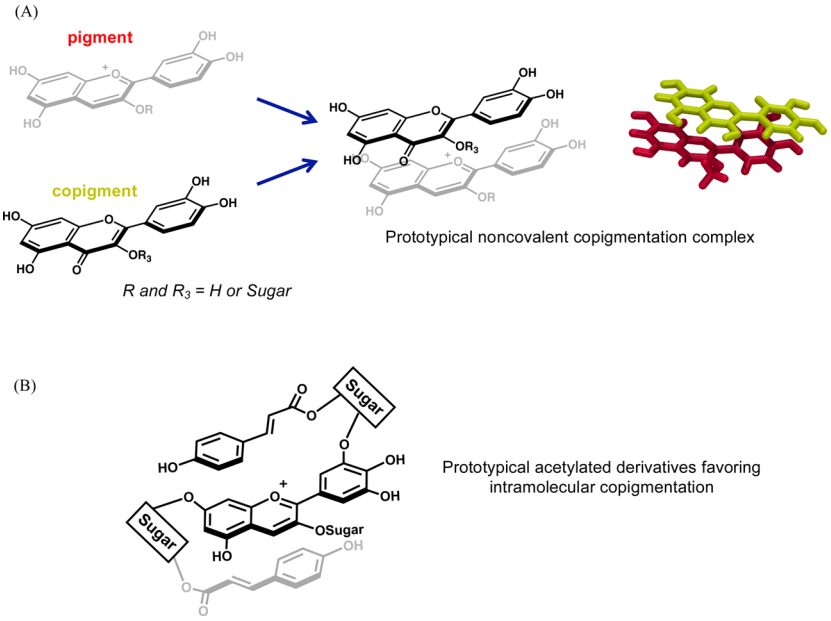

[a](A) Noncovalent association of a prototypical anthocyanin pigment and a prototypical flavonoid copigment (intermolecular copigmentation). (B) Prototypical acylated derivatives allowing copigmentation between the anthocyanin moiety and two phenolic acids covalently linked (intramolecular copigmentation).

The main anthocyanins in red wine are the 3-*O*-monoglucosides of five major anthocyanidins [i.e., cyanidin-3-*O*-glucoside (kuromanin), delphinidin-3-*O*-glucoside (myrtillin), peonidin-3-*O*-glucoside (peonin), petunidin-3-*O*-glucoside (petunin), and malvidin-3-*O*-glucoside (oenin), see Figure 1]. The last of these compounds is by far the most abundant.[9]

Many anthocyanins are acylated (generally at the C6-OH group of a glucose moiety), with either an aliphatic acid (e.g., acetic, malic, malonic, oxalic, or succinic acid) or a phenolic acid (e.g., *p*-hydroxybenzoic, caffeic, *p*-coumaric, ferulic, or sinapic acid). There are hundreds of known anthocyanins bearing multiple acyl groups linked to linear or branched oligosaccharides bound to the A-, B-, and/or C-rings of the anthocyanidin nucleus.[10]

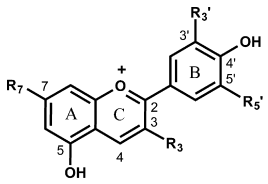

	Compound	R_3	$R_{3'}$	$R_{5'}$	R_7
Anthocyanidins	cyanidin	OH	OH	H	OH
	delphinidin	OH	OH	OH	OH
	malvidin	OH	OCH_3	OCH_3	OH
	pelargonidin	OH	H	H	OH
	peonidin	OH	OCH_3	H	OH
	petunidin	OH	OCH_3	OH	OH
Anthocyanins	kuromanin	*O*-Glucose	OH	H	OH
	myrtillin	*O*-Glucose	OH	OH	OH
	oenin	*O*-Glucose	OCH_3	OCH_3	OH
	callistephin	*O*-Glucose	H	H	OH
	peonin	*O*-Glucose	OCH_3	H	OH
	petunin	*O*-Glucose	OCH_3	OH	OH
	3',4'-dihydroxy-7-*O*-*β*-D-glucopyranosyloxyflavylium	H	OH	H	*O*-*β*-D-glucopyranosyloxy

Figure 1. Chemical structures of anthocyanidins (R_3 = OH) and anthocyanins (R_3 = glucose).

As demonstrated over the past decades, wine is a very complex system of dissolved and suspended pigments in which many chemical reactions involving anthocyanins occur including electrophilic aromatic substitutions on the electron-rich A-ring (hemiketal form) of the flavylium cation and nucleophilic addition to the electrophilic pyrylium ring (C-ring).[11,12] Consequently, a large variety of anthocyanin derivatives is formed during wine preparation and aging, including flavanol-anthocyanin adducts (with or without CH_3−CH bridges originating from ethanal formed by EtOH oxidation), anthocyanin dimers and related polymers, pyranoanthocyanins (e.g., vitisins A and B, oxovitisins), pyranoanthocyanin-phenols, pyranoanthocyanin-flavanols, the more recently discovered vinylpyranoanthocyanin-flavanol portisin, which is bluish at acidic pH (Figure 2), and pyranoanthocyanin dimers.[11,13−17] Most of these pigments form as the wine is stored and aged in bottles or barrels. All pyranoanthocyanins are colored as well as more than 50% of their ethyl-linked derivatives. These new pigments are known to (i) induce color shifts from red to orange or purple/blue;[18,19] (ii) enhance color intensity (i.e., to exert hyperchromic effects on the visible absorption band); and (iii) enhance resistance to water and sulfite addition and subsequent bleaching. They have extended π-conjugated systems and/or a comparatively high propensity for self-association, which allows colored forms to remain stable at higher pH values independently of any copigmentation effect.

2.1.2. Chemistry of Anthocyanins. Anthocyanins are *O*-glycosides of anthocyanidins (i.e., 3,4′,5,7-tetrahydroxyflavylium ions with additional OH and/or OMe groups at the C3′ and/or C5′ positions) (Figure 1). When considering their structures, anthocyanins are depicted in their flavylium cation (AH^+) form. However, extensive studies on their chemistry[20,21] have demonstrated that they can exist in various colored and colorless forms; the form that predominates under any given set of

DOI: 10.1021/acs.chemrev.5b00507
Chem. Rev. 2016, 116, 4937−4982

conditions is largely determined by pH. This chemistry is somewhat beyond the scope of this review, and it is assumed that the reader is broadly familiar with the contents of some recent reviews of this field (see for example refs 22 and 23). However, to understand copigmentation and its consequences for the expression of natural colors, it is necessary to clearly recall the structural transformations that anthocyanins can undergo in aqueous solution. Therefore, these transformations are briefly summarized below (see also Figure 3).

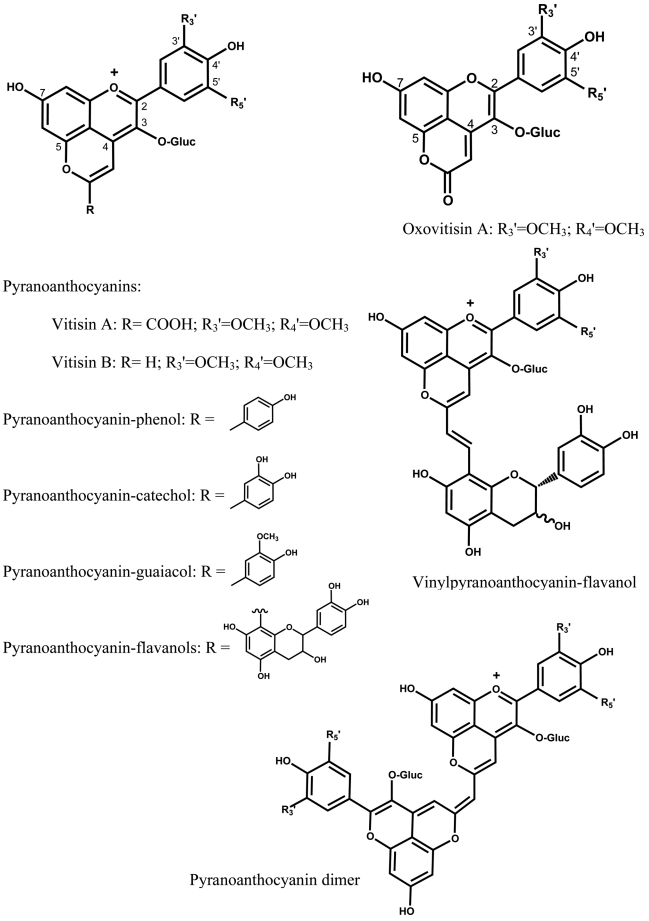

Figure 2. Chemical structures of pyranoanthocyanins (flavylium cation form).

The AH^+ form only predominates at very low pH values; experimentalists usually work below pH = 2 to ensure its exclusive presence in solution. In the pH range of interest in plants and plant products (pH = 3−8), anthocyanins are diacids with two successive pK_a values of about 4 and 7. Thus, AH^+ loses a proton under mildly acidic conditions and is converted into a mixture of neutral quinone methide tautomers, which are known as bases, formed after the deprotonation of one of the three most acidic phenolic OH groups (C7-OH, C4′−OH, or C5-OH, respectively). These quinonoid bases (A) lose a second proton around neutrality to form the anionic quinonoid bases (A^-). Above pH = 2, the flavylium cation of common (nonacylated) anthocyanins also becomes prone to water addition (hydration) at C2 to form a mixture of colorless hemiketal epimers (B or AOH) that exist in a fast cycle-chain equilibrium with a *cis*-chalcone tautomer (C_{cis}), itself in slow equilibrium with the *trans*-chalcone (C_{trans}). The thermodynamic constants of these three equilibria are designated K_h (hydration), K_t (hemiketal-chalcone

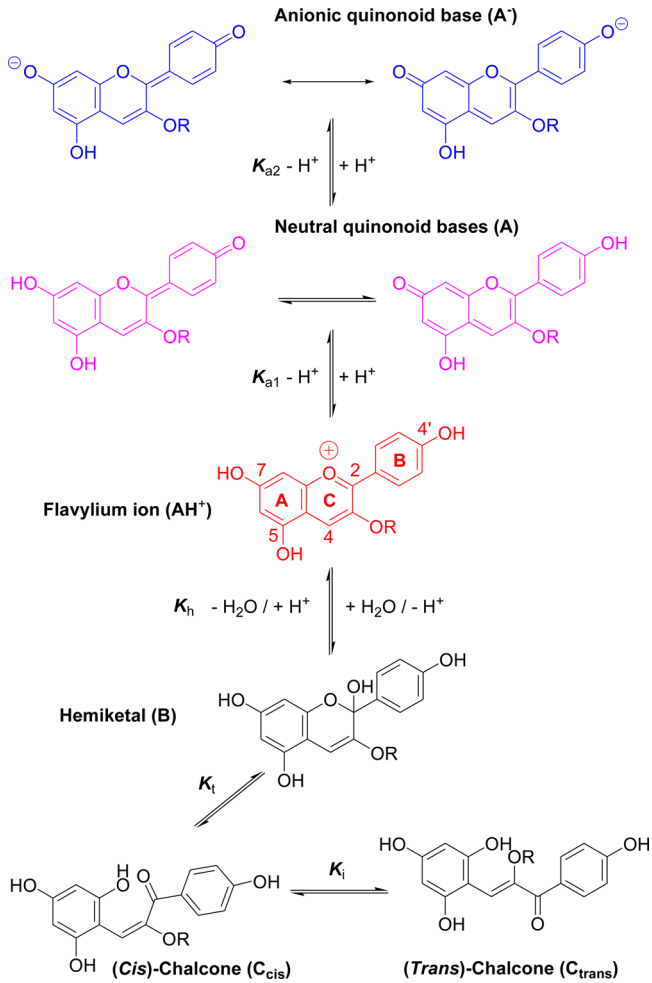

Figure 3. Structural transformations of anthocyanins in acidic to neutral solution. Proton loss from C5-OH omitted for simplicity.

tautomerization) and K_i (cis−trans chalcone isomerization), respectively. The overall hydration equilibrium connecting AH^+ and the other forms at equilibrium, is given by the overall thermodynamic constant K_h':

$$K_h' = K_h[1 + K_t(1 + K_i)] \quad (1)$$

The anthocyanidin core is a fully delocalized π-conjugated system, which is why these compounds can absorb visible light. However, the color is strongly affected by pH and hydration (see Figure 3). Namely, AH^+ is usually red, the different forms of A are purple, and the A^- anions are blue. Proton transfers cause (i) bathochromic (red) shifts of the lowest-energy visible absorption band, (ii) band broadening, and (iii) decreases in absorbance that are known as hypochromic effects.[24] In addition, B is colorless while both the C_{cis} and C_{trans} isomers are yellowish. Thus, based solely on their structural and electronic features, anthocyanins can exhibit many hues in solution. Depending on the conditions, their absorption may be UV-only (making them colorless) or may extend over the entire visible spectrum.

With natural anthocyanins, K_t and K_i are lower than 1, and chalcones only make a minor (<20%) contribution to the global pool of colorless forms. The pK_h' value, which is a relevant indicator of color stability, normally falls in the range from 2 to 3. Thus, considering the competitive fates of AH^+ (i.e., proton loss vs water addition), it can be stated that hydration is thermodynamically favored. However, it is much slower than

DOI: 10.1021/acs.chemrev.5b00507
Chem. Rev. 2016, 116, 4937−4982

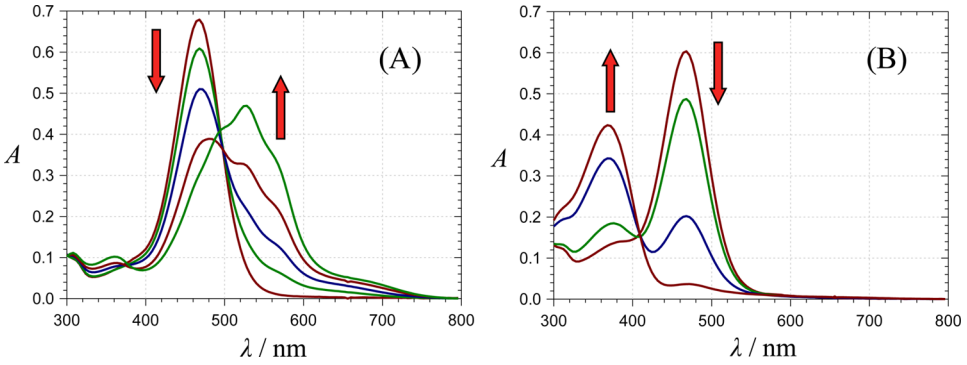

Figure 4. Structural transformations of the 3′,4′-dihydroxy-7-*O*-*β*-D-glucopyranosyloxyflavylium ion. (A) Fast formation of the quinonoid base. Spectral measurements immediately after addition of pigment to buffer, pH = 2.0 → pH = 6.0. (B) Slow accumulation of *trans*-chalcone (C_{trans}). Spectral measurements on solutions equilibrated overnight, pH = 2.0 → pH = 4.0. Adapted with permission from ref 25. Copyright 2013 Elsevier Ltd.

proton loss. In other words, in the reversible competitive fates of AH^+, the hemiketal (the most abundant colorless form) is the thermodynamic product while the tautomeric quinonoid bases are the kinetic products. Thus, at the pH values found in beverages or living plant cells, the concentration of strongly colored anthocyanin forms should in principle be low at equilibrium. However, the half-life of these colored forms is strongly pH-dependent and typically ranges from a few seconds at pH = 3 to several minutes at pH = 5−6. This is mainly because the proportion of electrophilic AH^+ in solution (which is the only colored form capable of undergoing water addition) declines as the pH is raised. The competition between the different forms can be illustrated with reference to the 3′,4′-dihydroxy-7-*O*-*β*-D-glucopyranosyloxyflavylium cation, a simple anthocyanin analog with no C3 substituent (Figure 1). In this case, C_{trans} accumulates and is the only significant colorless form present at equilibrium, as shown in Figure 4.[25]

2.2. Copigmentation

The pH effects and chemical variation (specifically, structural transformations, and different patterns of functionalization, mostly in the B-ring) alone cannot satisfactorily explain the great diversity of anthocyanin-derived hues observed in plants. This diversity is largely attributable to a process termed "copigmentation". Copigmentation can be defined as (i) the formation (in the presence or absence of metal ions) of noncovalent complexes involving an anthocyanin or anthocyanin-derived pigment (e.g., a pyranoanthocyanin or anthocyanin-flavanol adduct) on the one hand and a copigment on the other (Scheme 1) and (ii) the subsequent changes in optical properties of the pigment.

2.2.1. Types of Copigments. There are over ten-thousand compounds that could potentially serve as copigments. While an exhaustive list will not be provided, they can be classified into a number of distinct categories, thus giving an idea of the large number of plausible pigment-copigment pairs.

In general, copigments should have (i) sufficiently extended *π*-conjugated systems, which are supposed to favor *π*−*π* stacking interactions (see sections 5 and 7 for more details) and (ii) hydrogen bond donor/acceptor groups such as OH and C═O groups. The major natural copigments that have been identified are hydrolyzable tannins, flavonoids, and phenolic acids. Flavonoid copigments include flavonols, flavones, flavanols, and even dihydroflavonols (Figure 5). Due to extension of their *π*-conjugation over their entire tricyclic core structure (rings A, B, and C), flavones and flavonols (e.g., quercetin, kaempferol, isoquercitrin,[26] and rutin) appear to be the most efficient

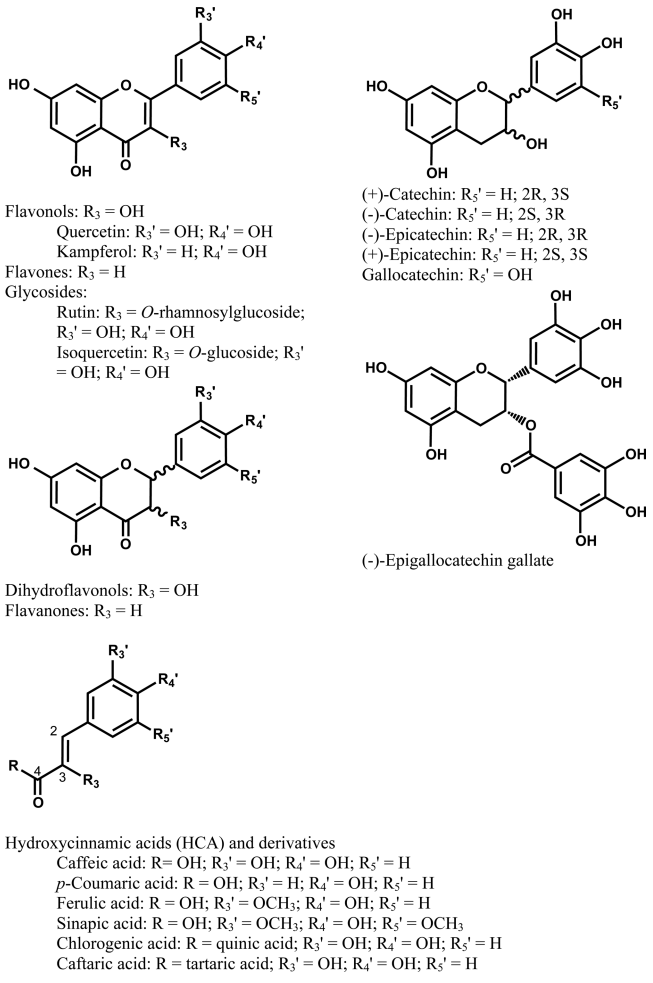

Figure 5. Chemical structures of series of copigments.

copigments (i.e., those that provide the strongest bathochromic and hyperchromic effects) and which have the highest Gibbs energies of association (see next sections for more details on binding energies and structure-affinity relationships).

Various hydroxycinnamic acids (HCA) and derivatives such as caffeic, *p*-coumaric, ferulic, sinapic, chlorogenic, and caftaric acids (Figure 5) are commonly described as relatively efficient copigments, with potencies comparable to those of flavanols and dihydroflavonols;[27] benzoic acids are generally less efficient copigments than HCAs.[28−32] HCAs are usually more efficient if

DOI: 10.1021/acs.chemrev.5b00507
Chem. Rev. 2016, 116, 4937−4982

they are linked to the pigment via acylation of a glycosyl group in a way that offers sufficient conformational flexibility for the pigment and copigment to be in close contact and form noncovalent intramolecular interactions (see section 6 for more details).

Anthocyanins themselves can also be regarded as copigments because self-association can be seen as a special case of copigmentation in which the two partners are colored if they both exist in the AH^+, A, or A^- forms. Although it is generally less efficient than copigmentation (at least with common non-acylated anthocyanins), self-association has been widely observed (see section 5). Some nonphenolic copigments have also been described, including alkaloids, amino acids, organic acids, nucleotides, and polysaccharides,[9] but their efficiency is typically much lower than that of polyphenols; it is still unclear whether such compounds can significantly contribute to color expression by anthocyanins.

2.2.2. Key Historical Milestones. The copigmentation phenomenon was first discussed in 1916 by R. Willstätter and E. H. Zollinger,[33] who noticed that the hue of the grape pigment oenin (malvidin 3-*O*-glucoside) could be changed by the addition of tannin or gallic acid. This was initially believed to be a rare phenomenon specific to oenin. R. Robinson subsequently investigated these findings in more detail and defined a copigment as a "substance in solution which intensifies and modifies the colour"; the terms "co-pigment" and "co-pigmentation" have later been replaced by "copigment" and "copigmentation", respectively. As a particular advanced concept, he discussed the modulation of anthocyanins' optical properties (bluing effects) in terms of intra- and intermolecular interactions.[34] Much later, S. Asen, R. N. Stewart, and K. H. Norris described bathochromic shifts in pigment-copigment pairs.[7,35] These authors stressed the crucial influence of the copigment concentration.[36] Copigmentation was thus described as a concentration-dependent process that is also sensitive to pH, temperature, and solvent.[37] The authors concluded that "the phenomenon of copigmentation offers a more logical explanation of the infinite variation in red to blue flower colors that exists in a pH range where anthocyanins alone are virtually colorless" and proposed for the first time that anthocyanins (e.g., aureusin from Yellow Rocket snapdragons) may be able to self-associate, which can also induce shifts in visible absorption bands.[38]

A few years later, T. Hoshino and T. Goto made a key contribution to the understanding of anthocyanin copigmentation (Scheme 2A) and self-association (Scheme 2B) by using CD experiments to demonstrate anthocyanin self-association.[39−44] This was made possible by the sensitivity of CD to the chirality of supramolecular assemblies. Their results confirmed that anthocyanin quinonoid bases can self-associate in water but not in DMSO.[39,42] The forces driving self-association were identified as "hydrophobic interactions among the aromatic nuclei stacked parallel to each other". The authors considered vertical stacking driven by $\pi-\pi$ interactions more likely than horizontal stacking driven by hydrogen bonding.[42] Interestingly, stacking between the neutral forms led to spectral shifts whose magnitude was comparable to those induced by the stacking of adjacent base pairs within DNA; the corresponding association constants were even larger than those observed for nucleic acids in solution.[45]

During roughly the same period, R. Brouillard proposed an advanced method for investigating the thermodynamics of copigmentation, which provided fundamental insights into the

Scheme 2. $\pi-\pi$ Stacking Interactions in Anthocyanins and Their Complexes[a]

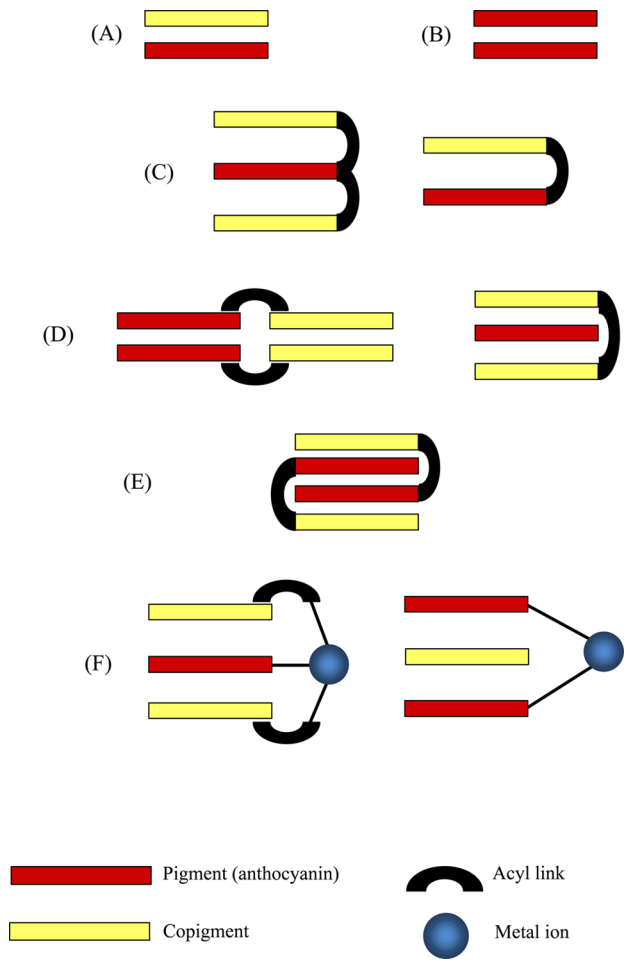

[a](A) Intermolecular copigmentation, (B) self-association, (C) intramolecular copigmentation in acylated anthocyanins, (D) self-association of acylated anthocyanins, (E) intercalation in intermolecular copigmentation, and (F) copigmentation in metal−anthocyanin complexes.

mechanisms of association between pigment and copigment. In particular, Brouillard et al. emphasized the importance of considering all of the equilibrating species when estimating the copigmentation binding constant.[46] This is important because copigmentation shifts the proton transfer and hydration equilibria (potentially suppressing the hydration reaction when AH^+ is part of the copigmentation complex), thus limiting the formation of colorless compounds. This phenomenon is known as color stabilization. Brouillard et al. confirmed that the main driving force of pigment-copigment binding is the hydrophobic effect. Intramolecular copigmentation was later observed in acylated anthocyanins;[47,48] in such cases, the pigment and copigment are covalently linked by a glycosyl spacer, allowing the two partners to come into close contact and form noncovalent interactions (Scheme 1). These authors also showed that copigmentation is dramatically weakened by the presence of organic cosolvents.

3. PIGMENT···COPIGMENT COMPLEXES IN NATURE

Virtually all plant organs that biosynthesize anthocyanins and flavonoids or phenolic acids could potentially provide pigment···

DOI: 10.1021/acs.chemrev.5b00507
Chem. Rev. 2016, 116, 4937−4982

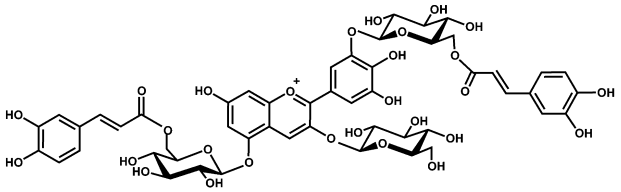

Gentiodelphin

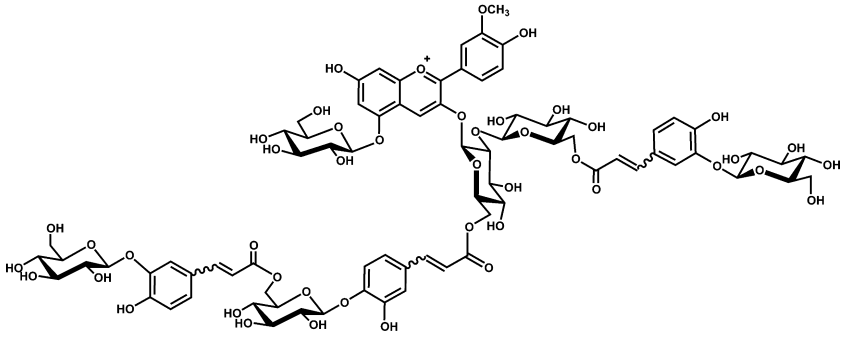

Heavenly blue anthocyanin - HBA

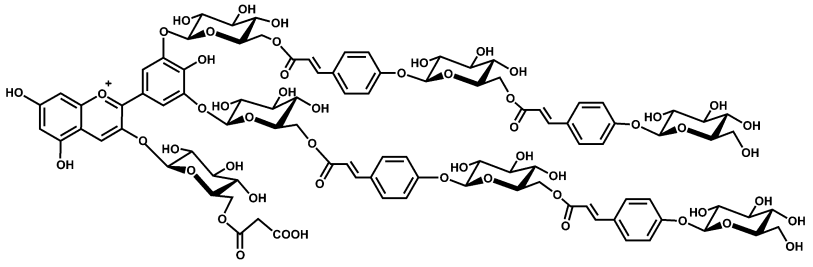

Ternatin

Figure 6. Chemical structures of three nonmetallic pigment···copigment assemblies.

copigment complexes (Schemes 1A and 2A), although in some cases they have only been hypothesized. Many binary systems (forming intermolecular copigmentation complexes, see Schemes 1A and 2A) have been studied by mixing a pigment and a copigment directly in solution, which is supposed to mimic plant and food environments. In two representative recent examples, oenin was mixed with five hydroxybenzoic acids[49] and with increasing concentrations of catechin, epicatechin, epigallocatechin, epigallocatechin gallate, procyanidin B3, and prodelphinidin B3.[50] Such studies performed in solution under various conditions (i.e., at different pH values and concentrations, in different solvents) have provided information on structure−efficiency relationships, as discussed in section 5.1. Many (poly)acylated anthocyanins have been reported, and such pigments may be involved in complex molecular assemblies that exhibit self-association and/or intra- or intermolecular copigmentation (Schemes 1B and 2).[1]

In addition to simple studies in solution, many pigment··· copigment systems have been investigated directly in plant and food matrices. Copigmentation has been studied intensively in blue flowers, which have attracted particular interest for many decades; there have been a number of reviews covering this field, including a recent one by Yoshida et al.[1] Over the past decade, numerous works have also examined copigmentation in wine, and in all food matrices in which copigmentation is likely to occur (see sections 3.2 and 3.3). The next three sections discuss copigmentation in these three representative environments.

3.1. Copigmentation in Blue Flowers

In ancient Greek, "antho" means flower and "cyanin" comes from cyan (blue); indeed, anthocyanin coloration is closely linked to blue and violet flowers such as hydrangea (hortensia), pansy, tulip, and morning glory. However, in mildly acidic to neutral conditions, blue flowers would hardly be blue without copigmentation; instead, they would be yellow or even colorless. The development of blue coloration has been studied intensively over the last 50 years or so.

As explained in the review by K. Yoshida, M. Mori, and T. Kondo,[1] the role of metal ions in copigmentation was initially ignored. This is partly because there are many known nonmetallic pigment···copigment assemblies in blue and violet flowers, such as gentiodelphin (from the blue *Gentiana makinoi*), heavenly blue anthocyanin (HBA from *Ipomoea tricolor* cv. HeavenlyBlue) and ternatin (from *Cliteria ternatea*). These systems feature anthocyanins that bear (poly)acylated branched chains on both A- and B-rings, the C-ring, and the B-ring, respectively (Figure 6). In aqueous solution, these chains adopt conformations that allow aromatic acyl moieties to stack on both sides of the anthocyanidin chromophore (Scheme 2C), thereby

DOI: 10.1021/acs.chemrev.5b00507
Chem. Rev. 2016, 116, 4937−4982

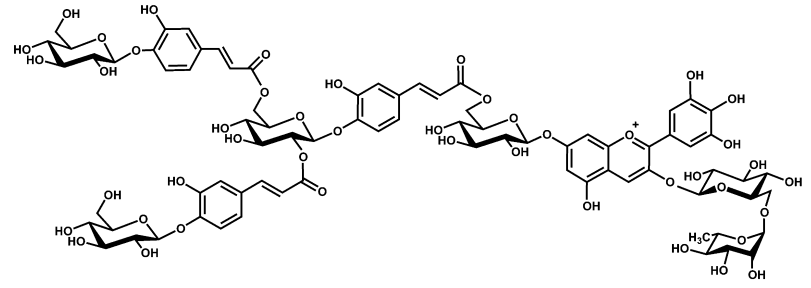

Tecophilin

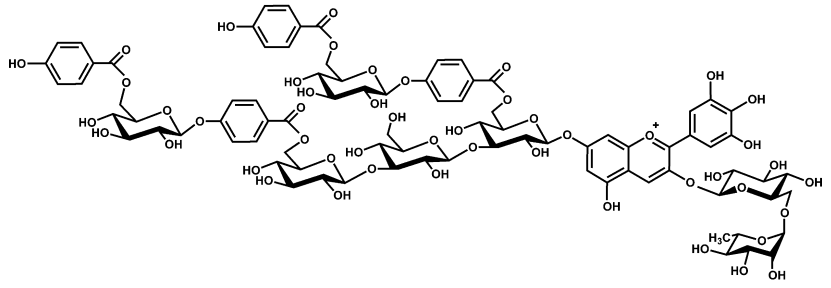

Cyanodelphin

Figure 7. Chemical structures of two polyacylated anthocyanins.

stabilizing the blue quinonoid form. Other polyacylated anthocyanins have different stabilizing copigmentation mechanisms. In tecophilin (from *Tecophilaea cyanocrocus*) and cyanodelphin, which both bear branched polyacylated chains on their A-rings (Figure 7), intra- and intermolecular stacking may occur simultaneously (Scheme 2E). Similar arrangements were proposed for phacelianin, alatanin, and petanin, all of which have linear (poly)acylated chains on the C-ring, and also for two other pigments, one from *Matthiola incana* with branched polyacylation on the C-ring and another that is linked to a flavonoid moiety (Figure 8). Fossen et al. also reported a covalently linked anthocyanin-flavone *C*-glycoside copigmentation system (Figure 9A) that was isolated from the leaves of *Oxalis triangularis*.[51] Two other pigments were found in Allium "Blue Perfume" (Figure 9B), which exhibited intramolecular copigmentation (i.e., they featured an anthocyanin core linked to a flavonoid via an acylglycoside moiety with sufficient conformational flexibility so that the chromophore and the flavonoid could come into close contact).[52] There is only indirect evidence of intramolecular stacking between pigment and copigment in these polyacylated anthocyanins, mainly derived from UV−vis absorption spectroscopy, CD, and NMR. Unfortunately, X-ray crystallography cannot be used to study these systems due to the difficulty of growing crystals of such labile molecular assemblies.

Copigmentation also occurs within metalloanthocyanin supramolecular complexes in petal cell vacuoles (Scheme 2F).[1] Copigments simply stack within metal−anthocyanin complexes (i.e., there is no binding between metal ion and copigment) or are connected to the anthocyanin via metal binding (a special case of intramolecular copigmentation). The structure of commelinin, the blue crystalline pigment of *Commelina communis*,[53] was elucidated for the first time in 1992. The structural description of this complex was based on the metal complex theory for blue color development, which was originally proposed by Shibata et al.[54] and brought to wider awareness by Yoshida et al.[1] It was shown to exist as a fascinating helical aggregate (see Figure 10 and section 5.4. for more details).

Many other metalloanthocyanin complexes have since been isolated and characterized, featuring various pigments (in various charge states), copigments, and metal ions. For example, the blue color of *Ceanothus papillosus* petals results from the intermolecular copigmentation of a polyacylated anthocyanin pigment (Figure 11) in its quinonoid base form with kaempferol 3-*O*-glycoside (Scheme 2, stackings A and F).[55] Protocyanin is the blue pigment of cornflower petals (*Centaurea cyanus*); crystallographic analysis suggests that it has a supramolecular structure of well-defined stoichiometry with stacking between a flavone derived from apigenin (6 equiv) and a cyanidin derivative (6 equiv), with two different coordinated metal ions (Fe^{3+} and Mg^{2+}) that stabilize the quinonoid base (Figure 12). Some other stoichiometric metal-pigment-copigment complexes are presented in Table 1.

3.2. Copigmentation in Wine

During winemaking and aging (in barrel or bottle), the initial red-purple color originating from the grapes is modified. Wine is by far the most studied beverage in which copigmentation has been repeatedly confirmed. It has been suggested that some of the reported copigments may originate from oak barrels in which the wine was stored, but this suggestion must be treated with some caution because the corresponding color modifications have not been comprehensively documented.[2] Regardless, grape contains significant amounts of flavonoids (flavonols and flavanols), phenolic acids, and mainly their derivatives such as caftaric acid largely found in wine. All these compounds favor the occurrence of copigmentation at all stages of winemaking. During storage, the levels of anthocyanins decline rapidly but those of copigments (e.g., the total quantity of flavonols) do not decrease over a month timescale.[66] This suggests that copigmentation in

DOI: 10.1021/acs.chemrev.5b00507
Chem. Rev. 2016, 116, 4937−4982

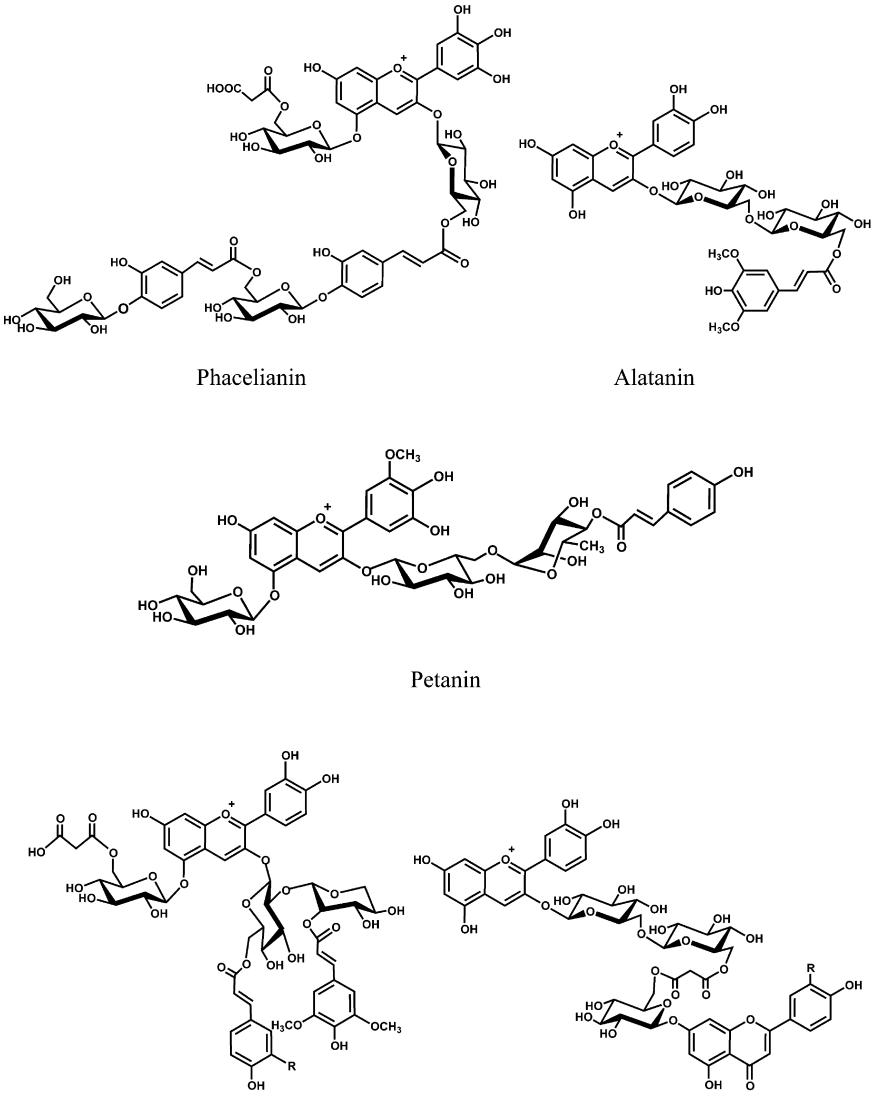

Figure 8. Chemical structures of polyacylated anthocyanins.

the beverage competes with other chemical reactions involving anthocyanins. Because it stabilizes the anthocyanins' coloration, copigmentation has a strong influence on the perceived color of wine; it has been shown to be responsible for 30−50% of the coloration in young red wines.[2,9,67,68] Anthocyanin copigmentation and self-association in wine can be demonstrated by gradually diluting young red wines at a constant pH, so as to at least partially dissociate the pigment···copigment and pigment··· pigment complexes. Because of this dissociation, Beer's law is not obeyed upon dilution, and a nonlinear color loss is observed.[2]

To estimate the extent of copigmentation in wine, the pigment and copigment contents of the different grape fractions (i.e., skin, pulp, and seeds) and different wine varieties must be carefully determined.[69] In wines, the total anthocyanin content varies from 150 mg/L (ca. 305 μM in oenin equivalents) to 800 mg/L (ca. 1620 μM) in some Pinot noir and Merlot wines, respectively. Most red wines contain ca. 300−500 mg/L of the most abundant anthocyanin (oenin) and thus have more than ten times the amount needed (ca. 35 μM, i.e., 17 mg/L) to enable sensitive detection of copigmentation in the visible range.[2]

Red wines contain many copigments. For example, in a study examining 34 hybrid grape varieties (22 red and 12 white),[70] 24 flavonol glycosides were identified, including derivatives of quercetin, myricetin, kaempferol, isorhamnetin, laricitrin, and syringetin. Other weaker copigments can be even more abundant in wine; for example, one publication reported a total concentration of phenolic acids and flavanols of 150 mg/L (800 μM in caffeic acid equivalents), compared to a total concentration of 30 mg/L (100 μM in quercetin equivalents) for myricetin, kaempferol, and quercetin.[2] Dihydroflavonols may also occur in wine and function as copigments,[27] although they are usually less abundant than other phenolic copigments. Overall, the copigment/anthocyanin molar ratios in wine are likely to be somewhere within the (rather wide) range of 0.05−2.

Many parameters influence the occurrence of copigmentation in wine, of which by far the most important are the concentrations of pigments and copigments. Rosé wines have much lower anthocyanin concentrations (20−50 mg/L) than reds[9,71] and, therefore, do not exhibit copigmentation producing the blue to purple tones. Surprisingly, certain phenolic

DOI: 10.1021/acs.chemrev.5b00507
Chem. Rev. 2016, 116, 4937−4982

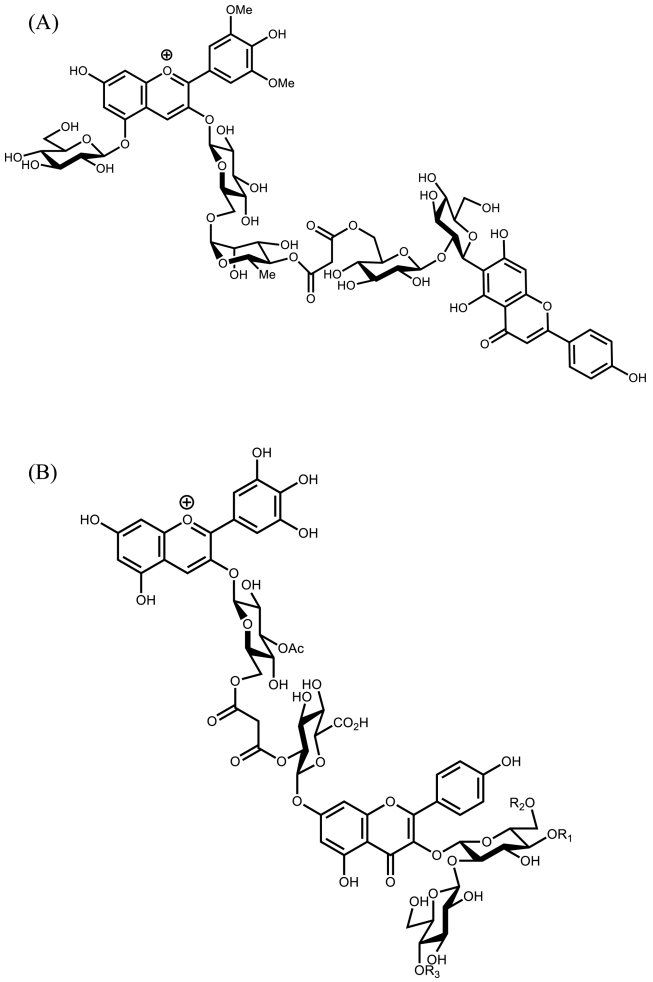

Figure 9. Anthocyanin-flavone *C*- or *O*-glycoside pigments with a malonate bridge from leaves of (A) *Oxalis triangularis* and (B) Allium "Blue Perfume".

compounds have been shown to produce color loss (hypochromism associated with anticopigmentation) rather than the expected hyperchromic effect due to copigmentation.[69] However, such anticopigmentation has only been reported once; further investigations will be required to verify its occurrence and clarify the underlying mechanisms.

Interestingly, it has been suggested that a ternary copigmentation complex consisting of an anthocyanin and two different flavonoids (oenin··· (+)-catechin··· quercetin-3-β-D-glucoside) may be formed in wine when all three species are present at high concentrations.[72] This may cause synergistic color-enhancing effects, depending on the pH, temperature, and presence of sulfites. A thorough characterization of the role of each partner would increase our understanding of color stabilization by ternary complex formation.

The relative contributions of self-association and copigmentation to wine coloration are a matter of intense debate. On the basis of CD analyses, R. Boulton concluded that self-association is not very relevant in young red wines.[2] Conversely, Gonzalez-Manzano et al. concluded that self-association accounted for 8% to 60% of the absorbance increases observed in wine-like solutions at 520 nm as the pigment concentration was increased from 50 to 600 mg/L.[2,73,74] Acylated anthocyanins are more prone to self-association than their nonacylated analogs.[75] With these pigments, intramolecular copigmentation and self-association may be tightly related and difficult to distinguish.[1] However, acylated anthocyanins are only minor pigments in wine.

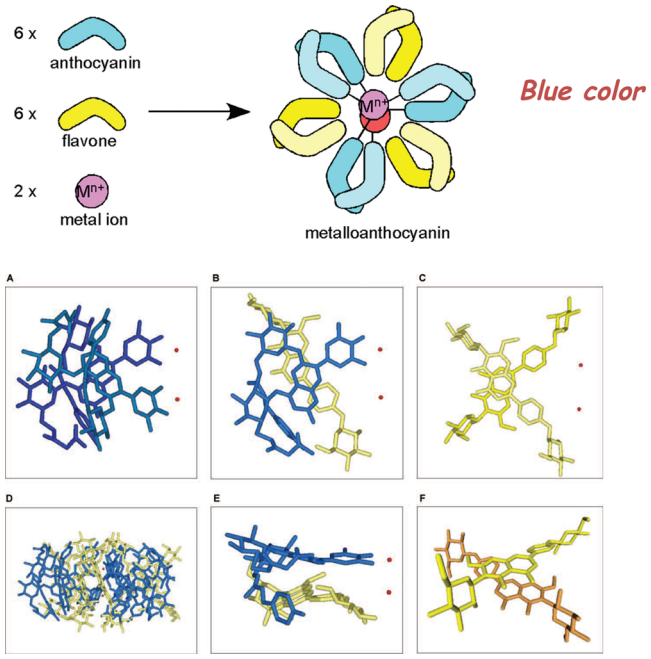

Figure 10. Structure of commelinin. Blue: malonylawobanin (MA), yellow and orange: flavocommelin (FC), red: Mg^{2+}(A). A side view of a left-handed stacking of two MA units that coordinate to different Mg ions. (B) A side view of a copigmentation of MA and FC in a right-handed stacking arrangement. (C) A side view of a left-handed stacking of two FC units. (D) A side view of commelinin. (E) A skew view of a copigmentation between MA and FC. (F) A skew view of the self-association of two FC units. Adapted with permission from ref 1. Copyright 2009 The Royal Society of Chemistry.

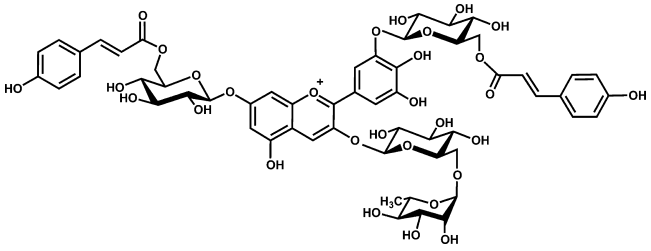

Figure 11. Chemical structure of the anthocyanin derived from *Ceanothus papillosus* petals.

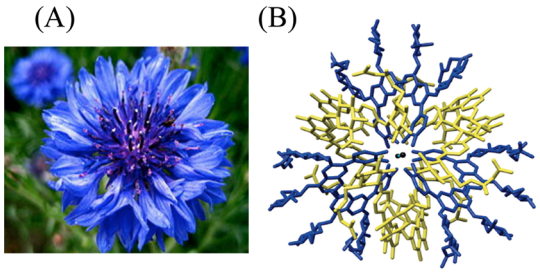

Figure 12. (A) Structure of protocyanins from *Centaurea cyanus* (cornflower). (B) X-ray diffraction crystal structure, showing the two metal ions Fe^{3+} and Mg^{2+} in the center of the supramolecular assembly. Adapted with permission from ref 1. Copyright 2009 The Royal Society of Chemistry.

DOI: 10.1021/acs.chemrev.5b00507
Chem. Rev. 2016, 116, 4937−4982

Table 1. Metal-Complex Pigments

common name	anthocyanin	copigments	metal	stoichiometry/pHv (vacuolar pH)	λ_{max} (nm)	source	ref
stoichiometric metal-pigment-copigment complexes							
commelinin	delphin 3-(6-p-coumaroylglucoside)-5-(6-malonylglucoside)	6-glucoside 4′-*O*-glucosylapigenin	Mg^{2+}	6 A: 6F: 2M	646	*Commelina communis*	56
protocyanin	cyanidin-3-*O*-(6-*O*-succinylglucoside)-5-*O*-glucoside	apigenin-7-*O*-glucuronide-4′-*O*-(6-*O* malonylglucoside)	Mg^{2+}; Fe^{3+}	6−8 A: 6−8F: 2M	676	*Centaurea cyanus* (corn flower)	57
protodelphin	delphin 3-(6-*p*-coumaroylglucoside)-5-(6-malonylglucoside)	7,4′-*O*-diglucosylapigenin	Mg^{2+}	6 A: 6F: 2M	–	*Salvia patens*	58
cyanosalvianin	delphin 3-(6-*p*-coumaroylglucoside)-5-(6-acetylmalonylglucoside)	7,4′-*O*-diglucosylapigenin	Mg^{2+}	6 A: 6F: 2M	–	*Salvia uliginosa*	59
nemophilin	petunin 3-(6-*p*-coumaroylglucoside)-5-(6-malonylglucoside)	7-*O*-glucoside 4′-(6-malonylglucosyl) apigenin 7,4′-*O*-diglucosylapigenin	Mg^{2+}; Fe^{3+}		712	*Nemophila menziesii*	1
nonstoichiometric metal-pigment-copigment complexes							
	delphinidin-3-glucoside	caffeoyl and coumaroyl derivatives of quinic acid	Al^{3+}, 4,5 equiv	pHv = 3.6 ± 0.3	586	*Hydrangea macrophylla* (blue color)	60,61
	delphinidin-3-glucoside	caffeoyl and coumaroyl derivatives of quinic acid	Al^{3+}, 1,2 equiv	pHv = 3.3 ± 0.2	539	*Hydrangea macrophylla* (red color)	60,61
	cyanidin-7-*O*-glucoside-3-*O*-(2-*O*-glucosyl)-glucoside	kaempferol derivatives	Mg^{2+}; Fe^{3+}	pHv = 4.8	646 and 606	*Meconopsis grandis*	62,63
	malvidin 3-*O*-glucoside-5-*O*-(6-*O*-acetylglucoside)	3-glucoside and 3-sophoroside of kaempferol and myricetin	–	pHv > 5.5		*Geranium*	64
	malvidin 3-*O*-(4-*O*-*p*-coumaroyl-rhamnosyl-6-*O*-glucoside)-5-*O*-glucoside	isovitexin (apigenin-6-*C*-glucoside)	–			*Iris ensata*	65
	Petunidin, delphinidin						

DOI: 10.1021/acs.chemrev.5b00507
Chem. Rev. 2016, 116, 4937−4982

Because grapes differ in their pigment and copigment contents, copigmentation in wines will obviously be sensitive to the grape varieties from which they are made. For example, Herras Roger et al. recently estimated that copigmentation is responsible for 31%, 22%, 22%, 16%, 15%, 14%, 11%, and 9% of the coloration of Ruby cabernet, Listan negro, Syrah, Merlot, Tintilla, Baboso, Negraoll, and Vijariego young red wines, respectively.[76] In another study, Tempranillo and Graciano monovarietal wines were compared to blended or "coupage" wines, which are made by grape blending (comaceration) and wine blending (covinification). Such winemaking techniques are intended to create wines with colors that are stable over time.[77] Forty-six pigments were identified in this study (including common anthocyanidin glucosides, their acylated analogs, and pyranoanthocyanins) as well as 12 flavonols (myricetin, quercetin, kaemferol, isorhamnetin, and their glycosides) and 12 phenolic acids (4 hydroxybenzoic acids and 8 HCA). Of the two monovarietal wines, the Graciano appeared darker and more intensely colored than the Tempranillo. Moreover, grape blending produced more bluish hues than wine blending. The authors concluded that copigmentation was enhanced in the early stage of winemaking. Moreover, copigmentation was enhanced in wines whose production involved pre- and postfermentative addition of rutin, caffeic acid, *p*-coumaric acid, and isoflavonoids.[78−82] Copigmentation also influences the extraction of anthocyanins from grapes into wine during winemaking; the efficiency of extraction was shown to depend on the concentrations of pigments and of certain copigments such as procyanidins from grape seeds.[2,83,84]

Other factors may influence the amount of pigments and copigments in wines, such as the soil on which the grapes are grown, the climatic conditions, the applied winemaking technique, and the degree of aging. For example, the copigmentation level in Cabernet sauvignon decreased from 42% to 0%, over the nine months immediately after the end of alcoholic fermentation, whereas its content in anthocyanin derivatives (including polymeric pigments), which are apparently much less prone to copigmentation, increased sharply.

Metal ions may also contribute to wine coloration if the wine has an appreciable content of anthocyanins with a catechol B-ring (e.g., cyanidin, petunidin, or delphinidin). High concentrations of copper are likely in certain grapes due to the use of copper-containing fungicides. However, metal-anthocyanin binding is poorly documented in wine and certainly has little impact on wine color.

Wine is a complex system that evolves as it ages, leading to the formation of diverse anthocyanin-derived pigments such as pyranoanthocyanins, which may also exhibit copigmentation. While anthocyanin copigmentation has been relatively well studied, the same is not true for copigmentation involving pyranoanthocyanins. Whereas anthocyanins and other flavylium derivatives like catechin-(4 → 8)-oenin express their maximal color intensity under acidic conditions, it was demonstrated that pyranoanthocyanin-flavanol pigments absorb visible light more strongly at wine pH (around 3.6), under which conditions their absorption is up to 30−50% stronger than at pH = 1.0. Such hyperchromic effects may indicate the occurrence of intramolecular copigmentation and/or self-association in pyranoanthocyanin-flavanols, which would produce higher molar absorption coefficients.[9] These results become even more interesting and surprising when one considers that pyranoanthocyanins, unlike anthocyanins, generally do not undergo water addition and therefore can only participate in proton transfer reactions as the pH increases.[85−87] On the other hand, the addition of (+)-catechin to a mildly acidic solution of the oenin-vinylguaiacol pyranoanthocyanin caused a large increase in visible absorption (even greater than that observed for oenin), illustrating the potential contribution of pyranoanthocyanins in the manipulation of wine color.[86]

In some cases, copigmentation is just the first step in a process of chemical change that anthocyanins undergo in aging wines and may be followed by the formation of covalent linkages between the components of the copigmentation complex.[88] For example, catechin-methylmethine-anthocyanins in wines are formed by the reaction between anthocyanins (pigment), catechin derivatives (copigment), and acetaldehyde (which is the source of the methylmethine bridge and functions as a covalent linker) produced by ethanol oxidation. This reaction is probably favored by the proximity of the reactants within the copigmentation complex.

3.3. Copigmentation in Food and Beverages

While there have been many studies on copigmentation in flowers and (to a lesser extent) in red wine, there have been far fewer on copigmentation in fruit, vegetables, and beverages other than wine. Nevertheless, copigmentation is likely to occur and stabilize coloration in fruit products (juices, purees, jams, and syrups). Early studies showed that metal ions stabilize the colors of products made from berries, such as strawberry puree,[89] cranberry juice cocktail,[90] and crowberry juice.[91] The blue color of blueberries (*vaccinium* sp.) has been linked to aluminum-anthocyanin complexes.[92] However, adequate pigment and copigment profiling or copigmentation measurements have not yet been conducted on fruit and vegetables.

One way of stabilizing color during food processing and storage is to add specific copigments; this technique has been studied especially intensively in the context of berry juices.[2,67,93] For example, phenolic acids have been shown to enhance color stability in some berry juices (strawberry, raspberry, lingonberry, cranberry, and orange juices) during storage.[93,94] Moreover, chlorogenic acid enhanced the color intensity of strawberry and chokeberry juices. Some authors have observed that the presence of flavone *C*-glycosides induced significant hyperchromic effects and enhanced anthocyanin stability in products rich in cyanidin glycosides, particularly açaí fruit beverages.[95] Flavonol glycosides such as rutin have repeatedly been identified as copigments that stabilize the color of fruit juices including blood orange and plum juices during storage.[94,96] In addition, the purplish-red color of jambolan anthocyanins is reportedly enhanced and stabilized by copigmentation with sinapic acid, caffeic acid, and rosemary polyphenolic extract.[97] The red color of pomegranate juice, which is due to cyanidin and delphinidin glycosides, was also stabilized by the addition of 2 equiv of phenolic copigments, although the addition of higher concentrations had negative effects, most probably due to the formation of aggregates.[98] Vitexin, orientin, and other flavonoid *C*-glycosides from pigeon pea leaves enhanced color stability in blueberry juices by intermolecular copigmentation, with pigeon pea leaf extract being the most effective.[99] It has been suggested that self-association is more important in berry coloration than in young red wines.[100] Finally, the ability of copigments (ferulic acid, caffeic acid, *p*-coumaric acid, rutin, and hesperidin) to limit bleaching in purple sweet potatoes has been tested, although none exhibited strong effects.[82]

DOI: 10.1021/acs.chemrev.5b00507
Chem. Rev. 2016, 116, 4937−4982

4. EXPERIMENTAL TECHNIQUES TO ANALYZE COPIGMENTATION

A full understanding of copigmentation requires a thorough analysis of the noncovalent interactions responsible for specific spectral variations. In wine chemistry for example, a comprehensive description of the supramolecular interactions involved in copigmentation would be advantageous at all stages of winemaking, from the selection of grape varieties in the vineyard to the characterization of an old wine in the glass.[2,85,101] Copigmentation and the associated interactions influence the wine's colorimetric ratios, including the color/colorless, red/blue, and red/orange ratios, and can thus affect consumers' perceptions of the product. These ratios are affected by grape variety, winemaking procedure (e.g., the protocol applied during maceration), as well as environmental and agricultural conditions. In the food industry, characterizing the contribution of copigmentation to the overall color requires the complete panel of available experimental techniques.

Copigmentation is an observable, so most of the color variation it produces is discernible by simple visual inspection, and many details of its functioning can be understood simply by using conventional UV−vis absorption spectroscopy. Although this technique is by far the most popular in this case, copigmentation complex characterization is amenable to other techniques widely used to characterize noncovalent assemblies, mainly NMR and CD spectroscopies. It is worth noting however that even the simplest (nonacylated) anthocyanins are typically available only in limited amounts, either by time-consuming extraction protocols or by multistep chemical synthesis or from a few commercial sources. Moreover, except in highly acidic (non-natural) conditions, aqueous solutions of anthocyanins are actually a mixture of several colored and colorless forms (vide supra), all characterized by their peculiar thermodynamics. These are probably the reasons why many nowadays standard and powerful techniques used in supramolecular chemistry, such as isothermal titration calorimetry (ITC), have been little applied to copigmentation so far. Even investigations of copigmentation by NMR are generally limited to the sole flavylium ion (highly acidic solution).

4.1. UV−vis Absorption

The most characteristic manifestation of copigmentation is the combination of color intensification and spectral shifts observed when a copigment is added to a mildly acidic solution of an anthocyanin. Monitoring by UV−vis absorption spectroscopy makes it possible to evaluate these phenomena in terms of hyperchromic effects and bathochromic shifts.[29,31,46,49,102−106] This is why UV−vis spectroscopy is by far the most widely used tool for studying copigmentation, also because rather low pigment concentrations (<0.1 mM) can be used, which is a valuable asset in this field. As an example of the spectacular spectral changes that can be observed, malvidin 3,5-di-*O*-β-D-glucoside (malvin) forms a highly stable copigmentation complex with 7-*O*-sulfoquercetin that triggers a bathochromic shift of nearly 40 nm in the flavylium visible band (λ_{MAX} = 525 nm for malvin), which is best evidenced at pH = 1. This bathochromic shift corresponds to a color change from red to purple. Moreover, a large hyperchromic effect of ca. 1 order of magnitude is also observed at pH = 3.5, reflecting the partial conversion of the free (colorless) hemiketal [largely dominant at pH = 3.5, pK'_h(malvin) ≈ 2] back to the (red) flavylium cation (Figure 13).[107] Raising the temperature markedly attenuates this color gain, which is consistent with a partial dissociation of the copigmentation complex and suggests that the binding of the two components is exothermic.

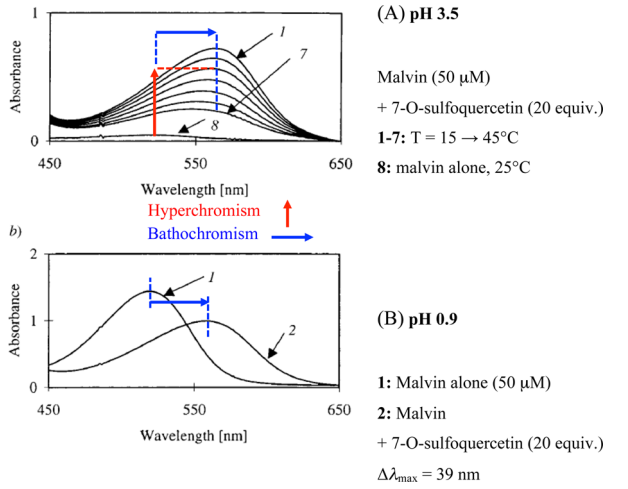

Figure 13. Copigmentation of malvin (malvidin 3,5-di-*O*-β-D-glucoside) by 7-*O*-sulfoquercetin. Reprinted with permission from ref 107. Copyright 2001 John Wiley & Sons.

This section focuses particularly on the dependence of the visible absorbance on temperature, pH, and copigment concentration. Assuming a 1:1 stoichiometry for the copigmentation complexes and no binding between the copigment and the colorless forms, the visible absorbance changes can be analyzed so as to estimate the pigment−copigment binding constants and the corresponding enthalpy and entropy.[102,106,108−111]

Briefly, the relative hyperchromic effect observed in copigmentation can be derived from simple solution chemistry combining Beer's law, the law of pigment conservation, and the expressions of the thermodynamic constants.[102] It can thus be written as

$$\frac{A - A_0}{A_0} = \alpha + \beta\frac{1}{[CP]} \tag{2}$$

where A and A_0 are the absorbance values at the same wavelength in the presence and absence of copigment, respectively, and [CP] is the copigment concentration. Parameters α and β are the following combination of a spectroscopic term K_S (involving molar absorption coefficients) and a second term K_C that only depends on proton concentration and thermodynamic constants: $\alpha = K_C/(K_S - K_C)$, $\beta = 1/(K_S - K_C)$.

$$K_S = \frac{r_{AHCP^+}K_{AHCP^+} + r_A r_{ACP}\frac{K_a}{[H^+]}K_{ACP}}{1 + \frac{K_a}{[H^+]}} \tag{3}$$

$$K_C = \frac{K_{AHCP^+} + \frac{K_a}{[H^+]}K_{ACP}}{1 + \frac{K_a + K_h'}{[H^+]}} \tag{4}$$

where K_a and K_h' are the acidity constant and overall hydration constant of the flavylium ion, respectively; K_{AHCP+} and K_{ACP} are the pigment−copigment binding constants for the flavylium ion and quinonoid bases, respectively; $r_A = \varepsilon_A/\varepsilon_{AH^+}$; $r_{AHCP^+} = \varepsilon_{AHCP^+}/\varepsilon_{AH^+}$; and $r_{ACP} = \varepsilon_{ACP}/\varepsilon_A$.

At low pH (<2), the flavylium cation and its complex are the sole species in solution and eq 2 is converted into the classical Benesi−Hildebrand relationship.[112] We must also note that at low pH, the hydration equilibrium is no longer established and

DOI: 10.1021/acs.chemrev.5b00507
Chem. Rev. 2016, 116, 4937−4982

no colorless forms are available for conversion into colored forms upon copigment addition. Hence, the hyperchromic effect is not observed and copigmentation only produces bathochromic effects, which may be very weak.[108]

Eq 2 can be used for the fitting of the pH dependence of the hyperchromic effect for fixed pigment and copigment concentrations.[102] For investigations of the dependence on temperature or copigment concentration, eq 2 can also be simplified by selecting a pH where either the flavylium ion ($pH < pK_a - 1$) or the quinonoid bases ($pH > pK_a + 1$) are present.[106,108−111] With anthocyanins that are especially sensitive to water addition such as 3,5-*O*-*β*-diglucosides ($pK'_h \approx 2$), the conditions $pH < pK_a - 1$ and $pH > pK'_h + 1$ can be met, thus permitting additional simplification:[46]

$$\frac{A - A_0}{A_0} = r_{AHCP^+} K_{AHCP^+}[CP] \quad (5)$$

A similar relationship can hold for quinonoid bases in mildly acidic conditions (pH 5−6):[113]

$$\frac{A - A_0}{A_0} = r_{ACP} K_{ACP}[CP] \quad (6)$$

Enthalpy and entropy changes of copigmentation are typically deduced by determining binding constants at different temperatures and constructing a linear Van't Hoff plot (assuming ΔH^0 and ΔS^0 are temperature-independent over the selected temperature range):

$$\ln K = -\frac{\Delta G^\circ}{RT} = \frac{\Delta S^\circ}{R} - \frac{\Delta H^\circ}{R}\frac{1}{T} \quad (7)$$

The simple situations described above (eqs 5 and 6) are particularly interesting as the hyperchromic effect is directly related to the copigmentation binding constants, without interference of the thermodynamics of proton transfer and water addition. This advantage can be exploited for the construction of structure-affinity relationships.[113] Thus, a direct plot showing the temperature dependence of the hyperchromic effect (for a fixed concentration of copigment in large excess) is possible, as follows:

$$\ln \frac{A - A_0}{A_0} = \ln(r[CP]) - \frac{\Delta G^\circ}{RT} = \ln(r[CP]) + \frac{\Delta S^\circ}{R} - \frac{\Delta H^\circ}{R}\frac{1}{T} \quad (8)$$

For a fixed CP concentration, the slope and intercept of $\ln(A - A_0/A_0)$ as a function of $1/T$ thus provide estimation of ΔH^0 and ΔS^0, respectively. The spectroscopic parameters r_{AHCP+} and r_{ACP} can be determined beforehand by comparing the spectra of the pigment alone and pigment plus copigment in large excess, both in the absence of colorless forms. The values of r_{AHCP+} and r_{ACP} can be determined in highly acidic solution and immediately after pigment addition in a pH = 5−6 solution, respectively, because hydration is either absent or slow under such conditions. Alternatively, the hyperchromic effect can be recorded at the isosbestic points of both the pigment and copigmentation complex, which are defined by $r_{AHCP^+} = 1$ (i.e., $\varepsilon_{AHCP^+} = \varepsilon_{AH+}$) and $r_{ACP} = 1$ (i.e., $\varepsilon_{ACP} = \varepsilon_A$), respectively.

Hyperchromic effects can be observed when a pool of colorless forms initially exists and are converted back to colored forms upon selective binding with copigment. Thus, it is clear that a pigment with a high K'_h value ($K'_h = [H^+][B']/[AH^+]$, where B′ is the global pool of colorless forms B, C_{cis}, and C_{trans}) (i.e., when the anthocyanin is especially prone to water addition) will usually produce a stronger hyperchromic effect. A simulation of the hyperchromic effect as a function of pH (Figure 14) also confirms that the color gain is maximal when it takes place from a mildly acidic almost colorless control solution (with no copigment).

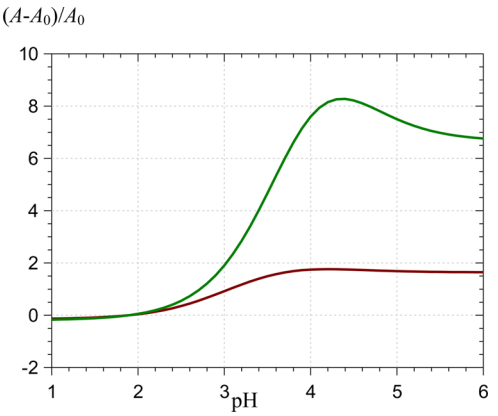

Figure 14. pH dependence of the copigmentation hyperchromic shift. Spectroscopic monitoring at λ_{MAX} of free flavylium. Simulations from eq 2 using the following parameters: CP concentration = 10 mM, pK'_h = 2.5, pK_a = 4.0, r_{AHCP+} = 0.8, r_{ACP} = 0.9, r_A = 0.7. Hydroxycinnamic acids (red line): $K_{AHCP+} = 3 \times 10^2$ M^{-1}, $K_{ACP} = 2 \times 10^2$ M^{-1}. Flavones and flavonols (green line): $K_{AHCP+} = 3 \times 10^3$ M^{-1}, $K_{ACP} = 10^3$ M^{-1}.

Many experimental studies have evidenced that bathochromic shifts require copigment-to-pigment charge transfer (CT).[105,108,114] On the basis of the explicit correlation between the free enthalpy of copigmentation and the difference between the copigment's ionization potential and the pigment's electron affinity, it was proposed that CT state formation contributes significantly to the driving force of copigmentation.[105] However, even relatively potent copigments such as vinylcatechin dimers can bind anthocyanins but induce no significant bathochromic shifts.[108] Stable copigmentation complexes may form with only marginal spectral changes if colorless forms are minor and CT negligible. This is the case for the 3-deoxyanthocyanidins (relatively abundant in red sorghum), which are known to be much more resistant to hydration than common anthocyanins.[115] Even when it has little visible impact on color, copigmentation may be quite important in limiting the accumulation of colorless forms and the subsequent (irreversible) degradation of pigments (see section 6.2).

By comparing the spectral changes at pH = 1 (pure flavylium and bathochromic shifts only) and at higher pH values (mixtures of colored and colorless forms), it is possible to outline the normally minor contributions of the colorless forms to copigment binding.[109,116] This contribution turned out to be very significant in the particular case of copigmentation by the purine caffeine, which was also observed to form 1:2 pigment-copigment complexes.[109,116,117] It may also be noted that the copigment-induced decrease in the apparent rate constant for water addition to the flavylium ion provides another method for estimating pigment-copigment binding constants.[113] Moreover, copigmentation can be interpreted by considering that the copigment increases the apparent pK'_h value (noted pK'^{CP}_h) (i.e., it extends the pH range over which the colored forms prevail) (Figure 15).[74,118]

DOI: 10.1021/acs.chemrev.5b00507
Chem. Rev. 2016, 116, 4937−4982

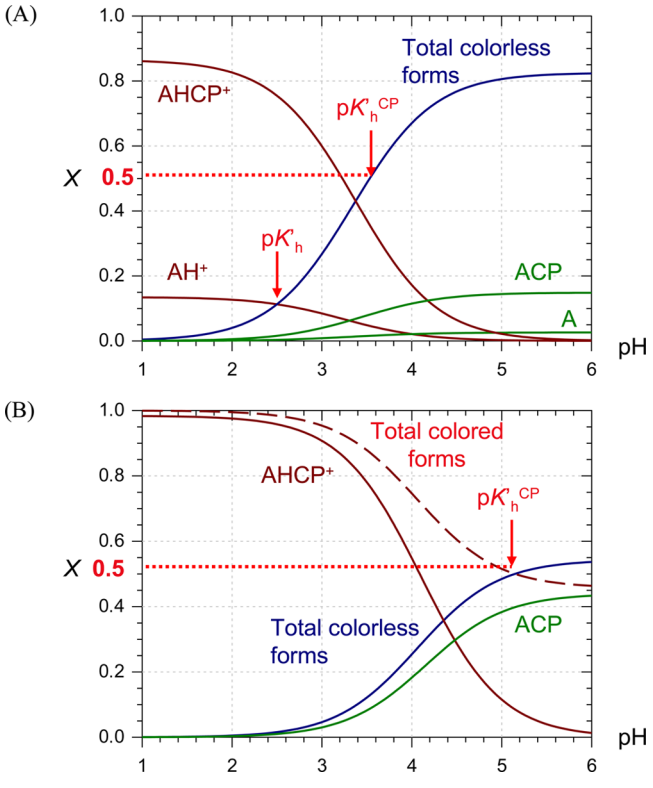

Figure 15. Distribution diagram of anthocyanin forms in the presence of a copigment. Parameters: $pK'_h = 2.5$, $pK_a = 4.0$, pigment and copigment concentrations = 10 and 30 mM, respectively. (A) Hydroxycinnamic acid, $K_{AHCP} = 3 \times 10^2$, $K_{ACP} = 2 \times 10^2$ M^{-1}, pK'^{CP}_h (pH of a 1:1 mixture of colored and colorless forms) ≈ 3.5. (B) Flavone or flavonol, $K_{AHCP} = 3 \times 10^2$ M^{-1}, $K_{AHCP} = 3 \times 10^3$ M^{-1}, $pK'^{CP}_h \approx 5.2$.

The preceding sections discussed the quantification and analysis of colors expressed by anthocyanins and their complexes in terms of the maximum absorption wavelength λ_{MAX} and increases in visible absorbance. However, color perception also depends on a number of factors that are inherent to the colorant, as well as its concentration, illumination, and interactions with the human eye. All of these factors should be well understood to analyze and/or modulate a specific visual impression of, for example, a wine. For a given pigment-copigment pair, the inherent optical properties are entirely contained in the details of the absorption spectrum, plotted in terms of the molar absorption coefficient, in a given solvent (e.g., water). Light scattering can be neglected if the number of associated chromophores is (very) small with respect to that of solvent molecules, as is usually the case in copigmentation. It is worth noting here that increasing concentrations give rise to hyperchromic effects but may also lead to the formation of larger aggregates and precipitation, which can dramatically modify optical behavior. For solid state samples, the description becomes much more complex, taking into account the specific chromophore assembly, which changes the colorant's optical properties via (long-range) intermolecular interactions, the size of the assembly, and the resulting reflectance and absorbance; for further details see, for example, refs 119 and 120.

Color perception can be robustly evaluated within the CIELAB (for 'Commission International de l'Eclairage' and L^*,a^*,b^*) model based on the color-opponent theory using hue or chromatic tonality (e.g., the amount of red vs green a^*, the amount of yellow vs blue b^*), saturation C^* (i.e., vivid or bright vs dull color perception), and lightness L^* (i.e., dark or light color perception) for standard illuminant D65 to mimic "average daylight".[121] For applications in the food industry, it is now mandatory to evaluate copigmentation using a combination of λ_{MAX} spectral shifts and total color difference ΔE^* measurements, which help refine the color perception assigned to copigmentation. As a general trend, copigmentation produces darker colors (lower L^*), bluing effects [higher Δh_{ab}, where $h_{ab} = \tan^{-1}(b^*/a^*)$ is the hue angle] and increased saturation (higher C^*).[72,122] The bluing effect of pigment···copigment association historically evidenced by *R.* Robinson was reevaluated by the conduction of colorimetric measurements of copigmentation between cyanidin 3,5-*O*-diglucoside and the flavonol rutin (quercetin 3-*O*-rhamnoglucoside).[121,123] The solutions containing the copigment provided a much more complex hue palette than would be expected for a simple bluing effect, with the eye perception of copigmentation strongly depending on the pH and the concentration of both pigment and copigment. ΔE^* values usually increase in the presence of copigments (e.g., when adding quercetagetin to anthocyanin solutions).[124] This was also shown with purple sweet potato anthocyanins[82] and grape juice, in which chlorogenic acid increased ΔE^* by almost 2 units.[125] The addition of rosemary polyphenols to jambolan (*Syzygium cumini*) fruit anthocyanins also yielded a more vivid purplish-red color with a decrease of lightness L^* and an increase of chroma C^*.[97] A decrease of L^* and b^* was also observed with the oenin-isoquercitrin pair.[26]

The concentration effect was confirmed and supported by colorimetric measurements. Molar ratio up to 1:7 (malvidin 3-*O*-glucoside···epicatechin) provided the lowest L^* and b^* values but the highest a^* values, meaning that this was the ratio at which the pigment-copigment pair exhibited the darkest and most vivid bluish color.[122] The modulation of the colorimetric parameters was used to evaluate the efficiency of copigments in anthocyanin-flavanol-flavonol ternary systems.[72] Quercetin 3-*O*-β-D-glucoside was shown to be more efficient than (+)-catechin at stabilizing color changes (in particular lightness) expressed by malvidin 3-*O*-glucoside. However, the synergism and antagonism within these ternary systems have not yet been elucidated.

Relative contributions to ΔE^* can be assessed by means of CIELAB measurements. Concentration-dependent decreases in L^* and increases in saturation can be evaluated in wine models.[27] These effects are associated with hyperchromic effects and bathochromic shifts, which remain noticeable two months after preparation. Chromatic changes typical of copigmentation (still visible two months after storage) were related to red-purple shifts. After two months, a gradual displacement toward red-orange colors was observed, suggesting the formation of new pigments. Colorimetric measurements pointing to copigmentation have also been conducted in various wines.[77]

4.2. Other Analytical Tools

^{1}H NMR provides direct evidence that copigmentation proceeds via (vertical) $\pi-\pi$ stacking interactions between phenolic nuclei. In the NMR spectra of copigmentation complexes, the aromatic proton signals of both pigment and copigment molecules are shielded (in comparison to those of the free molecules), suggesting that each phenol undergoes the ring current of the other's π-electrons.[42,107,126] The magnitude of these chemical shift modifications is comparable to those observed for stacked nucleotides in solution.[127] Moreover, each proton of the two partners is differently shielded, which provides information about their relative positioning in the complex. For example, the

DOI: 10.1021/acs.chemrev.5b00507
Chem. Rev. 2016, 116, 4937−4982

Table 2. Thermodynamic Parameters of Binding in Self-Association and Copigmentation Systems[a]

	K (M^{-1})[b]	ΔG^0 (kJ/mol)[b]	ΔH^0 (kJ/mol)	ΔS^0 (J/mol K)	pH	ref
self-association						
pelargonin	125	−12.0			1	44
cyanin	265	−13.8			1	44
peonin	325	−14.3			1	44
delphin	310	−14.2			1	44
petunin	625	−16.0			1	44
malvin	620	−15.9			1	44
malvin	900 (22 °C)	−16.9			6	45
malvin	200 (22 °C)	−13.1			9.8	45
myrtillin	1240	−17.7			1	128
oenin	976	−17.1			1	128
oenin	820 (27 °C)	−16.6			1	75
malvidin 3-*O*-*β*-D-(6-*O*-*p*-coumaroyl)-glucoside	1400 (27 °C)	−18.0			1	75
petunin	900	−16.9			1	128
kuromanin	700	−16.2			1	128
peonin	661	−16.1			1	128
callistephin	404	−14.9			1	128
copigmentation						
flavonols and flavones						
*m*alvin···rutin	2750	−19.6	−37.2	−59.0	3.5	130
malvin···3‴-*O*-sulforutin	350	−14.5	−33.0	−62.0	3.5	130
malvin···2‴,3‴-*O*-(2-carboxy-1-methylethylidene) rutin (2 epimers)	2320	−19.2	−16.7	8.4	3.5	130
malvin···2″,3″,4″,2‴,3‴,4‴-hexa-*O*-succinylrutin	1060	−17.3	−17.1	0.5	3.5	130
malvin···di-*O*-succinylrutin (3 regioisomers)	1820	−18.6	−13.6	16.7	3.5	130
malvin··· 4‴-*O*-succinylrutin	1700	−18.4	−7.9	35.3	3.5	130
malvin···quercetin 3′-*O*-*β*-D-(2,3,4,6-tetra-*O*-succinyl) glucoside	1560	−18.2	−23.6	−18.0	3.5	107
malvin···7-*O*-sulfoquercetin	14470	−23.8	−37.3	−45.6	3.5	107
malvin···4′,7-di-*O*-sulfoquercetin	8940	−22.6	−34.7	−40.0	3.5	107
pelargonin···isoquercitrin	1050 (20 °C)	−17.2			0.25	105
pelargonin···quercitrin	1740 (20 °C)	−18.5			0.25	105
delphinidin···baicalin	2020	−18.8	−35.2	−67.8	3.65	104
delphinidin···quercetin-5′-sulfonic acid	3290	−20.0	−51.7	−106.6	3.65	104
delphinidin···rutin	1150	−17.4	−55.2	−163.7	3.65	104
flavanols						
oenin···(−)-epicatechin	260	−13.8	−18	−14.2	3.6	31
malvin···catechin	185		−30.4	−58.6	3.5	113
malvin···catechin	215		−25.0	−39.2	5.5	113
oenin··· procyanidin B3	330	−14.4	−9.2	17.2	3.6	31
oenin···(9S,11R) vinylcatechin dimer	1930	−18.7			3.5	110
oenin···(9R,11S) vinylcatechin dimer	5420	−21.3			3.5	110
oenin···procyanidin B3	350	−14.5			3.5	110
catechin-(4→8)-oenin···(9S,11R) vinylcatechin dimer (10% EtOH)	311	−14.2	−17.8	−12.0	3.5	108
catechin-(4→ 8)-oenin···(9R,11S) vinylcatechin dimer (10% EtOH)	516	−15.5	−22.7	−24.2	3.5	108
catechin-(4→ 8)-oenin···procyanidin B3 (10% EtOH)	121	−11.9	−32.5	−69.2	3.5	108
hydroxycinnamic acids						
malvin···*p*-coumaric acid	129	−12.0	−32.1	−62.8	2.5	106
malvin···4-*O*-*β*-*D*-glucopyranosylcoumaric acid	111	−11.7	−26.0	−38.0		106
malvin···caffeic acid	243	−13.6	−25.6	−46.0		106
malvin···4-*O*-*β*-D-glucopyranosylcaffeic acid	244	−13.6	−21.6	−31.0		106
malvin···ferulic acid	331	−14.4	−29.0	−50.1	3.6	106
malvin···4-*O*-*β*-*D*-glucopyranosylferulic acid	277	−13.9	−33.8	−71.0		106
peonidin···ferulic acid	155 (20 °C)	−12.5			2.58	105
oenin···ferulic acid	243 (20 °C)	−13.6			2.58	105
pelargonin···ferulic acid	263 (20 °C)	−13.8			2.58	105
cyanin···ferulic acid	210 (20 °C)	−13.3			2.58	105
malvin···chlorogenic acid	220	−13.4	−24.1	−36.1	3.5	113
malvin···chlorogenic acid	140	−12.2	−18.3	−20.1	5.5	113
oenin··· chlorogenic acid	390	−14.8	−14.2	2.04	3.6	31
hydroxybenzoic acids						
pelargonin···protocatechuic acid	68 (20 °C)	−10.5			0.25	105
pelargonin···gallic acid	87 (20 °C)	−11.1			0.25	105

DOI: 10.1021/acs.chemrev.5b00507
Chem. Rev. 2016, 116, 4937−4982

Table 2. continued

	K (M^{-1})[b]	ΔG^0 (kJ/mol)[b]	ΔH^0 (kJ/mol)	ΔS^0 (J/mol K)	pH	ref
malvin···protocatechuic acid	80 (20 °C)	−10.9			3.65	105
oenin···*p*-hydroxybenzoic acid (12% EtOH)	12.1	−6.2	−10.7	−15.3	3.6	49
oenin···protocatechuic acid (12% EtOH)	14.6	−6.7	−13.5	−23.4	3.6	49
oenin···gallic acid (12% EtOH)	21.2	−7.6	−16.9	−31.9	3.6	49
oenin···vanillic acid (12% EtOH)	35.6	−8.9	−19.7	−37.1	3.6	49
oenin···syringic acid (12% EtOH)	50.6	−9.7	−21.1	−38.8	3.6	49
purines and aromatic amino acids						
malvin···caffeine	125	−12.0	−11.7	0.9	3.5	113
malvin···caffeine	180	−12.9	−17.6	−16.0	5.5	113
malvin···Trp	64	−10.3	−6.8	11.8	3.5	113
malvin···TrpOMe	36	−8.9	−12.3	−11.5	3.5	113

[a]All values were obtained in aqueous solution unless otherwise specified (presence of a certain % of EtOH). [b]Values at 25 °C, unless otherwise specified.

shielding of H2′ (B-ring) was greater than that for the other H atoms of the anthocyanins, providing the first evidence that anthocyanin stacking does not involve perfectly superimposed noncovalent interaction and confirming the importance of the B-ring. The B-ring's importance was further demonstrated by considering substituent effects.[44] In strongly acidic solution of an initially pure flavylium cation, plots of the pigment protons' diamagnetic shifts as a function of copigment concentration can be quantitatively analyzed to determine pigment-copigment binding constants. The method can also be used for the determination of self-association constants, using either a simple monomer-dimer model or the so-called isodesmic model, which assumes higher oligomers (i.e., the successive formation of *n*-mers with identical stepwise binding constants).[128,129]

The NOE (Nuclear Overhauser Effect) has also been used to evaluate noncovalent interactions in copigmentation, by measuring the transfer of nuclear spin polarization through space (rather than through covalent bonds). NOE experiments confirmed the occurrence of anthocyanin self-association. For instance, upon irradiation of malvin's anomeric protons, negative NOEs (decreases in the signal intensities of H4 and H6) were observed at room temperature (but not at 60 °C), which were attributed to a lowering of the pigment's tumbling motion caused by self-association.[44] NOESY experiments on malvidin 3-*O*-*β*-D-(6-*O*-*p*-coumaroyl)glucoside at different concentrations have shown that the coumaroyl group is oriented toward the anthocyanin chromophore. Cross-peaks between the H6 proton of the anthocyanidin moiety and the H*α* proton of the aromatic acyl group were detected, indicating that the chromophore and acyl group were associated with one-another in solution.[75]

The sugar residues of anthocyanins are chiral, so their self-association can result in chiral stacking, making CD a very powerful and sensitive tool for its study. In particular, CD is very convenient for discriminating between intramolecular copigmentation (which produces a flat CD spectrum in the visible region) and noncovalent dimerization of acylated anthocyanins with chiral stacking of the chromophores, for which a strong exciton-type Cotton effect is observed in the visible region.[1] The sign of the Cotton effect can be used to distinguish between assemblies with right-handed or left-handed screw axes in both metal-free aggregates and metalloanthocyanin complexes.[1,43,45,100] Exciton-type CD is allowed only if the transition dipole moments of both partners are not parallel or antiparallel. For example, due to electrostatic repulsion in A^-:A^-, the angle is higher than in A:A and so the CD magnitude is higher too.[45]

Despite their strong UV−vis absorption, anthocyanins are only very weakly fluorescent because of the many competing fates of their excited states. Consequently, fluorescence spectroscopy has only rarely been used to reveal and quantify copigmentation. For instance, in a strongly acidic solution, rutin was shown to quench the weak fluorescence of the flavylium ion of malvin at 600 nm (excitation at 540 nm). The binding constant between these two partners was estimated from their quenching curve ($K_{AHCP+} \approx 2.6 \times 10^3$ M^{-1}, in good agreement with the value determined by UV−vis spectroscopy).[130]

A relevant way of determining the supramolecular arrangement of copigmentation and self-association complexes is through X-ray crystallographic analysis. However, to date the only such complexes to have yielded X-ray quality crystals that enable full structural elucidation are the metalloanthocyanins commelinin from *C. communis*[131] and protocyanin from *C. cyanus*.[132] These complexes display a 3-fold symmetry axis and consist of six anthocyanin molecules bound to a core of two metal ions with six flavone copigments intercalated in between (vide infra).[1] Unfortunately, copigmentation and self-association (binary) complexes are usually labile, which make crystal growing virtually impossible and makes X-ray crystallography inapplicable to the analysis of most copigmentation systems with relevance to food. Moreover, significant to dramatic structural modifications from solution to the solid phase should be systematically envisaged, and the geometrical features of the copigmentation complexes should be analyzed with great care.

It is worth noting again that the experimental methods presented in this section are much less used than UV−vis absorption to characterize copigmentation, although NMR titrations are the most often used method to characterize supramolecular complexes and estimate binding constants. Indeed, copigmentation generally induces large changes in the pigment's visible spectrum; moreover, UV−vis spectroscopy allows working at low pigment concentration (<0.1 mM), for which the competing self-association of anthocyanins can be neglected, and data acquisition is fast enough to investigate many pigment-copigment systems for structure-affinity relationships. This shows however the lack of systematic studies based on advanced experimental methods in supramolecular chemistry, which should be developed in the future to gain further insight in structural and energetic description. At present, the only alternative to X-ray crystallography for directly investigating the 3D structures of anthocyanin complexes at the atomic scale is to perform molecular modeling calculations (see sections 8−10)

DOI: 10.1021/acs.chemrev.5b00507
Chem. Rev. 2016, 116, 4937−4982

and combine their results with experimental data from UV−vis absorption, NMR, and CD spectroscopy experiments.

5. STABILITY IN INTERMOLECULAR COPIGMENTATION

5.1. Structure−Affinity Relationships

As mentioned above, copigmentation has mainly been investigated qualitatively by comparing hyperchromic effects observed with different pigment-copigment pairs. However, since the hyperchromic effect may not be simply related to the copigmentation binding constants (vide supra), such data must be interpreted with care. Moreover, copigmentation is strongly pH-dependent, and most works reporting binding constants were conducted at a pH where the flavylium is the dominant-colored species. Despite these limitations, the known copigments can be ranked in order of decreasing binding constants based on the studies reported to date: flavones and flavonols ($K_{AHCP+} > 10^3$ M^{-1}) > hydroxycinnamic acids ($K_{AHCP+} = 2-4 \times 10^2$ M^{-1}) > flavanols ($K_{AHCP+} = 1-2 \times 10^2$ M^{-1}) > hydroxybenzoic acids ($K_{AHCP+} < 10^2$ M^{-1}) (see Table 2).[29,31,46,49,102−106,113] Unexpectedly, the simple aroma component 3,5-dimethoxy-4-hydroxyacetophenone also turned out to be a rather potent copigment of malvin.[133] This ranking suggests that any extension of the π-conjugated system beyond the phenolic ring (e.g., conjugation through the 2,3-double bond of flavonoids, substitution by electron-donating hydroxyl and methoxyl groups, or conjugation with an electron-withdrawing keto groups) has a positive impact on copigmentation. This reflects an enhancement of dispersion interactions to favor $\pi-\pi$ stacking (higher copigment polarizability) and subsequently the formation of noncovalent complexes. Interestingly, 7-*O*-sulfoquercetin is an excellent (negatively charged) copigment of the malvin flavylium ion ($K_{AHCP+} \approx 10^4$ M^{-1}), possibly because of the additional ionic interaction it can form (Table 2).[107] Similarly, the ferulate ion (produced by deprotonating the free carboxyl group of ferulic acid, $pK_a \approx 4.2$) binds malvin much more avidly than ferulic acid itself, reflecting a possible combination of ionic interactions and enhanced copigment-to-flavylium CT.[105]

Copigments with multiple phenolic units are more efficient than simpler analogs due to geometrical flexibility, which allows the formation of numerous molecular contacts between the pigment and copigment. For example, catechin dimers (condensed tannins) are slightly better copigments than catechin itself, although much less efficient than the vinylcatechin dimers ($K_{AHCP+} > 10^3$ M^{-1}) found in red wine.[110] Similarly, gallotannin penta-*O*-galloyl-β-D-glucose forms a much more stable complex with malvin ($K_{AHCP+} \approx 10^3$ M^{-1}) than does gallic acid, possibly by accommodating the pigment between the galloyl residues at C1-OH and C6-OH of the D-glucose core.[126] The ability of gallotannins to function as copigments in plants was confirmed with sylvatin, which is unusual in that it carries acetyl residues on its D-glucose moiety.[134] By contrast, the more rigid ellagitannins, vescalagin and castalagin, exhibited little affinity for malvin.[126]

The chemical features of the anthocyanin partner, and particularly the difference between 3,5-di-*O*-glycosides and 3-*O*-glycosides, had a relatively modest impact on the stability of the copigmentation complexes.[109] A modest impact of B-ring substitution was also observed, although some works reported that pigments having methoxyl substituents on the B-ring tend to bind copigments more strongly than their hydroxylated counterparts,[104] suggesting a weaker role of hydrogen bonding with respect to $\pi-\pi$ stacking. Pigments bearing bulky di- or trisaccharides at C3-OH form less stable copigmentation complexes than 3-*O*-β-D-glucosides.[135,136] The bulky substituents most probably induce strong steric repulsion that counteracts the stabilizing $\pi-\pi$ stacking and hydrogen-bonding interactions. Interestingly, sterically demanding vinylcatechin dimer copigments were reported to bind oenin more strongly than malvin[110] and catechin-(4 → 8)-oenin.[108]

Structure-affinity relationships have further been established with non-natural model anthocyanin analogs (flavylium cations substituted by OH, OMe and/or glycosyloxyl groups) more accessible to chemical synthesis.[109,116] For a given copigment, the binding constants appeared weakly influenced by the flavylium substitution. It must be noted that unlike anthocyanins, the simple aglycones (anthocyanidins) are accessible from their two faces, as indeed both 1:1 and 1:2 pigment-copigment bindings have been evidenced with chlorogenic acid. Moreover, upon water addition, flavylium ions unsubstituted at C3 give the C_{trans} as the sole accumulating colorless form (while the main colorless form of natural anthocyanin is by far the hemiketal). As the C_{trans} is flatter and more polarizable than the hemiketal (thus, more prone to develop dispersive interactions), copigmentation with the colorless forms was also observed with these model pigments, thus limiting the color gain.[109,116]

5.2. Environmental Effects

The stability of intermolecular copigmentation complexes is highly sensitive to temperature, pH, and the presence of organic cosolvents. As already stressed, the pH dependence of hyperchromic effects largely reflects the sensitivity of anthocyanins to water addition. However, the relative affinities of the flavylium cation and quinonoid bases to the copigment also contribute to the overall process. Although only a few studies have compared K_{AHCP+} and K_{ACP} binding constants, the trend for phenolic copigments (e.g., flavonoids and HCA) is that the flavylium cation binds slightly more strongly that the corresponding quinonoid bases.[102,113] As an example, the K_{AHCP+} and K_{ACP} binding constants for the malvin···rutin pair were around 3×10^3 and 10^3 M^{-1} at 25 °C, respectively. However, the opposite was true for caffeine; for this copigment, the two constants took values of about 10^2 and 2×10^2 M^{-1}, respectively, at 25 °C (Table 2).[113] In keeping with this finding, the apparent pK_a value of cyanidin 3-*O*-β-D-glucoside declined from 3.8 to 3.3 in the presence of a large excess of caffeine (0.08 M), which is consistent with a more efficient stabilization of the bases.[117]

The thermodynamic constants of copigmentation, proton transfer, and hydration can be used to construct distribution diagrams showing the relative abundance of free and bound colored forms as well as colorless forms as a function of pH (Figure 15). Even at high pigment and copigment concentrations, as found in plant vacuoles, a moderately efficient copigment such as HCA only mildly increases $pK_h'^{CP}$ (i.e., the pH value at which the relative abundances of colored and colorless forms are equal) and hence the pH range in which the colored forms prevail (Figure 15A). By contrast, the effect of flavones and flavonols is much more significant and, for instance, three equivalents of copigment are enough to shift $pK_h'^{CP}$ by 2 to 3 pH units (Figure 15B).

The temperature dependence of the hyperchromic effect must also be interpreted with care as it may reflect the thermodynamics of both the hydration and copigmentation steps. For instance, raising the temperature of a catechin-(4 → 8)-oenin-vinylcatechin dimer solution (pH = 3.5) leads to an unexpected

DOI: 10.1021/acs.chemrev.5b00507
Chem. Rev. 2016, 116, 4937−4982

color gain that is ascribed to the exothermic character of the hydration step.[108] However, copigmentation itself is typically exothermic and thus a color loss is generally observed when temperature is increased.[29,31,46,103,104,106,107,113]

At pH = 3.6, the association enthalpies of gallic acid, vanillic acid, and syringic acid with oenin were −7.6, −8.9, and −9.7 kJ/mol, respectively (Table 2).[49] The entropy change of the copigmentation process is generally negative. Thus, for the same systems as before, the ΔS^0 values were −31.9, −37.1, and −38.8 J/mol K, respectively, at pH = 3.6. Similar trends were obtained in ref 32. That is to say, the formation of the noncovalent copigmentation complex driven by $\pi-\pi$ stacking and hydrogen bonding is a wholly ordering process.

A separate ^{1}H NMR investigation provided early evidence of heterodimerization involving colorless forms.[137] Studies on the pH and concentration dependence of the different malvin forms revealed that the flat C_{trans} (unlike the hemiketal and C_{cis}) binds the flavylium ion.

The decisive contribution of water to the driving force of copigmentation is evident, and the addition of organic cosolvents is strongly destabilizing.[46] For instance, even the remarkably stable malvin···7-*O*-sulfoquercetin complex (with its record high binding constant of ca. 10^4 M^{-1} at 25 °C) does not persist in a 1:1 water−methanol mixture.[107] Small concentrations of ethanol (4−6%) tend to increase the exothermicity of the interaction between the malvin flavylium cation and common copigments, suggesting that ethanol molecules preferentially accumulated in the first solvation shells of these complexes.[113] The formation of such organized assemblies would be entropically costly, making the overall thermodynamics of the process less favorable and producing a lower binding constant in the presence of cosolvents. Nevertheless, this result is consistent with the persistence of copigmentation complexes in wine, which contains a moderate percentage of ethanol.

5.3. Self-Association

At relatively high concentration (> 0.1 mM), the flavylium cation of common anthocyanidin 3,5-*O*-*β*-D-diglucosides forms noncovalent dimers with a left-handed chiral stacking and association constants in the range of 1 to 6 × 10^2 M^{-1}, depending on the B-ring substituents (Table 2).[44] Self-association of the flavylium cation is enhanced when the number of hydroxyl and methoxyl substituents in the B-ring is increased. The same trend was observed with common anthocyanidin 3-*O*-*β*-D-glucosides, albeit with slightly higher dimerization constants ranging from 4 to 12 × 10^2 M^{-1} (Table 2).[128]

Interestingly, the self-association of flavylium cation tends to reduce K_h and increase K_a. Thus, self-association protects the flavylium cation against hydration (like copigmentation) and favors its conversion into the quinonoid bases.[128] The latter result suggests that the self-association of the neutral quinonoid bases is stronger than that of flavylium cations. This is not unexpected because the self-association of flavylium cation is impeded by electrostatic repulsion. These data are in agreement with the results of ^{1}H NMR studies on malvin in acidic to mildly alkaline solutions,[44,45] which provided the following association constants: $K_{AH+/AH+}$ = 600, $K_{A/A}$ = 900, $K_{A-/A-}$ = 200 M^{-1} (Table 2). Moreover, spectroscopic titrations of malvin around neutrality have shown two successive proton transfers consistent with the sequence A···A → A···A^- → A^-...A^- with pK_a = 7.0 and 8.2 at 5 mM.[43] By contrast, in dilute solution (50 μM), a single proton transfer is observed with pK_a = 7.0. The persistence of the neutral quinonoid bases above neutrality in concentrated solutions is further evidence that noncovalent dimerization is more favorable for neutral than for anionic bases.

It is worth noting that self-association is in competition with intermolecular copigmentation. In such cases, the dominant process, in plant and food, will be determined by the relative concentrations of pigment and copigment.[85] Studies on wine models have suggested that self-association of oenin, the main grape anthocyanin, is more important to color stabilization than copigmentation in young red wine.[31]

5.4. Metal−Anthocyanin Complexes

Metal ions may participate in stabilizing copigmentation complexes. Anthocyanins with a catechol or pyrogallol B-ring (cyanidin, petudinin, and delphinidin derivatives) can bind hard metal ions such as Al^{3+}, Fe^{3+}, and Mg^{2+} with the simultaneous loss of two protons.[25,109,138,139] Metal-anthocyanin binding is crucial for the expression of blue coloration, although it must be noted that blue coloration can also be achieved with metal-free acylated anthocyanins, especially when the vacuole pH is relatively high. However, metal-anthocyanin binding must typically be combined with intermolecular copigmentation (the other common source of bathochromic shifts in the visible spectrum) to achieve a stable blue. The most intriguing anthocyanin-based supramolecular assemblies that have been examined to date are known as "metalloanthocyanins" and consist of metal-pigment-copigment complexes with a well-defined 2:6:6 stoichiometry; see Table 1.[1] In these complexes, each metal ion is bound to the B-ring of three anthocyanin ligands and anthocyanins bound to different metal ions stack in a left-handed mode. Moreover, pairs of copigment (flavone) molecules, also stacked in a left-handed mode, fill the empty spaces and stack onto anthocyanin moieties in a right-handed arrangement.

The structure of commelinin (Figure 10) was elucidated by X-ray crystallography, which represented a major breakthrough in the understanding of natural coloration due to anthocyanins.[131] The CD spectra associated with anthocyanin complexation were shown to be typical of molecular exciton coupling as first described by Kasha et al.,[140] indicating the formation of stacks with right- or left-handed screw axes.[40] In commelinin, malonylawobanin (the acylated anthocyanin pigment) and flavocommelin (the flavone glucoside copigment) are arranged in stacked pairs with interaromatic ring distances of ca. 0.40 and 0.35 nm for pigment and copigment pairs, respectively. Chiral anticlockwise supramolecular arrangements were observed for pigment···pigment and copigment···copigment pairs, whereas a clockwise arrangement was observed for pigment···copigment pairs, with interaromatic distance of 0.45 nm. This supramolecular assembly has been characterized extensively and is now taken as the prototypical example of a distinct class of copigmentation complexes.

Overall, the available data indicate that various $\pi-\pi$ stacking interactions coexist in metalloanthocyanins, including anthocyanin self-association, copigment (flavone) self-association, and anthocyanin-copigment association (copigmentation). Moreover, the anthocyanin components of metalloanthocyanins quite often bear a 6-*O*-*p*-coumaroyl-D-Glc substituent at C3-OH, which was shown to form long-range NOEs with the flavone nucleus.[59] Here, anthocyanin molecules all interact via their metal-stabilized anionic quinonoid bases.

DOI: 10.1021/acs.chemrev.5b00507
Chem. Rev. 2016, 116, 4937−4982

6. STABILITY IN INTRAMOLECULAR COPIGMENTATION

6.1. Conformational Folding of Acylated Anthocyanins

Anthocyanins acylated by HCA are prone to intramolecular copigmentation or self-association (noncovalent dimerization) depending on their structure.[1,100,141,142] Intramolecular stacking requires a flexible acyl link that makes possible close contacts between the anthocyanidin chromophore and copigment moiety (Scheme 2, panels C−E). The interacting partners in such folded conformations are covalently linked but also share a number of noncovalent interactions based on $\pi-\pi$ stacking and possibly hydrogen bonding. Conversely to intermolecular copigmentation, the association energies of intramolecular copigmentation are less amenable to experimental determination as they pertain to a conformational equilibrium. The stabilization is typically qualitatively described in terms of structural features, about which NMR analysis can provide precious information.

The observation of long-range NOE correlations between the flavylium nucleus and HCA residues is a direct evidence for the existence of folded conformations in which both moieties are in close (van der Waals) contact (i.e., intermoiety distance of 0.3−0.4 nm). Moreover, the ^{1}H NMR spectra of HCA residues in contact with a chromophore typically contain proton signals that are shielded relative to those of the equivalent protons in the corresponding HCA methyl esters under the same conditions. It is significant that HCA groups capable of folding back onto the chromophore are typically linked to the primary C6-OH group of a sugar moiety (most frequently, β-D-glucopyranose). Thus, rotation about the C5−C6 bond seems to provide just about enough flexibility for stacking to occur. The folding increases the percentage of *gt* (gauche−trans) conformers as evidenced by analyzing the $J_{H5,H6}$ coupling constants of the linker.[142] Conversely, when acylation occurs at a secondary sugar OH group such as the C4-OH group in the case of the monoacylated anthocyanin petanin, no flavylium-HCA NOE correlations were observed; in such cases, NMR analysis instead suggested the formation of a head-to-head extended dimer in which both flavylium nuclei on the one hand and both HCA residues on the other hand were in close contact.[143,144] Interestingly, petanin is closely related to alatanin C as both pigments bear a single HCA group at the terminal sugar moiety of a 1,6 disaccharide moiety. However, unlike petanin, alatanin C is acylated via a primary C6-OH group and its NOESY (nuclear overhauser effect spectroscopy) spectrum reveals flavylium-acyl contacts.[145] It is also remarkable that in the triacylated anthocyanin tecophilin, which displays a diacylated D-glucose unit with HCA residues at C2-OH and C6-OH, only the acyl group at C6-OH stacks onto the chromophore.[146] The fact that long-range NOE correlations within acylated anthocyanins can even be observed in non-aqueous environments (DMSO-d_6) emphasizes the stability of such molecular stacks and shows that they do not necessarily require the assistance of the hydrophobic effect to form.[147,148]

Such arrangements may also form with wine pigments and models in which the C6 and/or C8 atoms of flavylium and flavanol units are linked through a CH_3−CH bridge originating from ethanol after its oxidation to ethanal.[149] These pigments are consistently far more resistant to water addition than the corresponding flavylium cations. Spectroscopic titrations of these pigments are also consistent with sequential proton loss within dimers.[150,151] Similarly, the wine pigment formed by electrophilic aromatic substitution at oenin's C8−H position by the carbocation derived from vescalagin (by dehydration at C1-OH), a common ellagitannin transferred from oak barrel to wine upon aging, exhibits long-range NOEs between the flavylium nucleus and a galloyl unit; a moderately improved color stability in aqueous solution and a bathochromic shift of the visible band by ca. 20 nm were observed with respect to oenin.[152] These observations together suggest the formation of a folded conformation allowing intramolecular $\pi-\pi$ stacking interactions and CT.

The structural features that predispose a given molecule to intramolecular copigmentation or self-association are subtle and only partially understood. In brief, when HCA residues are linked to the B- or C-ring by short sugar spacers (monosaccharides or 1,2-disaccharides), intramolecular copigmentation seems to be favored. With more extended spacers (*e.g.*, 1,6-disaccharides) or repeating D-Glc-HCA sequences, especially at the A- or C-ring, chiral (left-handed or right-handed) self-association seems to be the rule. It must also be emphasized that depending on the position of the sugar moiety on the chromophore, HCA residues bound to C6-OH sugar groups by acyl linkages do not exhibit the same propensity for $\pi-\pi$ stacking. For species with a single D-Glc spacer, the following ranking has been proposed: C3′ ∼ C5′ > C7 > C3.[141,153]

The capacity of acylated anthocyanins for intermolecular copigmentation has not been studied extensively. In principle, the folding of an internal HCA residue onto the chromophore should make it less available for $\pi-\pi$ stacking interactions with external copigments. In other words, intermolecular copigmentation should compete with intramolecular copigmentation and self-association. The CD spectrum of alatanin C and its concentration dependence are suggestive of a strong noncovalent dimerization, even at low pigment concentration (50 μM).[145] However, the addition of a potent flavone copigment (flavocommelin, 8 equiv) cancels the Cotton effect, suggesting that copigmentation outcompetes self-association under these conditions. In the case of the Morning glory anthocyanins (*Pharbitis nil*), which undergo intramolecular copigmentation, a single HCA residue has little impact on the stability of the copigmentation complexes with chlorogenic acid, perhaps suggesting that one face of the chromophore remains accessible to the copigment.[135] However, the binding of chlorogenic acid to the diacylated anthocyanin was greatly weakened, in agreement with the pigment adopting a sandwich-like conformation that blocks both faces of its chromophore. On the other hand, the monoacylated pigment cyanidin 3-*O*-β-D-[2-*O*-β-D-xylosyl-6-*O*-β-D-(6-*O*-*p*-coumaroyl)glucosyl)]-galactoside does not seem to bind free HCAs.[136] However, as this is also true for its deacylated counterpart, it appears that it is the bulky trisaccharide rather than the acyl moiety that is responsible for the chromophore's inaccessibility to external copigments.

Being quite prone to noncovalent dimerization, the wine pigments, in which anthocyanins are linked to a flavanol unit through a CH_3−CH bridge, show very little affinity for chlorogenic acid.[150,151] Conversely, the diacylated *Ceanothus papillosus* anthocyanin, which has two HCA residues that interact with the chromophore (based on the diamagnetic shifts observed in its ^{1}H NMR spectrum), cannot express the blue color of the flower without its major copigment, kaempferol 3-*O*-β-xylosyl-(α-1,2)-rhamnoside.[55] Interestingly, this unusual metal-free combination of intermolecular copigmentation with intramolecular copigmentation or self-association is not observed with other (more common) flavonol 3-*O*-glycosides.

There is relatively little physical-chemical information on acylated anthocyanin dimerization constants or the impact of

DOI: 10.1021/acs.chemrev.5b00507
Chem. Rev. 2016, 116, 4937−4982

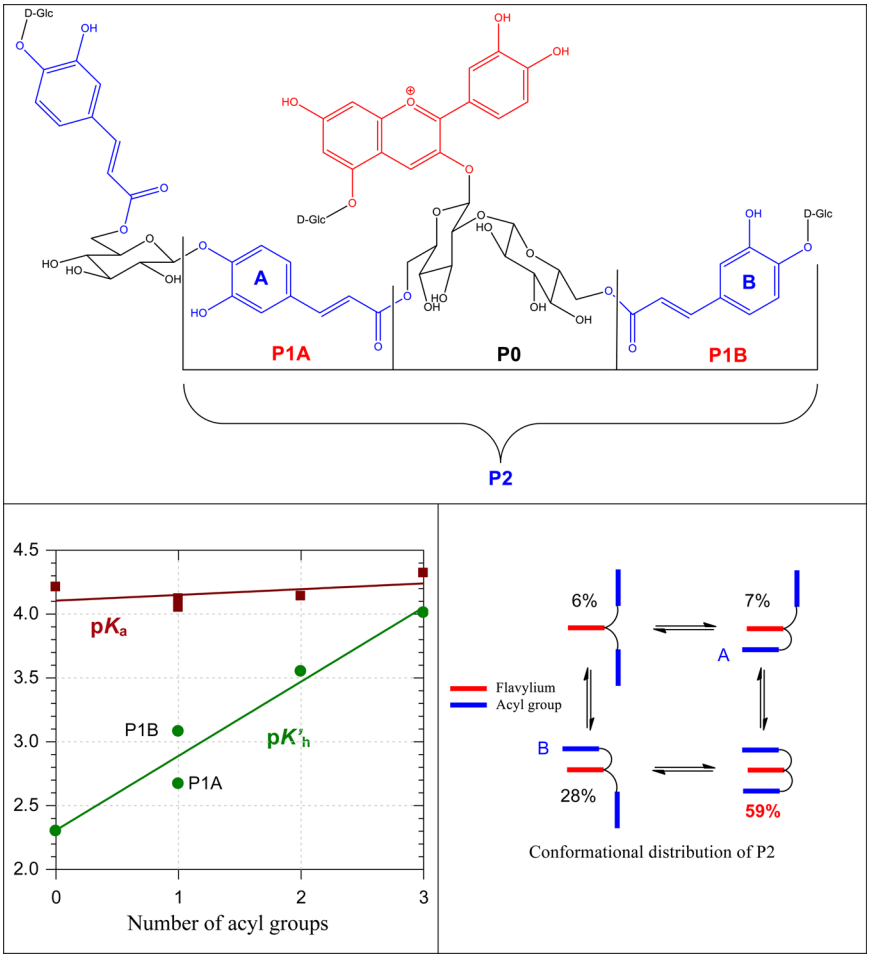

Figure 16. Morning glory (*Pharbitis nil*) anthocyanins (inspired from ref 135).

acylation on the thermodynamics of water addition and proton transfer. A recent ^{1}H NMR study showed that malvidin 3-*O*-*β*-D-(6-*O*-*p*-coumaroyl)glucoside is more prone to noncovalent dimerization [$K_{AH+/AH+} \approx 1400$ M^{-1} in D_2O−DMSO-d_6 (7:3)] than its deacylated counterpart (oenin, $K_{AH+/AH+} \approx 800$ M^{-1}), see Table 2.[75] Interestingly, even in the most dilute solution, some proton signals of malvidin 3-*O*-*β*-D-(6-*O*-*p*-coumaroyl)-glucoside remain more shielded than the corresponding protons of oenin. This observation suggests that intramolecular copigmentation also plays a role, a conclusion supported by the long-range NOE observed between the malvidin 2′,6′ protons and the vinylic *α* proton of the acyl residue.

By forcing water away from the chromophores, intramolecular copigmentation and self-association are expected to make them more resistant to water addition. In keeping with this expectation, the pK'_h values of the Morning glory (*Pharbitis nil*) anthocyanins increase with the number of HCA residues, acylating the primary C6-OH groups of the D-glucosyl-*β*-1,2-D-glucosyl moiety at C3-OH.[135,154] Interestingly, the color stability is greatly enhanced on going from the monoacylated to the diacylated pigment. By assuming that the difference in the Gibbs energy of water addition in the series only reflects the selective stabilization provided by the HCA residues to the flavylium ion, it was even possible to estimate the distribution of the diacylated pigment into open, half-folded and fully folded (sandwich) conformations (Figure 16); the latter was estimated to be dominant, with a relative abundance of ca. 60%. Unlike pK'_h, the pK_a value is not strongly affected by acylation, which suggests that the intramolecular *π*−*π* stacking interactions are as strong with the flavylium cation as with the quinonoid bases, and that the conformation distributions of the two species are broadly similar. Other studies on acylated anthocyanins have confirmed that acylation increases pK'_h.[47,48] This color-stabilizing effect is also observed with a remarkable pigment in which delphinidin 3-*O*-*β*-D-glucoside is covalently linked to apigenin 7-*O*-*β*-D-glucoside via a malonyl residue that bridges the two Glc C6-OH groups.[48] Interestingly, pK_a lowering was also observed with *Matthiola incana* anthocyanins, which are closely related to the Morning glory anthocyanins but also bear a 5-*O*-*β*-D-(6-*O*-malonyl)glucosyl moiety.[47] This may reflect intramolecular hydrogen bonding between the malonyl group and the O atom at C7 of the quinonoid bases.[116] A series of di- and triacylated anthocyanins bearing *p*-hydroxycinnamic and *p*-hydroxybenzoic acid residues on the sugar moieties of both the A- and B-rings were found to be so resistant to water addition that no pK'_h values could be determined.[155] It is however not clear whether this spectacular color stabilization reflects intramolecular copigmentation or noncovalent dimerization.

To better appreciate how noncovalent dimerization tends to erase water addition in polyacylated anthocyanins, a distribution diagram as a function of pH can be constructed with tentative stability constants for the different dimers AH$^+$···AH$^+$, AH$^+$···A, and A···A (Figure 17). Even by assuming that the monomer itself is stabilized by intramolecular copigmentation (accounting for a relatively high pK'_h value of 3), very high dimerization constants

DOI: 10.1021/acs.chemrev.5b00507
Chem. Rev. 2016, 116, 4937−4982

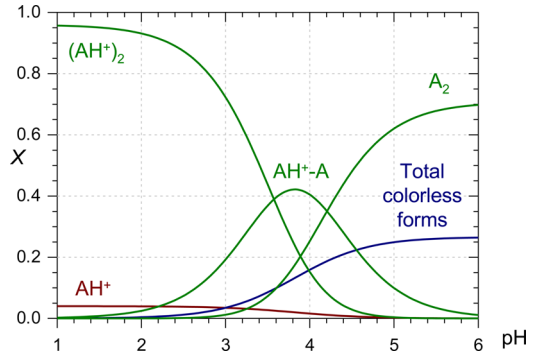

Figure 17. Distribution diagram for a prototypical acylated anthocyanin forms showing the strong influence of noncovalent dimerization. Parameters: pK'_h = 3.0 (assuming partial protection against water addition owing to intramolecular copigmentation in monomer), pK_a = 4.0, pigment concentration = 10 mM. Tentative values for the dimerization constants: $K_{AH+/AH+} = 3 \times 10^4$, $K_{AH+/A} = 8 \times 10^4$, $K_{A/A} = 5 \times 10^4$ M^{-1}.

in the range of 10^4−10^5 M^{-1} are required to minimize the abundance of the colorless forms over the pH range of 3−6.

6.2. Improving the Chemical Stability of Anthocyanins by Copigmentation

The chemical stability of anthocyanins must be clearly distinguished from the stability of their color, which was the subject of the preceding discussion. Color stability relates to the reversible equilibrium between colored and colorless forms, whereas chemical stability relates to the irreversible chemical degradation of pigments, mainly arising from cleavage of the C2−C1′, C2−C3, or C3−C4 bonds of the chromophores.[111,156−159] The former is fast while the latter takes place over time scales of hours to days, even months, depending on the conditions (e.g., pH, temperature, dioxygen, irradiation, and copigments).[160] Regardless, whether thermal or photochemical, anthocyanin degradation imposes serious limitations on the industrial use of anthocyanins as colorants for food and cosmetic applications. The mechanisms involved have not been fully elucidated but probably involve a combination of hydrolytic and auto- or photo-oxidation steps.

Some works on the photochemistry of anthocyanins have provided information relevant to this issue. Generally, anthocyanins are only weakly fluorescent and simple flavylium ions in their excited state are strong acids (pK_a < 0), rapidly transferring a proton to water. The excited quinonoid base thus formed is then deactivated by a combination of radiative and nonradiative pathways.[161] In the presence of a copigment, a very efficient alternative pathway emerges, namely the direct ultrafast (τ < 1 ps) nonradiative deactivation of the copigmentation complex via a low-lying copigment-to-flavylium CT state. Interestingly, acylated anthocyanins in their excited state are also very efficient at dissipating excess energy to water. In particular, when UV−B light is absorbed by the HCA moiety, an ultrafast energy transfer to the chromophore takes place, which successfully competes with (*Z*-*E*)-isomerization of the vinyl moiety.[162] In the sophisticated polyacylated Heavenly blue anthocyanin, this efficient HCA-to-chromophore energy transfer only takes place in neutral conditions (i.e., when the pigment adopts a quinonoid structure). Under acidic conditions, the dominant pathway remains the (*Z*-*E*)-isomerization of the most external HCA residues.[60] In parallel with those observations, the Heavenly blue anthocyanin was demonstrated to be chemically much more stable (and also much more fluorescent) at neutral pH than under acidic conditions, whereas the opposite usually holds with common anthocyanins. Overall, these results suggest that π−π stacking in anthocyanins, whether inter- or intramolecular, provides efficient pathways for energy dissipation, thereby competing with alternative pathways for the excited states that may lead to degradation. For instance, it may be noted that monoacylated anthocyanins were shown to accumulate from diacylated anthocyanins upon UV irradiation.[163]

On the other hand, the thermal degradation of anthocyanins is well-known to be slower for acylated anthocyanins or when efficient copigments are present.[164] In some cases, copigmentation by HCAs seems to compete with intramolecular copigmentation, thus leading to a net decrease in pigment stability.[136] Upon thermal treatment of weakly acidic solutions of anthocyanins and anthocyanin-rich extracts, a likely scenario is (i) the endothermic formation of C_{trans}, (ii) the rate-limiting hydrolysis of the glycosidic bond at C3, and (iii) the fast degradation of the chalcone aglycone to yield the *p*-hydroxybenzoic acid derived from the B-ring and other cleavage products.[158] The same sequence is much less favorable in acidic conditions, first because the flavylium cation is relatively insensitive to acid-catalyzed hydrolysis and because anthocyanidins are only stable at low pH (under their flavylium form).[165] It may thus be speculated that copigmentation, although typically weaker at high temperature, somewhat still limits the formation of C_{trans}, thereby slowing down the whole degradation process. This is consistent with the fact that chalcone glycoside intermediates could not be detected during the degradation of acylated anthocyanins.[158]

It must be noted that alternative routes not involving the C_{trans} intermediate may also occur, for instance oxidative pathways leading to B-ring elimination and formation of the corresponding coumarin.[164] A mechanism starting with addition of hydrogen peroxide (of undetermined origin) at C2 of the flavylium nucleus and subsequent Bayer-Villiger rearrangement was also proposed for the degradation of oenin in a wine model.[157] It may be speculated that copigmentation could protect the chromophore from H_2O_2 addition in the same way it opposes water addition.

7. DRIVING FORCES OF COPIGMENTATION

From the large collection of experimental studies, the driving forces of copigmentation have clearly been identified as π−π stacking interactions. Hydrophobic effects have also been suggested as a crucial contribution, as the most stable copigmentation complexes in water vanish in water:methanol (1:1) mixtures. Although both contributions are interrelated, the different attractive/repulsive contributions should be carefully distinguished.[166]

π−π Stacking had first been described by solvophobic effects of entropic origin mainly, except in water where enthalpic effects are important. Later, electrostatic interactions have been pointed out as a major driving force.[167] In particular, the electrostatic substituent effect is of crucial importance to predict aromatic stacking geometries [e.g., edge-to-face (T-shaped) arrangement vs face-to-face (displaced) parallel stacking].[168−170] The stability of a given noncovalent stacking involving aromatic rings has exhibited correlation with the Hammett substituent constants. Even substituents at aromatic rings which have little influence on the π-electron distribution [i.e., with only an inductive (± I) but without a mesomeric (±M) effect] might exhibit a clear effect on the electrostatic potential; this allows, for example, parallel stacking of substituted benzene, whereas nonsubstituted benzene

DOI: 10.1021/acs.chemrev.5b00507
Chem. Rev. 2016, 116, 4937−4982

forms T-shaped noncovalent dimers.[171] The electrostatic contribution can be seen as pairwise interactions between maxima and minima of the electrostatic potential in both partners, a consideration of importance to quantify such intermolecular interaction.[172] In principle, parallel stacking complexes require one partner bearing strong electron-donor and the other strong electron-acceptor groups.[169,170] In copigmentation, the (multiple) OH substitution pattern in both pigment and copigment is of crucial electrostatic importance to favor parallel stacking due to the considerable +M effect of the OH group.[173] Here, the relative positioning of both partners is driven by the electrostatic contribution.

In many situations, it became however clear that dispersion forces make the dominant contribution to attractive $\pi-\pi$ interactions. The (London) dispersion interactions stem from correlation of transient dipoles among atoms and molecules.[174] They are by far the dominant noncovalent interactions between nonpolar molecules. They also contribute if the molecules are originally polar, although in this case, the noncovalent effects would also incorporate other electrostatic-driven contributions including hydrogen bonding (vide infra). It is known that parallel-displaced arrangements maximize dispersive attraction,[170] which may appear as an indicator of the ideal dispersive-type arrangement in copigmentation complexes; every variation from this geometry is driven by the other contributions. Due to the small polarizability of water molecules, dispersion interactions in intermolecular complexes are maximized in water with respect to other solvents, as in this case, the competition with solvent molecules is weakened.[166]

As said above, the copigmentation complexes are observed mainly in water and highly in polar solvents (i.e., water:alcohol mixtures with excess of water). Therefore, besides the pure pigment−copigment interaction, further contributions arising from solute−solvent interactions are likely to occur. The description of all aspects of this complex process is beyond the scope of the review (details can be found in literature refs 175 and 176), and here we only focus on some aspects which are considered important in copigmentation. Solvents with high cohesive interactions prefer to interact with bulk solvent molecules rather than to solvate the complementary apolar surfaces of solute molecules,[170] hence favoring solute aggregation by the hydrophobic effect. It is not a special type of molecular interaction but a collective effect with entropic ("classical" hydrophobic effect) and enthalpic ("nonclassical" hydrophobic effect) origin.[176] In the vicinity of a hydrophobic solute (or a hydrophobic region of a larger molecule), water molecules form a particularly organized network that maximizes the number of hydrogen-bonding interactions among them.[175] When two hydrophobic surfaces, of both a pigment and a copigment are brought together (in the copigmentation complex), the ordered water molecules are released from the intermolecular region (hydrophobic cavity) into the bulk solvent, causing an increase in entropy; that is to say, the system gains Gibbs energy. In some conditions, this can be reinforced by enthalpy gain due to the formation of new hydrogen bonds upon this water release ("nonclassical" hydrophobic effect).[176] Nonetheless, copigmentation also involves an ordering process, as the rotational and translational contributions to entropy decrease when pigment and copigment associate. This counterbalances entropic changes due to the hydrophobic effect and the overall change in entropy during the copigmentation process results from a subtle balance between these multiple effects, in which the numerous OH groups of polyphenols may participate through the (intra- and intermolecular) hydrogen-bonding network. In most copigmentation systems experimentally studied, the entropy variation is negative (Table 2). Only the negative enthalpy of association enables formation of the copigmentation complexes. This agrees with the fact that with flat molecular surfaces, hydrophobic effects are minor, and the dispersive forces mainly drive stacking.[176] Positive entropy changes were rarely observed, namely, for the interaction of malvin with highly water-soluble rutin derivatives bearing acylated succinyl groups on the sugar moiety.[130]

Hydrogen bonding between the phenolic pigment and copigment may also play a role in stabilizing noncovalent copigmentation complexes. Although its role in copigmentation is not sufficiently documented so far, it is usually weakened in water media. This agrees with the recent QM/MM calculations performed on a prototype copigmentation system, showing more planar OH groups (i.e., weakening intermolecular H-bonds between both the pigment and the copigment) with respect to calculations performed in implicit solvent (see section 10.3 and ref 173). It is thus important to recall that copigmentation is a complex phenomenon resulting from subtle combinations of different noncovalent interactions; since anthocyanins and phenolic copigments can be regarded as amphiphilic compounds, their complexation is influenced by all of these effects. The stability of a mixture of amphiphilic molecules in an aqueous environment can be maximized in two ways, namely by maximizing the solvation of their hydrophilic parts (e.g., via intermolecular hydrogen bonding with water molecules) and by minimizing the exposure of the hydrophobic parts to the polar solvent. This latter factor promotes the formation of intra- and intermolecular stacks driven by dispersion forces and, to a lesser extent, hydrogen bonding. These forces naturally lead to the copigmentation process. In accordance with the thermodynamic balance of complexation, copigmentation complexes can be stable, metastable, or unlikely; usually the entropy decrease associated with complex formation counteracts the negative enthalpy of association, as evidenced experimentally by enthalpy−entropy compensation.[113]

Because the typical intermolecular distances of parallel stacking is about 3.5 Å, a distance also obtained in copigmentation complexes (vide infra), short-range repulsive interactions (exchange term related to the Pauli exclusion principle) are most likely to contribute to the energetic balance of copigmentation. Charge transfer is suggested to contribute mainly in excited state and little in energetic stability of noncovalent complexes; however, exchange can significantly influence interplanarity.[167] One should keep in mind that other contributions could also be at stake in the stability of large copigmentation complexes, namely CH-π interactions (mainly driven by dispersion), OH-π interactions (mainly driven by electrostatics), cation-π interactions, and anion-π interactions.[170,171,177]

The available experimental data on physicochemical factors relevant to the formation of copigmentation complexes include information on modes of binding and energies of association. However, theoretical chemistry has become a mandatory support to experimental works, which may help figure out driving forces of copigmentation and subsequent observed changes. So far, little has been made to draw conclusions from the experimental data on the nature of the interactions and to compare the results, for example, with energetic stabilities. Theoretical studies on prototypical copigmentation complexes are required to support such comparison, which would allow a comprehensive distinction of all energetic contributions. In the future, phenolic

DOI: 10.1021/acs.chemrev.5b00507
Chem. Rev. 2016, 116, 4937−4982

molecular balances[166,171,178] could be designed to investigate and quantify noncovalent interactions in copigmentation. In any event, the molecular recognition between the two partners of a given copigmentation complex should only be interpreted with care in solvent-accessible systems.[178]

The available experimental data suggest that noncovalent copigmentation complexes may exist in various conformations and mutual orientations (i.e., they are not rigid and their structures fluctuate around minima). This makes it necessary to thoroughly sample their conformational space (i.e., the space of all their possible conformations and mutual arrangements) (also known as hypersurface), when attempting to study their behavior with computational tools. The need to explore a large number of structures prohibits the use of QM ab initio methods, necessitating the use of empirical methods in order to obtain stabilizing energies of noncovalent complexes in a reasonable time frame. Moreover, the hydrophobic effect is a collective phenomenon and the only way to properly evaluate its physical-chemical consequences is to describe the solvent explicitly. Given the size of a typical copigmentation complex, the only theoretical chemistry methods suitable for performing such calculations are MM and MD simulations. Such methods account for all of the relevant forces (i.e., electrostatic interactions, dispersion, and repulsion). However, they also face some limitations as discussed in the very next section.

8. CONFORMATION AND THERMODYNAMICS IN COPIGMENTATION FROM MOLECULAR DYNAMICS

8.1. Molecular Dynamics Challenges

It is assumed that the basic concepts of MM and MD simulations are a prerequisite for comprehensive understanding of this section; more details can be found in literature.[179−181] MM relies on several approximations[179] and compensation of errors to produce useful results.[182] It should be noted that a force field is a rather complex "tool" that sometimes needs reparameterization or even the addition of new parameters, both of which are delicate tasks that can only be achieved with much care.[183] Classical MD simulations can be used to monitor the evolution of a molecular system over time.[184] They are performed using dedicated software tools (e.g., AMBER,[185] CHARMM,[186] NAMD,[187] GROMACS,[188] etc.) and usually last for between hundreds of nanoseconds and a few microseconds depending on system size and the available computational power. It is worth noting that MD simulations provide atomic and femtosecond resolutions simultaneously.

8.1.1. Exploring Conformational Space. A key objective when attempting to sample the conformational space of a system with many degrees of freedom as in copigmentation complexes is to reduce the number of conformations that must be considered by focusing on those that are most heavily populated under the relevant conditions. Conformations with lower energies (ε_i) have greater populations (p_i) according to the Boltzmann distribution (eq 9):

$$p_i = Q^{-1} e^{-\beta \varepsilon_i} \tag{9}$$

where Q represents the partition function and β equals to $1/k_B T$ (i.e., inverse product of the Boltzmann constant and the temperature). One way of sampling conformational space is to identify one (or a few) reasonable conformation(s) (e.g., by geometry optimization) and then to run a classical MD simulation starting from that optimized structure.

Since MD simulations are usually carried out at room temperature (ca. 300 K), they produce conformations that are in principle accessible under experimental conditions but only over the time scale of the simulations. This means that MD simulations cannot describe "long-lasting" processes of around the microsecond time scale or above. In the case of copigmentation, nanosecond time scales are sufficient to explore the conformational space of the simplest molecular systems. However, in most real-world copigmentation complexes, jumping the energetic barriers from one potential well to another (i.e., from one conformer to another) would require a longer time. In such cases, classical MD rarely enables robust conformational space sampling. As alternatives, stochastic Monte Carlo methods based on randomly generated geometries (Figure 18)[189] as well as biased methods of MD can be employed.

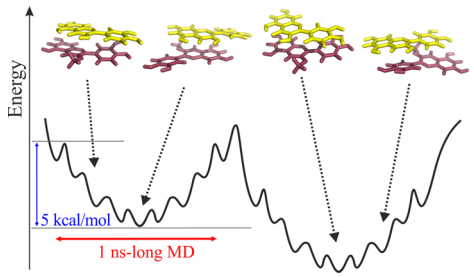

Figure 18. Schematic (1D) potential energy surface (PES) showing many local minima accessible by 1 ns-long MD simulation and the necessity to properly explore the entire PES to reach the real valley via long MD simulation or biased techniques to force random exploration. (The noncovalent complex represented here is just a pictorial representation.)

8.1.2. Biased vs Unbiased Molecular Dynamics. Many techniques for performing biased MD simulations have been developed. An important one is simulated annealing, which creates bias by performing successive artificial simulated loops of heating/cooling. In this process, the system is quickly heated to a high temperature (up to several thousand Kelvin) then cooled slowly. This enables the molecular system to escape from its initial minimum then to explore the rest of its hypersurface, systematically escaping from local minima. Simulated annealing procedures have been employed regularly in studies on copigmentation (see Section 8.2).

Other more advanced methods have been developed for efficient exploration of the hypersurface,[190] including MD with quenching (MDQ), replica exchange MD (REMD), and meta-dynamics (MetaD). These methods could provide important new insights into the conformational space of copigmentation complexes.

MDQ is a variant of the classical MD, which is carried out at ambient or elevated temperature (e.g., 500 K) to facilitate escape from the initial minimum.[191] The structures along the MDQ trajectory are collected at particular time steps and minimized (quenched) using the applied force field. This technique has been efficiently used to sample the conformational space of small noncovalent complexes (e.g., the acetic acid dimer[192] and microhydration of nucleobases).[193]

In the temperature REMD (T-REMD) method, a set of several parallel MD simulations each at different temperatures are executed simultaneously, and at specific time steps a Monte Carlo step is performed to exchange structures between neighboring temperatures.[194] This method helps to overcome

DOI: 10.1021/acs.chemrev.5b00507
Chem. Rev. 2016, 116, 4937−4982

energetic barriers; however, some conformational transitions are not facilitated by the T-REMD method if the system is entropically biased.[195] This behavior may significantly limit the usefulness of T-REMD as a tool for studying the conformational space of copigmentation complexes.

MetaD[196] requires the definition of one or more collective variables, which are typically the root-mean-square-deviation from a given structure, radius of gyration, and number of intermolecular hydrogen bonds. During a MetaD simulation, a biasing potential is deposited at given time steps to the collective variable, filling potential wells of the hypersurface. The biasing potentials are collected and integrated after the MetaD run, enabling reconstruction of the Gibbs energy surface from the obtained negative picture. This method is very effective and many flavors of MetaD have been developed to date. The selection of a suitable collective variable(s) remains the major challenge of MetaD.[197]

8.1.3. Estimation of $\Delta G_{binding}$. Theoretical modeling of copigmentation mostly focuses on conformations and related stabilities, which are well expressed in terms of Gibbs energies of association (binding), $\Delta G_{binding}$. In accordance with the first principle of thermodynamics, the Gibbs energy of binding is negative for complexes that form spontaneously; the lower the $\Delta G_{binding}$, the more stable the complex. As noted above, classical MD simulations enable identification of the favored conformations quite effectively.[198] Because the various copigmentation complex conformers usually differ in Gibbs energy by only a few kcal/mol,[108] the quality of force field is crucial. It may bias the differences among individual conformers and could even create erroneous ordering. In this case, it is recommended to further minimize the different identified conformers using QM methods and to evaluate the differences among individual conformers using high-level QM calculations.

Postprocessing methods have also been developed to estimate the Gibbs energy of association. They are known as MM with Poisson−Boltzmann surface area (MM-PBSA) and MM with generalized Born Surface Area (MM-GBSA).[199] Both methods are based on the thermodynamic cycle (Scheme 3), which makes

Scheme 3. Thermodynamics Cycle for the Formation of Copigmentation Complexes in Water (Comprising Complex Formation in the Gas Phase and the Transfer of the Process from the Gas Phase to Solvent)

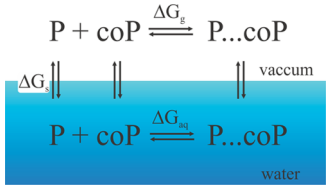

it possible to split the process into two parts, one corresponding to complex formation in the gas phase and the other to the transfer of the process from the gas phase to a solvent (usually water).

The Gibbs energy of association is then estimated using the following formula:

$$\Delta G_{binding} = \langle \Delta H_{MM} \rangle - T\langle \Delta S_{MM} \rangle + \Delta \langle G_{solv} \rangle \quad (10)$$

where ΔH_{MM} is the MM enthalpy in the gas phase; ΔS_{MM} is the entropy of the solute in the gas phase; and ΔG_{solv} is the solvation Gibbs energy and all these terms are averaged along the MD trajectory.

The solute entropy is computed under the quasiharmonic approximation by means of normal mode calculations.[200,201] The electrostatic contribution to the solvation Gibbs energy is estimated using continuum solvation models based on the generalized Born (GB)[202] or Poisson−Boltzmann (PB)[203] equations, and the nonpolar terms are derived using surface area (SA).[204] In principle, the absolute values of the estimated Gibbs energies of association may be biased by the used approximations; however, they can be more safely used for ranking various complexes or their conformational states (see section 8.2.1 for further details).

8.2. Molecular Picture of Copigmentation

8.2.1. Molecular Dynamics Based Studies: Early Stages. The first MM calculations on copigmentation complexes were performed with the MM+[205] force field both in vacuo and in a water box.[47] Indirect molecular information was actually available in both these studies because the calculations were performed on the pigments alone (in absence of explicit copigments), namely delphinidin 3-*O*-gentiobioside and cyanidin 3-*O*-rutinoside, with both favylium and hemiketal forms being considered. Low intramolecular distances were predicted which supported the possibility of hydrogen bonding between the pigment and the sugar moieties. More recently, Yoshida et al. performed MM calculations on the pigments albireodelphin A and monodeacylgentiodelphin (two acylated gentiodelphin pigments linked, at different locations, to one caffeic acid as copigment).[141] The interacting potential was described by the CHARMM force field, and an implicit water solvent was used. Various geometrical features were constrained according to NMR data. In particular, distances were fixed at 2.5 ± 0.5 Å and 4.0 ± 1.0 Å when strong and weak NOE contacts were observed, respectively. Interestingly, no interaction was observed between the pigment and the copigment for the former compound, whereas some conformers of the caffeoyl moiety approached the pigment at the van der Waals distances. The most stable conformers were obtained from the analysis of several thousand conformers. However, in this case, one can expect that several conformations were relatively close to each other in energy and could have been considered as well.

At about the same period, MM simulations were performed on theaflavin self-association and theaflavin−caffeine complexation.[206] Again NOE-NMR contacts were evidenced between the two partners, which were used to perform constrained simulated annealing. The proposed supramolecular arrangements confirmed the importance of $\pi-\pi$ stacking and hydrogen-bonding intermolecular interactions, which was revealed by the predicted formation of a spatial arrangement in which the electron deficient tropolone ring lies directly over the electron-rich catechol ring.

MM calculations were carried out as an initial step to evaluate the conformational features of (i) a series of anthocyanins (peonidin-3-*O*-glucoside, pelargonin, cyanin, oenin, and malvin) complexed with several phenolic derivatives (gallic acid, protocatechuic acid, ferulic acid, caffeic acid, and quercitrin), using the MM+ force field;[105] (ii) oenin and five phenolic compounds (caffeic acid, catechin, proanthocyanin B, rutine, and ellagic acid), using the AMBER force field;[207] and (iii) oenin and five different hydroxybenzoic acids (*p*-hydroxybenzoic acid, protocatechuic acid, gallic acid, vanillic acid, and syringic acid).[49] However, these reports included only a few details on the procedures used to ensure comprehensive coverage in the conformational analysis. Some other studies have been reported

DOI: 10.1021/acs.chemrev.5b00507
Chem. Rev. 2016, 116, 4937−4982

in which more care was taken to ensure adequate conformational sampling, and more comprehensive details of the MD simulation procedure or simulated annealing protocol were provided. For example, the geometrical features of the cyanidin···baicalein 7-*O*-glucuronide copigmentation system was explored based on a joint simulated annealing and 300 ps-long MD simulation procedure using the Tripos force field and the SPC explicit solvent model.[208] A thorough conformational analysis of 115 conformations and mapping of hydrophilic and hydrophobic spots on the Connolly surface demonstrated the importance of hydrogen bonding and the hydrophobic effect in this system. Water was excluded from the space between the interacting partners, leading to the formation of a so-called lamellar stacking system (see Figure 19 for similar arrangements).

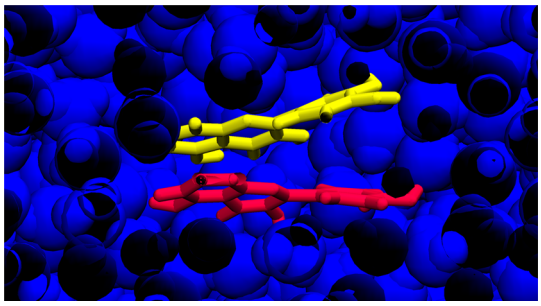

Figure 19. Molecular dynamics snapshot of the 3-*OMe*-cyanidin··· quercetin noncovalent complex (the pigment 3-*OMe*-cyanidin in red; the copigment quercetin in yellow), showing the space between both partners depleted from water molecules.

MD simulations were also performed on the malvidin···ellagic acid complex.[209] The AMBER force field was used to treat the solute, whereas the solvent was treated with the TIP3P model, using different mixtures of solvents to evaluate the effects of ethanol (0% and 14% ethanol in volume). A 100 ns equilibration period was used, which was considered sufficient to characterize all intermolecular reorganizations in the first solvent shell. Over this time scale, the ethanol molecules clearly aggregated around the copigmentation complex, and with the 14%:86% ethanol:-water mixture, the first solvent shell consisted of 50%:50% ethanol:water. The authors assigned this behavior to strong entropic effects when water was replaced by ethanol in the first solvent shell, thus modifying subsequent enthalpy−entropy compensation. This is seemingly consistent with the fact that the entropy of water decreases locally around the hydrophilic moieties of the copigmentation complex, which counteracts the noncovalent association. The magnitude of this effect was probably eliminated by replacing water by ethanol in the first solvent shell. This is perfectly consistent with the experimental work described above using malvin and common copigments in the presence of moderate amounts of ethanol molecules and shows that ethanol preferentially accumulate in the first solvation shells.[113]

A conformational search procedure using CONFLEX (conformational analysis of flexible molecules) with the MM3 force field was used to explore the conformational space of three oligomeric pyranoanthocyanin···flavanol pigments isolated from Port wines (pyranomalvidin-3-*O*-glucoside···procyanidin B3, pyranomalvidin-3-*O*-glucoside···(+)-catechin and pyranomalvidin-3-*O*-glucoside···(−)-epicatechin).[16] The authors confirmed intramolecular $\pi-\pi$ stacking between the pyranoanthocyanidin chromophore and the second catechin moiety of B3, with an interatomic distance between the aromatic rings of 3.25 Å. Pyranomalvidin-3-*O*-glucoside···(+)-catechin exhibited a less closed structure than pyranomalvidin-3-*O*-glucoside···(−)-epicatechin, which impacted the copigmentation process, the latter pigment having a stronger hyperchromic effect.

Regular MD simulations were performed with copigmentation complexes formed by the noncovalent interaction between two pigments (oenin and malvin) and three copigments (two vinylcatechins and procyanidin B3).[110] With the general AMBER force field (GAFF)[180] for the pigment···copigment systems and TIP3P for water, a 100 ps equilibration step was followed by a 10 ns-long simulation, which was suggested to enable exploration of the potential energy hypersurface. The same procedure was applied on oaklin compounds formed in red wines aged in oak barrels, namely guaiacylcatechin-pyrylium and syringylcatechin-pyrylium, with common copigments including catechin, epicatechin, chlorogenic acid, epigallocatechin, and procyanidin B3.[210] The average minimal distances between pigment and copigment were greater than 4.65 Å, which is slightly greater than the optimal distance for efficient $\pi-\pi$ stacking. Hydrogen bonding was also observed in all pigment··· copigment complexes (indicated by an interatomic distance of ca. 2.7 Å).

The MM-PBSA technique has thus been used successfully in two separate studies to score the relative binding energies of copigmentation association. The MM-PBSA method provided the correct ordering of the formed complexes, thus making it possible to confirm previously proposed structure-affinity relationships. Moreover, it was shown that vinylcatechin and epicatechin provided the most efficient copigmentation stabilization in both studies, respectively. The quantitative description failed with respect to experimental binding Gibbs energies, which was attributed to the approximations underpinning the MM-PBSA method.

Interestingly, classical MD has also been used to study self-association of polyphenols in complex environments. As polyphenols are amphiphilic compounds, they distribute into biological membranes in cells.[211−214] Biased and free MD simulations highlighted the formation of self-association complexes and complexation with vitamins in lipid bilayers (Figure 20). This was confirmed by spectroscopic measurements. In this case, complexation occurred over a time scale of several nanoseconds, between the lipid chains of the bilayer (i.e., in a hydrophobic environment). In this case, the driving force of self-association and complexation was $\pi-\pi$ stacking and hydrogen bonding to a lesser extent. It should be noted that MD simulations are sufficiently mature to enable simulation of

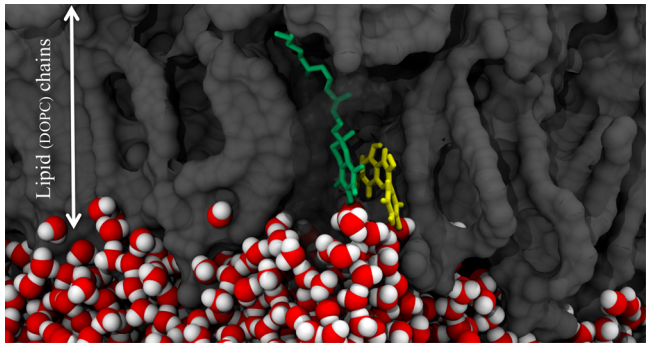

Figure 20. $\pi-\pi$ Stacking complexes between quercetin (yellow) and vitamin E (green) in lipid bilayer membranes.

DOI: 10.1021/acs.chemrev.5b00507
Chem. Rev. 2016, 116, 4937−4982

such complex environments (e.g., lipid bilayers, micelles, etc.) and impact of such environments on copigmentation processes.

8.2.2. Challenges in the Theoretical Description of Copigmentation Complexes. The results presented in the preceding subsection strongly suggest that the precise choice of force field one makes will not necessarily greatly change the conclusions one obtains concerning geometrical features of copigmentation. Indeed, all regular force fields can adequately cover the essential noncovalent interactions occurring during copigmentation. Also the use of explicit solvent enables a qualitative description of the hydrophobic effect. Therefore, one might anticipate that a qualitative description can generally be reached when using regular MM-based calculations. In any case, the exploration of the conformational space, and identification and energy ordering of all possible copigmentation complex arrangements remains the real challenge. Again, the reader should be aware that sampling the conformational space requires sufficiently long MD simulations, properly parametrized simulated annealing procedures or sophisticated-biased MD simulations (see section 8.1.2).

Another critical issue that, in principle, could be addressed using MD is the real capacity to form copigmentation complexes, which is determined by the Gibbs energy of association $\Delta G_{binding}$ (see section 8.1.3). Obtaining accurate estimates of such Gibbs energy changes (with errors of less than 1 kcal/mol) remains an important challenge in contemporary computational chemistry. As noted above, there are several specialized methods that can be used to estimate $\Delta G_{binding}$ from classical and biased MD simulations. The predictive potential of these methods is mostly limited by the robustness of their sampling and the accuracy of the force field used. As the Gibbs energy of association is based on both enthalpic and entropic contributions, the quality of the force field is mostly reflected in the enthalpic term, whereas the sampling is in the entropic term. This is useful when attempting to improve the estimated association energies obtained with empirical methods.

The enthalpy can be estimated using QM calculations. In principle, using high-level QM methods the electronic energy can be accurately calculated, but there are still some uncertainties in calculations of zero-point vibrational energy (ZPVE). ZPVE is usually calculated using the harmonic approximation, which is generally sufficiently accurate around the minima for many molecular systems but might be not valid especially for low-frequency vibration modes (intermolecular breathing modes) of noncovalent complexes. Accounting for anharmonic contributions may improve the estimation of ZPVE. It should be noted that the errors in ZPVE estimation account usually to ~1 kcal/mol. Anyway, the accurate estimation of the entropy remains difficult for accurate estimation of association energies, especially for QM methods, which assess the entropy using the apparatus of statistical mechanics and adopting the ideal gas, rigid rotor, and harmonic oscillator approximations.[215]

9. CONFORMATION AND THERMODYNAMICS IN COPIGMENTATION FROM QUANTUM CHEMISTRY

The geometries identified by MM-based calculations can be subsequently used as inputs for QM-based calculations in order to: (i) describe in detail the electronic configurations of both the separated monomers and the weakly bound complex; (ii) study any chemical property (e.g., deprotonation) or bond rearrangements that occur upon complexation; (iii) distinguish between attractive and repulsive energetic contributions, which are governed by the complex's underlying electronic structure; and (iv) evaluate all kinds of specific optical features, which arise from the properties of excited states (see section 10). It is important to apply QM methods rigorously and on the basis of a sound understanding of the underlying theories and to select methods with care from the wide range that are available. Our aim here is to provide a comprehensive and brief listing of computational methods suitable for studying copigmentation. This is necessary because the field is so broad that it is important to cater to researchers with widely varying levels of expertise in different aspects.

In the context of conformation and thermodynamic stability of copigmentation complexes, dispersion (London) forces must be accurately evaluated. Dispersion interactions originate from electron correlation effects, which are not fully captured by theoretical approaches based on the mean-field approximation, such as Hartree−Fock (HF) theory. This means that it is necessary to study these phenomena using alternative first-principles methods such as density functional theory (DFT) or post-HF methods.

9.1. Computing Copigmentation with DFT

The correlation functionals that are most commonly used in DFT studies are considered semilocal; i.e., they compute the correlation energy as a functional of the electron density at a given point r in space, and its gradient, $E_c[\rho(r),\nabla\rho(r)]$, as well as higher-order derivatives, $E_c[\rho(r),\nabla\rho(r),\nabla^2\rho(r)]$. These approaches neglect long-range electron−electron correlation effects. In this section, we briefly describe how current dispersion-corrected functionals address this problem, making possible an accurate modeling of the interactions that enable copigmentation (for some relevant reviews, see refs 216−226).

The most commonly utilized (semi)classical picture expresses dispersion energy (E_D) as a sum of pairwise interactions between the relevant weakly overlapping entities (atoms, molecules, or atoms-in-molecules):

$$E_D = -\sum_{J>I} \frac{C_6^{IJ}}{R_{IJ}^6} \tag{11}$$

where R_{IJ} is the separation of entities I and J, and C_6^{IJ} is the interatomic dispersion coefficient. We also note that these interactions are not limited to the dipole−dipole case; more generally speaking, the energy can be written as a multipole expansion:

$$E_D = \sum_{J>I} \left(-\frac{C_6^{IJ}}{R_{IJ}^6} - \frac{C_8^{IJ}}{R_{IJ}^8} - \frac{C_{10}^{IJ}}{R_{IJ}^{10}} - \dots \right) \tag{12}$$

where the different terms represent dipole−dipole, dipole−quadrupole, and quadrupole−quadrupole (or dipole-octupole) effects, respectively. The dispersion coefficients depend on the polarizabilities as described by the Casimir-Polder expression:[227]

$$C_6^{IJ} = \frac{3}{\pi} \int_0^\infty \alpha_I(i\omega)\alpha_J(i\omega)\, d\omega \tag{13}$$

with $\alpha(i\omega)$ being the frequency-dependent polarizability. While C_6^{IJ} can be computed explicitly, the other coefficients are normally calculated recursively [e.g., $C_8^{IJ} = 3C_6^{IJ}(Q_I Q_J)^{1/2}$ with Q being related to $< R^n >$ multipole-type expectation values and nuclear charges].[228−232] However, these coefficients can be computed using more sophisticated schemes; for example, the XDM method calculates them very accurately from the exchange-hole dipole moment.[233−235] At this point, we would like to note that

DOI: 10.1021/acs.chemrev.5b00507
Chem. Rev. 2016, 116, 4937−4982

the distance dependence (R^{-6} and beyond) of the dispersion energy is clearly of a long-range nature, meaning that it influences both thermodynamic parameters and chemical reactivity in solvated environments. The energy expression given in eq 12 is asymptotically correct; however, it diverges at small interatomic separations. The simplified form is also used in the Lennard-Jones potential, $E_D = 4\epsilon[(\sigma/R_{IJ})^{12} - (\sigma/R_{IJ})^{6}]$, which is used in many force fields and where the latter term stands for the dispersive (attractive) interaction. Although it is widely used and remarkably accurate for most systems, it is important to recall that this pairwise additivity scheme does not fully reflect the collective nature of the dispersion interactions (i.e., the relevant many-body effects).

The binding (or association) energy ($\Delta E_{\text{binding}}$) for two weakly interacting M and N (sub)systems has a profound effect on the supramolecular self-assembly of copigments. This energy is given simply by

$$\Delta E_{\text{binding}} = E(M\cdots N) - E(M) - E(N) \tag{14}$$

where the $M\cdots N$ notation is used throughout this text to emphasize the key role of weak interactions, and where $E(M)$ and $E(N)$ are the energies of the isolated pigments (which must all be computed at the same level of theory). This expression can be easily generalized to describe the copigmentation association of more than two molecules by using the many-body expansion.[236,237]

The most popular and reasonably successful DFT-based methods describing dispersion are those which include pairwise additive corrections. The direct application of a classical dispersion correction, $E_D \propto -R^{-6}$, is inappropriate because it will lead to a double-counting of the energy at intermediate distances and a divergence at shorter distances. Coupling the energy terms with some parameter fitting can avoid the double-counting problem, whereas introducing a damping function[238−240] allows managing the transition from short-to-long distances in order to avoid the problem of divergence.

Actually, the reparameterized -D3(BJ) method[241−243] illustrates the state-of-the-art of current corrections. There are also various simplified versions of this correction; while the primitive -D1 variant has gradually been discarded,[244] the -D2 method[245,246] is still widely and successfully used. To further illustrate the use of the above correction in the field of natural polyphenols, taking into account the diversity of this review's intended readership, Figure 21 shows the magnitude and shape of the dispersion energy as a function of the interatomic distance for three pairs of interacting IJ atoms: C−C, C−H, and H−H. Note that we have truncated the expression for E_D at first-order and used a value of $s_6 = 1.0$ for the sake of readability. Broadly speaking, we can clearly see that: (i) the energy peaks at approximately the average van der Waals radii of the two atoms involved; (ii) less energy is introduced for less polarizable atoms; (iii) the expression displays the correct asymptotic behavior; and (iv) it augments the electronic energy for all of the interacting atoms, at a negligible computational cost.

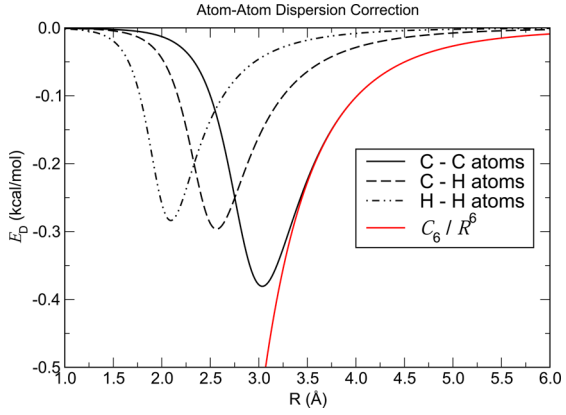

Figure 21. Dispersion energy as a function of the interatomic distance for a set of selected atomic pairs.

We also wish to mention some other approaches, namely the vdW-TS method;[247] the density-dependent energy correction (dDsC) which introduces a density-dependent damping function[248] and reduces the severity of intramolecular errors without perturbing the good performance achieved for long-range dispersion interactions;[249,250] and the DFT-*lg* method.[251,252] Seamless additive corrections have also been developed, in which the missing dispersion energy can be obtained by considering the coupling of the electronic densities $\rho(r)$ and $\rho(r')$ at two different points within the electronic coordinate space, r and r'. The corresponding general correlation functional expression[253−256] includes a coupling function $\Phi(r, r')$ partially accounting for nonlocality (DFT-NL methods), which naturally vanishes at short electron−electron distances and concomitantly describes intramolecular dispersion interactions.[257−261] Other recent refinements have been proposed[262,263] whose development has led to the VV10 final form.[264−269] This approach has yielded some remarkably accurate results.[270−272] Figure 22 outlines the two approximations (DFT-D3 and DFT-NL) discussed so far. Finally, we mention that nonpairwise effects may be important in inhomogeneous systems or in cases where there is a large region of vacuum between weakly interacting molecular fragments. Furthermore, it has recently been shown that the size dependence of the dispersion interactions deviates from the expected rule $E_D \propto k^2$ (where k is the number of weakly interacting entities), with some unusual behavior observed depending on the dimensionality of the system.[273,274]

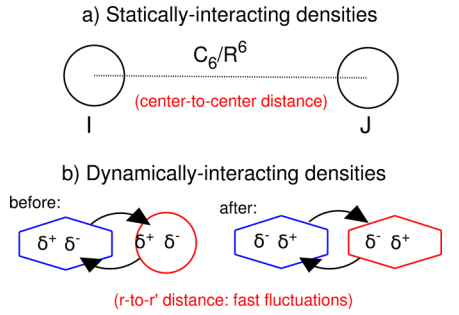

Figure 22. Sketch of the two main DFT-based corrections discussed: the statically averaged interaction (top) and the dynamically interacting densities (bottom).

9.2. Other Methods to Compute Copigmentation

Post-HF methods can minimally describe the dispersion energy by truncated perturbation theory, in which the intermolecular correlation energy is introduced by coupling both monomers with their respective excited-state via a long-range term that has a stabilizing effect. Double excitations are very important for electronic correlation, and therefore the simplest size-extensive ab initio method (e.g., Møller−Plesset perturbation theory

DOI: 10.1021/acs.chemrev.5b00507
Chem. Rev. 2016, 116, 4937−4982

truncated at second-order, MP2) can at least partially describe dispersion effects. However, this method cannot be used to simultaneously describe multiple excitations within and between the interacting molecules, and it is thus not recommended for an accurate description of the copigmentation process due to its well-known overestimation of binding energies.

Coupled-cluster single and double (CCSD), or more appropriately the extension known as CCSD(T), including a perturbative-like correction Δ(T), is considered to be the "gold-standard" method of computational chemistry.[275] Other perturbative corrections that have been investigated, such as the CCSD[T] method, are also very accurate[276] and reaffirm the excellent trade-off between accuracy and computational cost inherent to CCSD(T).

We hasten to note that the CCSD(T) method seamlessly covers all types of noncovalent interactions in an accurate way. Unfortunately, its computational cost is very high because it formally scales with system size as $O(N^7)$, where N is related to the system size. This makes it difficult to use CCSD(T) to model large (real-world) copigmentation complexes. Furthermore, the performance of these high-level techniques is strongly dependent on the manifold of virtual orbitals available for excitations (the larger, the better), so it is important to use very large basis sets to achieve nearly converged results at the complete basis set (CBS) limit. This truncation of the basis sets space leads to the undesired basis set superposition error (BSSE), which is known to overestimate artificially the strength of the binding energy. Even when the use of a counter-poise corrections is sometimes recommended, which simply aims at subtracting that additional energy by a set of additional calculations, it has been recently questioned too. Various strategies have been proposed, but their description is beyond the scope of the review. One can mention MP2-F12 and CCSD(T)-F12;[277−281] domain-based local pair-natural-orbitals (DLPNO) CCSD(T) method;[282−295] and spin-component-scaled (SCS) variants of MP2 and CCSD.[296,297] The latter approach (SCS-MP2) has been theoretically rationalized[298,299] and leaves the opportunity to reweigh each contribution specifically for noncovalent interactions (e.g., SCSN-MP2,[300,301] SCS-MP2-D2,[302] SCS(MI)-MP2,[303] DW-MP2,[304] SCS-S66-MP2,[305] and SCS(MI)-CCSD[306] to name just a few applications).[307−313]

Table 3 stresses again the computational demands of the available post-HF methods, showing their formal scaling. All

Table 3. Formal Scaling of Different Methods Belonging to the Wavefunction Family

method	CCSD(T), CCSD[T]	CCSD, SCS-CCSD	MP2.5, MP2.X	MP2, SCS-MP2
scaling	$O(N^7)$	$O(N^6)$	$O(N^6)$	$O(N^5)$

DFT-based methods formally scale from $O(N^3)$ (pure) to $O(N^4)$ (hybrid) to $O(N^5)$ (double-hybrid) in the worst case, so their scaling is a few orders of magnitude lower than the wave function-based methods discussed previously.

The interaction between molecules typically involves electrostatic, polarization, dispersion, and repulsion contributions. It is worth noting that these contributions are difficult to separate experimentally, and to this end, the symmetry adapted perturbation theory[314,315] may assess the role of individual contributions.[316−318]

While density-fitting or resolution-of-the-identity techniques can substantially alleviate the computational costs of wave function-based calculations, they are also applicable to DFT methods, so the latter will always be favored in terms of their balance between accuracy and cost. However, there might be situations where even DFT is too costly for rapidly screening noncovalently bound systems, in solvated or unsolvated environments, and so alternative low-cost methods may be needed. If we also take the need for large basis sets when using common ab initio methods into account, it is clear that major savings can be achieved by using methods that can provide qualitatively (or better still, semiquantitatively) correct results with minimal basis sets. The recently developed HF-3c method[319−321] (the suffix -3c denotes a triple pairwise correction) is an outstanding method of this kind. A valence variant (HF-3cv) also exists, in which the core electrons are treated with pseudopotentials (relativistic effective core potentials) reducing the computational cost even further.[322] We should note that a density-based variant, dubbed as PBEh-3c, has been also recently proposed.[323]

The only way to achieve greater computational speedups would be to neglect three- and four-center integrals in the HF treatment, leading to the semiempirical OMx or PMx methods[324−326] with some supplementary corrections for dispersion and/or hydrogen bonding. This approach has resulted in the development of improved semiempirical methods such as OM3-D3[327,328] and PM6-DH(2).[329,330] The density functional tight binding (DFTB) method also uses a minimal basis set and provides reasonably accurate results at a fraction of the cost of a standard calculation thanks again to some parametrization of the integrals.[331,332] Novel features are the use of dispersion corrections[333] and the self-consistent charge density functional tight binding method (SCC-DFTB) for the treatment of charged systems.[334]

It is important to note that the list of methods and applications presented herein is not exhaustive because of the vast and rapidly growing number of possibilities in this vast field. We have nevertheless tried to give a first comprehensive (although necessarily limited) view of the complex and rich physics of dispersion interactions and to demonstrate why there is such a large range of available methods with very different formal scalings with respect to system size.

9.3. Quantum Chemistry Studies on Copigmentation: Failures and Successes

9.3.1. Conformational Analysis. Only a few purely QM studies on the conformational analysis of copigmentation complexes have been published so far.[114] QM calculations (mainly using DFT) are typically performed on the most stable conformers, which are generally identified using MD (see section 8.2). Indeed, for most real-world copigmentation systems, the number of degrees of freedom is too high to permit random exploration of their conformational space using robust but costly QM methodologies. However, such approaches are viable for systems with a very limited number of degrees of freedom. For example, we recently reported a systematic scan of the 3D space of intermolecular coordinates for the copigmentation pair consisting of 3-*OMe*-cyanidin (with the pigment in its flavylium form) and quercetin (the copigment).[114] Scanning along the *z*-axis, which was defined as being perpendicular to the coplanar and cofacially oriented partners, revealed an energy minimum at an intermolecular separation of 3.3 Å, which is typical for $\pi-\pi$ stacking interactions. Scanning in the *xy* plane then resulted in the identification of five conformers (named conformers 1−5 in the related publication), which may be stabilized by a

DOI: 10.1021/acs.chemrev.5b00507
Chem. Rev. 2016, 116, 4937−4982

combination of $\pi-\pi$ stacking and (in some cases) intermolecular hydrogen-bonding interactions [e.g., between the OH groups of the two partner's B-rings in the most stable conformer (conformer 5) or involving the keto group at C5 of quercetin (conformer 2)] (see Figure 23, panels A and B). Even with such a simple binary copigmentation system, there is considerable flexibility in the stacking of the two partners. As was suggested previously, the system was shifted slightly away from pure cofacial stacking, with both B-rings being parallel-displaced (Figure 23A). Note also that, as suggested by Hondo et al.,[131] chiral (clock-wise or anticlockwise) rearrangements are likely, as confirmed by this QM study (Figure 23C). In addition, the individual partners sometimes "bend" away from purely coplanar stacking arrangements, mainly because of intermolecular hydrogen bonding (Figure 23D). The identification of these different geometries prompted further MD simulations in a box of water,[173] which confirmed the coexistence of the five conformers and revealed large hydrophobic effects, with the space between the two fragments being completely devoid of water molecules (Figure 19).

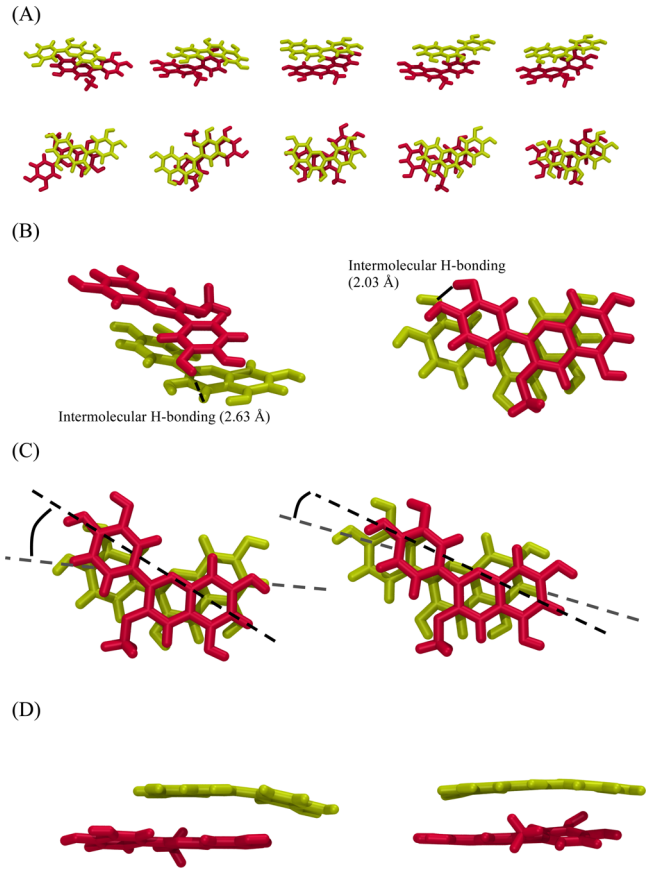

Figure 23. Five stable conformations of the 3-*OMe*-cyanidin··· quercetin noncovalent complex (A) side-view and top view showing the parallel-displaced arrangement; (B) side-view showing the intermolecular hydrogen bonding of conformers 2 and 5; (C) top view showing the supramolecular chirality in conformers 3 and 5; and (D) side-view showing the slight bending in conformers 1 and 5.

We wish to stress that with the 3-*OMe*-cyanidin···quercetin copigmentation prototype, the only way to obtain a potential well along the *z*-axis within the DFT framework was to include dispersion forces, through the DFT-D correction. The use of uncorrected hybrid functionals, such as B3P86 or B3LYP, precluded the description of a stable complex (Figure 24). Interestingly, the copigmentation complex of oenin and ellagic acid, with and without the presence of ferrous and ferric ions, has also recently been studied with great success using B3LYP.[209,335] The presence of such ions clearly enhanced the electrostatic interactions between the two partners and helped drive the stacking that was ultimately identified, with the cation thus promoting the formation of a sandwiched structure in which it is "trapped" between the two active partners (e.g., malvidin-Fe(II)-ellagic acid). The incorporation of the cation increased the stacking distance between the two partners from roughly 2.6 to 5.0 Å, again demonstrating its important effect. These results demonstrate that such through-space cation-π interactions can be (semi)quantitatively described by uncorrected DFT-based methods. Note, however, that the distance between the stacked molecules in the absence of ions is generally below the sum of their van der Waals radii,[336] and thus indicates some mismatch between electrostatic and dispersion interactions. This again highlights the need to use dispersion-corrected methods that adequately balance all kinds of noncovalent interactions when studying this type of complexes.

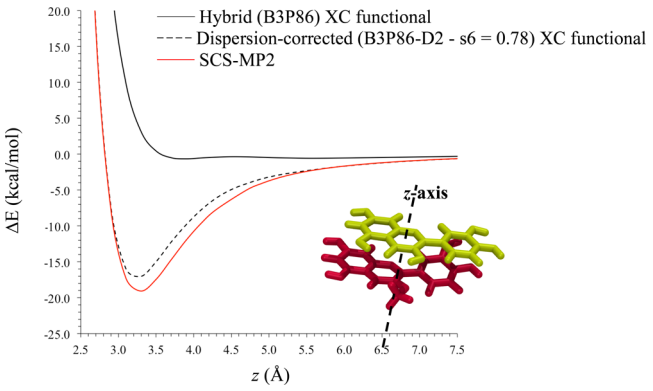

Figure 24. Potential energy curve along the *z*-axis defined perpendicular to the planar π-conjugated system, as obtained by three methods of calculation.

Systematic QM evaluations of the potential energy curve along the *z*-axis would be particularly instructive when studying copigmentation. However, such methodologies cannot be recommended as standard tools for describing the geometrical features of copigmentation complexes. Combining QM with MD simulations appears a much better way of dealing with these complexes' geometrical flexibility; the MD simulation is performed first (it should generally be unbiased, but biased simulations may be preferable if reliable experimental data can be used to constrain the geometries) followed by QM calculations on selected geometries to confirm their relative stabilities.

9.3.2. Association Energies. So far little has been made to establish a quantitative comparison between experimental and theoretical $\Delta E_{binding}$, which, as detailed above, remains a complex challenge. Nonthermally corrected association energies were computed for the five conformers found for 3-*OMe*-cyanidin··· quercetin at the B3P86-D2/cc-pVDZ level, yielding values of −13.3, −13.1, −12.8, −13.4, and −13.9 kcal/mol, respectively.[114] From these results obtained at the dispersion-corrected DFT level, the Boltzmann distribution was predicted to be 16.2%, 12.9%, 7.0%, 19.9%, and 44.4% for the five conformers, respectively. This distribution gave a weighted association energy

DOI: 10.1021/acs.chemrev.5b00507
Chem. Rev. 2016, 116, 4937−4982

of −13.3 kcal/mol, which was rather close to the experimental enthalpy (−13.9 kcal/mol) obtained for a similar system.[30]

Interestingly, self-association was also observed between the two partners, with a slightly higher association energy (corresponding to a lower stability) of ca. −12.7 kcal/mol being determined for the self-association of the flavylium form of 3-*OMe*-cyanidin. As previously suggested, the self-association between two flavylium cations appeared feasible based on our dispersion-corrected calculations, confirming that noncovalent interactions can counteract the repulsive electrostatic interactions between two positively charged species.

Table 4 lists some energies computed for the five conformers of the 3-*OMe*-cyanidin···quercetin system using the DFT-D2, DFT-D3, and DFT-NL variants with the very large def2-QZVP basis set, in the presence and absence of solvent effects. We can clearly see the pronounced influence of the solvation shell (even when described using a continuum model) and, concomitantly, the robust behavior of all the dispersion corrections considered. For example, the (solvated) weighted association energy is predicted to be −12.4 kcal/mol at the COSMO-B3P86-D3(BJ)/def2-QZVP level, with conformer 5 (the most stable) of 3-*OMe*-cyanidin···quercetin contributing most heavily to this value. Interestingly, the low-cost HF-3c method performs rather well. Note, however, that further and more detailed benchmark studies are required to establish a global consensus concerning method selection for the accurate description of copigmentation complexes.

Table 4. Calculated Association Energies (kcal/mol) for the Prototypical Copigmentation System 3-*OMe*-Cyanidin··· quercetin, in Their Five Stable Conformers

	conformer 1	conformer 2	conformer 3	conformer 4	conformer 5
HF-3c	−15.8	−18.1	−17.8	−15.8	−20.1
B3P86-D2/def2-QZVP	−12.6	−16.5	−14.1	−13.8	−17.3
B3P86-D3(BJ) def2-QZVP	−14.5	−18.2	−16.6	−15.8	−19.2
B3P86-NL/def2-QZVP	−17.6	−21.7	−19.9	−19.2	−23.4
SCS-S66-MP2/def2-QZVP	−17.6[a]	−22.6[a]	−20.0[a]	−19.4[a]	−23.5[a]
COSMO-B3P86-D2/def2-QZVP	−6.9[b]	−8.6[b]	−6.8[b]	−7.5[b]	−10.6[b]
COSMO-B3P86-D3(BJ)/def2-QZVP	−8.8[b]	−10.3[b]	−9.3[b]	−9.5[b]	−12.5[b]
COSMO-B3P86-NL/def2-QZVP	−11.7[b]	−13.6[b]	−12.4[b]	−12.8[b]	−16.5[b]

[a]Values may be considered as reference for gas phase estimates. [b]Values for the water phase represented by a continuum solvent.

Evaluating the Gibbs energy of association of copigmentation complexes is even more challenging than estimating their electronic energy and enthalpy, not least because of the difficulty of estimating the entropy correction. The translational, rotational, and vibrational contributions to entropy are evaluated using expressions from statistical thermodynamics, subject to the ideal gas, rigid rotor, and harmonic approximations. However, some features of copigmentation complexes go beyond these approximations. It is also important to note that QM calculations are performed either in vacuo or using implicit solvent models, mainly polarizable continuum models (e.g., PCM or COSMO) in which the solute is placed in a shape-adapted cavity surrounded by a continuum dielectric medium. This approach usually accounts for mean-field polarizable effects reasonably well but all specific interactions with water are ignored, which can be critical in the case of copigmentation. It also means that hydrophobic effects and related entropic contributions cannot be accounted for directly. An explicit description of the first solvent shell would enhance the results but dramatically increase the computational effort. The use of implicit solvent also has direct consequences for the evaluation of energies and enthalpies of binding because stabilizing hydrogen bonds between the pigment and copigment may compete with intermolecular hydrogen bonding between the two partners and water molecules. Again, further developments based on combining QM and MM calculations (QM/MM) are probably required to improve the prediction of $\Delta G_{binding}$.

10. UNDERLYING CONCEPTS OF SPECTRAL SHIFTS IN COPIGMENTATION

Having identified QM methodologies based on cost-effective dispersion-corrected DFT methods as particularly appropriate tools for studying pigment-copigment systems,[337] we now turn our attention to the prediction of their electronic and optical properties with the aim of better understanding their UV−vis absorption spectra. This is particularly important because, as noted above, UV−vis spectroscopy is the most important experimental tool for studying copigmentation. There have only been a few publications reporting the successful interpretation of copigmentation complexes' spectral behavior on the basis of computational investigations.[105,108,114] However, several investigations along these lines have been initiated because copigmentation is a complex electronic process (vide infra). On one hand, it involves electronic properties arising from the pigment and the effects of the copigment, such as the stabilization of specific (de/protonated) pigment forms at a specific pH values due to its close contact with the copigment. Moreover, it involves cooperative pigment-copigment electronic interactions that enable the formation of energetically low-lying CT states. Both factors can significantly, and simultaneously, contribute to energetic (bathochromic) shifts and hyperchromic effects affecting the pigment's UV−vis spectrum. The understanding of experimental UV−vis spectra is further complicated by the fact that electronic transitions in the visible range, including the CT states, are close in energy.[114] Moreover, the corresponding bandwidths are large, so the apparent "main" absorption is actually a collective response of different electronic excitations. Consequently, spectral shifts and intensity enhancements cannot necessarily be interpreted using a simple scheme.

10.1. Charge Transfer and Underlying Theory

For anthocyanins not engaged in copigmentation complexes, various QM-based studies have calculated the UV−vis absorption features, mainly of their flavylium cation forms, which were the subject of a recent review.[173] These studies have highlighted the crucial importance of: (i) the choice of method and (ii) the description of the environment (water solvation mainly). With respect to the first of these points, the available options include the semiempirical ZINDO method,[152,338] post-HF methods for excited states (e.g., configuration interaction: CI, CIS(D), CC2, or CASPT2)[339] and TD-DFT methods.[50,69,108,114,340−343] In terms of computational feasibility and accuracy, TD-DFT appears to currently represent the optimal

DOI: 10.1021/acs.chemrev.5b00507
Chem. Rev. 2016, 116, 4937−4982

compromise between computational cost and accuracy when studying the optical properties of anthocyanins.

The electronic description of the excited states presents an additional challenge due to the potential for the existence of CT states. These states can form because of the energetic offset between the frontier MOs of the pigment (which commonly acts as the electron acceptor, A) and the copigment (typically the donor, D), as shown in Scheme 4. In the simplest approximation (i.e., a one-electron case with no mixing of the D and A MOs), the energy of the CT state is given by

$$E_{CT} = \varepsilon^{A}_{LUMO} - \varepsilon^{D}_{HOMO} \tag{15}$$

Scheme 4. (A) Simplified MO diagram for CT and exciton formation of a DA and AA pair (H = HOMO, L = LUMO)[a]

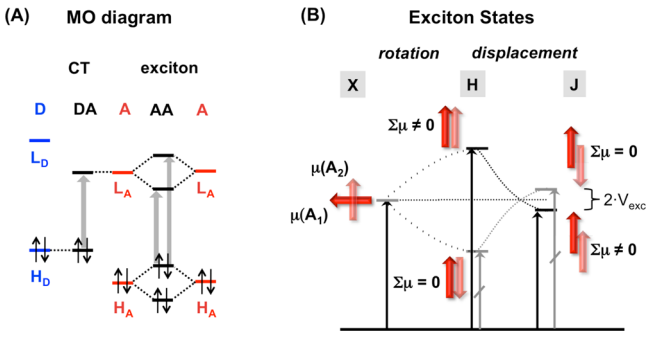

[a]Grey arrows indicate lowest electronic transitions in a one-electron picture. (B) Resulting exciton states for rotated and laterally displaced AA pair (qualitative quantum-chemical corrected Kasha picture at π-stacking distance).

In reality, MO mixing, configuration interaction (CI), and mixing with higher allowed excited states through perturbation significantly change this picture, which is highly dependent on the electronic natures of D and A as well as their mutual orientation (intermolecular distance, rotation, and lateral displacements). However, as a rule of thumb, the energy of the CT state is still mainly driven by $E^{A}_{L} - E^{D}_{H}$, and the oscillator strength by the degree of MO mixing (i.e., mainly by the energetic offsets $\Delta E_L = E^{A}_{L} - E^{D}_{L}$ and $\Delta E_H = E^{A}_{H} - E^{D}_{H}$).[344] This also suggests a basic correlation between the amount of bathochromic shift and decrease of the oscillator strength for the CT state.

This facile picture is significantly altered in more accurate time-dependent approaches such as TD-DFT. In fact, CT states are usually predicted to have very unrealistically low energies,[345,346] which renders the standard TD-DFT treatment almost meaningless. This behavior can be understood by combining purely electrostatic arguments with the underlying TD-DFT equations that are routinely employed.[347] Assuming that, during CT excitations, some charge density is transferred from one region to another that is distant in space, and that these separated charge densities can be approximated as point charges separated by a distance R, the distance-dependent excitation energy is estimated as

$$E_{CT} = IP_D - EA_A - \frac{1}{R} \tag{16}$$

where IP_D is the ionization potential of the donor, EA_A is the electron affinity of the acceptor, and $1/R$ is the electrostatic separation at the distance R between pigment and copigment.

However, when one applies and develops the TD-DFT linear-response equations for a pure functional, taken here as an example, and assuming that the relevant CT excitation is dominated by a HOMO to LUMO transition, this energy is estimated in terms of one-electron orbitals as

$$E^{TD-DFT}_{CT} = \varepsilon^{A}_{LUMO} - \varepsilon^{D}_{HOMO} + \iint \frac{\phi^{A}_{LUMO}(r)\phi^{D}_{HOMO}(r)\phi^{A}_{LUMO}(r')\phi^{D}_{HOMO}(r')}{|r - r'|}\,dr\,dr' + \iint \phi^{A}_{LUMO}(r)\phi^{D}_{HOMO}(r) f_{XC}(r, r')\phi^{A}_{LUMO}(r')\phi^{D}_{HOMO}(r')\,dr\,dr' \tag{17}$$

with f_{XC} being the exchange-correlation kernel (i.e., the functional derivative of the exchange-correlation potential) defined by the selected functional. However, due to the orbital localization imposed, $\varphi_i \to 0$ in the limit of large separation between pigment and copigment, which also implies a small density overlap in the intermolecular region, due to the exponential decay of the latter property, so that the previous expression indeed simply (and wrongly) collapses to

$$E^{TD-DFT}_{CT} = \varepsilon^{A}_{LUMO} - \varepsilon^{D}_{HOMO} \tag{18}$$

with ε_i being the corresponding eigenvalues in a one-electron picture. This clearly shows how and why the TD-DFT excitation energy underestimates the real value; it misses not only the $-1/R$ component, but it approximates $IP_D - EA_A$ as $\varepsilon^{A}_{LUMO} - \varepsilon^{D}_{HOMO}$ rather than giving the correct expression $\varepsilon^{A}_{LUMO} - \varepsilon^{D}_{HOMO} + \Delta_{xc}$, with Δ_{xc} being the correction to the HOMO−LUMO gap (also known as the derivative discontinuity).

Note that within this one-electron scheme, the bathochromic shift against the monomer, say the acceptor A (with excitation energy roughly equals to $\varepsilon^{A}_{LUMO} - \varepsilon^{D}_{HOMO}$), is given by

$$\Delta E = \varepsilon^{D}_{HOMO} - \varepsilon^{A}_{HOMO} = \Delta\varepsilon_{HOMO} \tag{19}$$

Eq 19 corresponds to the energetic offset of the HOMO of the weakly bound donor and acceptor molecules. When this approximation is used, the CT state is predicted to be dark (i.e., oscillator strength $f^{CT} = 0$) since CT is complete (i.e., transfer of 1|e| from D to A), and no dependency on the mutual orientation is expected.

Experience has also shown that for short-range (e.g., intramolecular) CT excitation, the use of hybrid functionals (including a certain percentage of exact-like exchange (e.g., 50% for BH and HLYP) can partly alleviate this drawback. This alleviation can be traced back to TD-HF, the HF-analogue of TD-DFT, for which at large separations:

$$E^{TD-HF}_{CT} = \varepsilon^{A}_{LUMO} - \varepsilon^{D}_{HOMO} + \iint \frac{\phi^{A}_{LUMO}(r)\phi^{D}_{HOMO}(r)\phi^{A}_{LUMO}(r')\phi^{D}_{HOMO}(r')}{|r - r'|}\,dr\,dr' \tag{20}$$

reproducing (qualitatively) the CT excitations since now $E^{TD-HF}_{CT} = \varepsilon^{A}_{LUMO} - \varepsilon^{D}_{HOMO} - 1/R$. Thus, the use of a hybrid functional, where a HF-like exchange term is weighted by a value C_{HF}, in practical calculations would lead to $E^{TD-HF}_{CT} \to \varepsilon^{A}_{LUMO} - \varepsilon^{D}_{HOMO} - C_{HF}/R$, partially correcting the error. One disadvantage of this procedure is that the weight of the HF-like exchange is often system-dependent, demonstrating a need for more accurate and general solutions that can be applied to all systems.

DOI: 10.1021/acs.chemrev.5b00507
Chem. Rev. 2016, 116, 4937−4982

Furthermore, in the case of long-range (e.g., intermolecular) CT excitations, a more efficient and conceptually correct model would enable automatic switching from short- to long-range regions, with the full HF-like term being dominant in the latter. In this correction, the two-electron operator $1/|r - r'| = 1/r_{12}$ is divided by the error function into two separate contributions (short- and long-range):

$$\frac{1}{r_{12}} = \frac{1 - \mathrm{erf}(\mu r_{12})}{r_{12}} + \frac{\mathrm{erf}(\mu r_{12})}{r_{12}} \quad (21)$$

μ is a parameter to be determined, or even fine-tuned from first-principles, for each functional. This has led to the family of range-separated functionals (e.g., CAM-B3LYP[348] or ωB97XD[349,350]), which are applied below. Note also that not only excitation energies but also oscillator strengths are more accurately predicted by these methods than with standard hybrid functionals, as demonstrated by a recent comparison to benchmark EOM-CCSD values.[351]

It should be noted that the theoretical treatment of the pigment-copigment CT states differs from the molecular exciton picture for self-aggregation of pigments (i.e., AA systems). For a simple rotation of two pigments, one starts with H-aggregates (with the relevant transition dipole moments, μ, oriented in parallel to give a bathochromically shifted, symmetry-forbidden state, and a hypsochromically i.e., blue-shifted, allowed state) and moves to a situation in which the dipole moments are perpendicular (no shift); see Scheme 4. Starting again from the H-aggregates, lateral displacements lead successively to the formation of J-aggregates corresponding to permitted lower energetic states. At $\pi-\pi$ stacking distances (~3.5 Å), the H/J inversion point and the extent of the splitting cannot be described in terms of classical dipoles as attempted by Kasha[140] and must instead be handled using an appropriate QM treatment that incorporates all of the relevant (inter)molecular parameters.[120]

In accordance with the considerations discussed above, the CT character depends critically on the electronic nature of the co/pigments as well as the intermolecular geometrical parameters. For a reliable description of CT states, it is therefore essential to use a theoretical method capable of reflecting and reproducing this structural sensitivity.

10.2. Theoretical Investigations of Spectral Shifts in Copigmentation

Methodologies that exclude long-range interactions have failed to reproduce the bathochromic shifts associated with copigmentation. For example, ZINDO//AM1 and TD-B3LYP calculations were performed for the two hybrid pigments, 1-deoxyvescalagin-(1β → 8)-oenin and 1-deoxyvescalagin-(1β → 8)-malvidin. At wine pH, these two pigment-copigment systems exhibit a bathochromic shift compared to the corresponding anthocyanin and anthocyanidin derivatives, which is responsible for the well-evidenced red-to-purple hue evolution.[152] On the basis of experimental data, these spectral effects were clearly assigned to noncovalent interactions between the pigment and copigment moieties. However, neither of the two tested computational methods could properly describe the excited state (ES), in which CT was expected to play a significant role.

Post-HF methods are known to correctly account for CT. In one notable example pertaining to phenolic compounds that are not strictly related to copigmentation, a post-HF method, namely the second-order approximate coupled cluster (CC2) approach CC2/aug-cc-pVDZ, was used to successfully predict CT effects in isoflavonoid fluorescence, using geometries computed at the PBE0/TZVP level.[352] However, such methodologies are very time-consuming when applied to copigmentation systems. A rather delocalized MO with components on both fragments was identified in PCM-MP2/6-311++G(d,p) calculations on the malvidin···ellagic acid complex (Figure 4 of ref 209). However, it is difficult to establish a link between this MO description and CT excited states because the cited work did not focus on optical properties, and so no ES calculations were reported.

Remaining within the TD-DFT framework, the XC functional is known to have a major impact on the quality of the results, particularly when studying CT systems. Hybrid DFT (PCM-mPW1PW91/6-31+G(d,p)) calculations showed that the first ES of 4-methyl-7-methoxyflavylium chloride···ferulic acid, which is described by a HOMO → LUMO transition, has strong CT character with the HOMO and LUMO being localized on the copigment and pigment, respectively.[105] Consequently, this ES ($S_0 \rightarrow S_1$), lying at 594 nm, was essentially dark in optical terms, with an oscillator strength of 0.002. The other two ES (without CT character), $S_0 \rightarrow S_2$ and $S_0 \rightarrow S_3$, were only slightly shifted (402 and 390 nm, respectively). Unfortunately, as in many cases, there are no conclusive experimental data available with which to verify the computational conclusion because weak low-lying CT states are difficult to detect under the broad features of the intense pigment-localized transition.

CT states can be properly characterized using range-separated hybrid (RSH) functionals such as ωB97X and CAM-B3LYP that (mathematically) split the particle−particle interaction operator into short- and long-range interactions, as it was previously explained. These functionals have only recently been developed but have made obsolete the use of hybrid functionals for extended π-conjugated systems and systems in which CT plays a determinant role. DFT calculations employing long-range corrections (SS-PCM-ωB97XD/cc-PVDZ) confirmed the bathochromic shift occurring in the copigmentation complex of 3-*O*-methylcyanidin···quercetin.[114] UV−vis absorption spectra were predicted for the five stable conformers of this complex (Figure 23) on the basis of COSMO-B3P86-D2(s_6 = 0.780)/cc-pVDZ geometry optimizations. The bathochromic shift, obtained from a Boltzmann-weighted analysis of the five conformers, was predicted to be 0.14 eV (23 nm), which is consistent with the experimental result (11.7 nm) presented in ref 30 given that complete complexation would not have been achieved under the reported experimental conditions.[107] In accordance with the calculations, the main absorption band was assigned to the first excited state, which exhibited considerable CT character. The HOMO is mainly delocalized on quercetin, whereas the LUMO is on the pigment (Figure 25) and CT occurred from the copigment to the pigment. The global bathochromic shift that had been observed for many years was thus rationalized as a new band originating from the noncovalent $\pi-\pi$ stacking arrangement. Also, in this case, high-energy lying states such as $S_0 \rightarrow S_2$ contribute to the global bathochromic shift. In this model 3-*O*-methylcyanidin···quercetin copigmentation system, it was clearly seen that the MO and ES description was strongly conformation-dependent. Specifically, the CTs for the five conformers were 0.09, 0.06, 0.13, 0.30, and 0.73 |e|, respectively, and the corresponding bathochromic shifts were 3.7, 5.7, 10.8, 20.9, and 37.8 nm, respectively; the correlation between the bathochromic shift and the CT character confirms the rule of thumb stated above.

Thus, all of the molecular conformational arrangements and conformational diversity of pigment···copigment complexes

DOI: 10.1021/acs.chemrev.5b00507
Chem. Rev. 2016, 116, 4937−4982

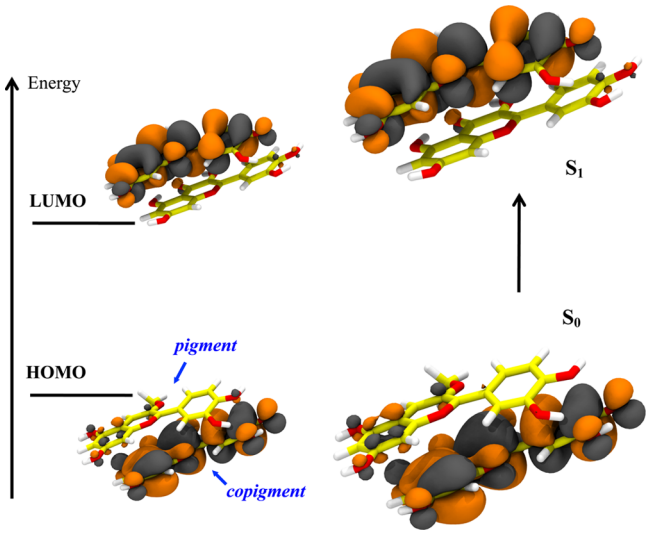

Figure 25. MO orbital diagram related to the maximum absorption wavelength HOMO and LUMO (left) and NTO analysis (right). Both schemes show the strong CT character of $S_0 \rightarrow S_1$.

must be identified and characterized in order to understand the spectral shifts associated with copigmentation. This point has also been made by other authors, many of whom also stressed the role of thermally activated intramolecular vibrations.[353] The 3-*O*-methylcyanidin···quercetin complex exhibits rather few degrees of freedom, so a systematic evaluation of its conformational space can be performed using QM-based approaches. However, for most real-world copigmentation systems, such approaches are too computationally demanding, and the identification of all possible conformers requires the application of MM-based approaches. We have recently used such an approach with the catechin-(4 → 8)-oenin pigment, which is copigmented with two vinylcatechins and procyanidin B3.[108] A 10 ns MD simulation was used to sample the conformational space, yielding a set of averaged geometries. DFT-D optimization of these geometries provided three conformers on which TD-ωB97XD/6-31+G-(d,p) calculations were performed. Interestingly in this system, new UV−vis absorption bands were identified. Theoretical calculations predicted that the B- or E-rings of the pigment participated in parallel-displaced $\pi-\pi$ stacking interactions with the C-, A-, D-, and F-rings of the copigment. While the main absorption (λ_{MAX}) was assigned to the $S_0 \rightarrow S_1$ transition (which exhibits CT character), the new absorption bands were mainly attributed to the $S_0 \rightarrow S_2$ and $S_0 \rightarrow S_3$ excited states. The electronic transitions describing these two ESs appeared to be complex, involving lower-lying occupied MO but were always to the LUMO, and for most of them there was evidence for a contribution from intramolecular CT within the hybrid pigment (catechin-(4 → 8)-oenin). We believe a posteriori that the sampling in this study was not sufficient, since the 10 ns time scale of the MD simulation is unlikely to have been sufficient to permit escape from local minima. However, the overall qualitative description of the experimentally observed optical properties clearly was sufficient.

10.3. Environmental Effects and Peak Broadening

Even more than conformational diversity, the description of the environment is a matter of utmost importance when studying molecular spectroscopy in solution. The rearrangement of the solvent in response to changes in the solute's charge distribution induces inhomogeneous polar broadening.[354] Most theoretical works on anthocyanins and copigmentation have described the solvent using implicit models, mainly COSMO[355] and PCMs[356] mainly IEFPCM and (C)PCM; some gas phase (i.e., in vacuo) studies have been reported, although these are becoming less common. However, it is important to stress that the conventional application of PCM in TD-DFT calculations is in principle not physically relevant because the effective Hamiltonian is defined in a static way, whereas the electronic vertical transition is a dynamical process. Simply applying PCM within TD-DFT fails to capture the time dependence of solvent relaxation. Therefore, even though this approach is attractive due to its very competitive accuracy/computational cost ratio, great care must be taken when interpreting results obtained in this way. Various approaches have been developed to circumvent this problem.[356] These techniques can be divided into two families, namely state-specific (SS) and linear-response (LR) methods. SS methods solve the effective Schrödinger equation for each state of interest. LR-methods aim to directly compute the vertical excitation energies, describing the time-dependent wave function as a linear perturbation of the time-independent wave function. In one case, SS-PCM and PCM were found to provide similar qualitative descriptions of the spectral shifts occurring in a copigmentation complex (i.e., both predicted the occurrence of a bathochromic shift) but the quantitative description was different in that PCM underestimated the shift compared to SS-PCM.[114]

Whatever progress may be made in the development of implicit models, such models are inherently incapable of describing specific solute−solvent interactions. Copigmentation is a phenomenon associated with pigments and copigments that are both phenolic and which mainly occurs in aqueous solution. Therefore, as noted above, hydrogen-bonding interactions are expected to play important roles in stabilizing the complexes and structuring the first solvent shell surrounding them. These supramolecular structures are dynamic in nature and may strongly influence the complex's optical properties. Implicit solvents cannot capture this aspect of the system, so the only way to investigate these dynamic supramolecular architecture at present is to perform MD-based calculations, and in this case, the optical properties cannot be calculated. So the MD simulations must be somehow combined to QM-based calculations of the excited states.

In an evaluation of CT in the isoflavonoid daidzein, the system was microsolvated with different numbers of water molecules (limiting to one water molecule per OH group), which may contribute to its intermolecular hydrogen-bonding network.[352] The S. Baroni group has rationalized the spectral shifts of cyanidin 3-*O*-glucoside using an explicit solvent description: they performed ab initio MD (within the Car−Parrinello scheme) within TD-DFT using the plane wave pseudopotential approach and periodic boundary conditions in a 20 × 20 × 12 Å^3 supercell.[353] Their results indicated that the first solvent shell is highly anisotropic, featuring water molecules interacting both (i) in-plane with the OH groups of the anthocyanidin moiety and (ii) out-of-plane with the π orbitals of the aromatic rings; the former interaction is attractive, whereas the latter is repulsive. The authors concluded that static models such as QM calculations with a PCM model may not be appropriate for characterizing the spectral changes observed with these pigments. The dynamic solvent description appeared to be crucial but mainly because it influenced intramolecular thermal fluctuations, which dramatically impact the energies and π-character of the frontier MOs involved in light absorption. Band broadening and modifications of UV−vis absorption spectra

DOI: 10.1021/acs.chemrev.5b00507
Chem. Rev. 2016, 116, 4937−4982

were mainly attributed to these dynamic distortions of the (co)pigment's structures rather than direct solvation effects. This again highlights the importance of sampling conformational space: not just that of the solutes, but also that of the supramolecular solute−solvent assembly. Interestingly, only a few water molecules appeared to directly influence absorption in the visible range (i.e., had detectable effects on the π-conjugated frontier MOs).

On the basis of similar calculations, the same authors developed a color morphing procedure to expedite the theoretical evaluation of anthocyanins' optical properties in solution.[357] Rather than providing absorption wavelengths and oscillator strengths, the TD-DFT results can also be expressed in terms of three-color parameters *XYZ* using the transmitted light intensity:

$$XYZ = N \int I_T(\lambda)\bar{x}\,\bar{y}\,\bar{z}(\lambda)\,\mathrm{d}\lambda = N \int I_0(\lambda)e^{-\kappa(\lambda)l}\bar{x}\,\bar{y}\,\bar{z}(\lambda)\,\mathrm{d}\lambda \quad (22)$$

where I_0 is the incident light; κ is the absorption coefficient as obtained from the theoretical (TD-DFT) oscillator strengths; l is the actual path length of light through the sample; $\bar{x}\,\bar{y}\,\bar{z}$ are the tristimulus color matching function giving the chromatic response of an observer as defined by CIE; and N is a normalization factor.

As regards simulations with explicit solvent, we recently performed QM/MM-MD simulations on the prototypical 3-*OMe*-cyanidin···quercetin copigmentation system. This method predicted a bathochromic shift of 0.36 eV, which is very close to that obtained using SS-PCM-TD-ωB97XD/cc-PVDZ calculations (0.41 eV, see above).[173] This case study confirmed that the direct impact of the solvent on the absorption properties of anthocyanin systems is relatively weak, and that conformational fluctuations are important. In addition, these simulations also revealed five copigmentation conformers arranged in very similar ways to those identified in our earlier systematic pure-QM search. The dynamic network of intermolecular solute−solvent hydrogen bonding appeared to weaken all of the intramolecular hydrogen bonds (C3-OH···O4, C3′−OH···O4′, and C4′−OH···O3′) except for the strong C5-OH···O4 intramolecular hydrogen bond in quercetin (which was present for 98.6% of the MD simulation time). This QM/MM approach is based on a fully self-consistent polarizable embedding (PE) scheme.[358,359] A series of snapshots along the MD simulation is collected, and TD-DFT calculations are performed on each snapshot to evaluate the optical properties that are averaged on the whole collection of geometries. As far as the series of snapshots is sufficiently characteristic of rearrangements occurring in real solutions, this technique is adapted for calculations of UV−vis as well as CD spectra.[360] It is much relevant and promising to tackle unresolved questions of copigmentation.

The spectral shifts observed in copigmentation are usually small, on the order of 0.01−0.2 eV (i.e., 2−40 nm at ca. 500 nm). Therefore, the method must be as accurate as possible and any potential sources of error should be accounted for and controlled. We wish to strongly emphasize that an inappropriate choice of XC functional combined with classical PCM models may result in error compensation, producing a seemingly correct qualitative description that must be interpreted with great care. Such approaches are very unlikely to produce reliable quantitative predictions other than by pure chance. Ideally, such error compensation should be avoided and recent theoretical studies have paved the way toward a safe method based on coupled TD-DFT/MM approaches.[173,353,357]

Last but not the least, the vibrational structure of copigmentation spectra must be analyzed. To minimize computational time, most works in this field focus on computing the vertical transition energy, which is then compared to the experimental E_{MAX} (λ_{MAX}). However, estimating the performance of a QM method based on vertical transition calculations is likely to systematically bias the conclusion. A rough 0.1−0.3 eV shift is expected when comparing a vertical transition wavelength to the maximum absorption wavelength, simply because these two values do not actually provide the same information.[361] The comparison to experimental data is affected by conformational and solvent broadening and also by vibrational corrections (via the Franck−Condon factor). The first-moment ^1M therefore appears to be a more robust parameter for such purposes; it can be compared to experimental λ_{MAX}, values using the expression:[361,362]

$$^1M = \int \upsilon L(\upsilon)\,\mathrm{d}\upsilon \quad (23)$$

where υ is the frequency and $L(\upsilon)$ is the absorption spectrum line shape, which can be obtained by

$$L(\upsilon) = \sum_{i,f} \rho_i(T)|\langle w_i|\mu_{if}|w_f\rangle|^2\delta(E_f - E_i + h\nu) \quad (24)$$

where $\rho_i(T)$ is the Boltzmann distribution of the vibrational state i; $\langle w_i|\mu_{if}|w_f\rangle$ is the transition dipole moment; $|w_i\rangle$ and $|w_f\rangle$ are the initial and final states, respectively; and E_i and E_f are their respective energies. In other words, ^1M is the center of gravity of the spectrum in a given region.

11. CONCLUDING REMARKS, FUTURE NEEDS, AND APPLICATIONS

There is everlasting interest for safe and efficient ways to prepare foods with a wider variety of dyes and pigments that are stable under the conditions used in food preparation and conservation, as well as safe and suitable for consumption. Copigmentation has recently attracted great interest in food industry. The reason for this interest can be attributed to the recent advances in the field, which offer opportunities to design new combinations of natural pigment and copigment (dye and co-dye) with stable and finely tuned colors. The joint theoretical and experimental studies can now provide a molecular understanding of copigmentation with the sake of such real-world applications. However, although experimental techniques have provided insight into many aspects of copigmentation, there remain a number of major challenges to be addressed. Namely, comprehensive structure affinity relationships have still to be established and the different contributions to copigmentation complex stability should be better unraveled. This is a complex issue as this process is particularly environment-dependent (solvent, pH, temperature, and metal ions), which is of crucial importance in food applications. This underdeveloped field should benefit from the application of advanced techniques (e.g., isothermal titration calorimetry, NMR with NOE, and molecular balances), which have already provided useful insights in the field of supramolecular chemistry. Further research may also benefit from the systematic design of model copigmentation complexes to better establish structure-affinity and structure-optical-property relationships.

State-of-the-art theoretical calculations are increasingly capable of addressing the conformations and supramolecular bonding arrangements of pigment-copigment pairs. To accu-

DOI: 10.1021/acs.chemrev.5b00507
Chem. Rev. 2016, 116, 4937−4982

rately evaluate the Gibbs energy of association and spectral features of such copigmentation complexes, it is necessary to adopt a combination of (biased) MD simulations and DFT with modern functionals, including corrections for dispersion and/or long-range separation. The advanced theoretical calculations may support experimental data in the identification of individual contributions to copigmentation complex stability (e.g., hydrophobic effect, dispersion forces, $\pi-\pi$-stacking, exchange term, and hydrogen bonding). By understanding these interactions, we can rationalize their spectral consequences (i.e., bathochromic and hyperchromic shifts). Many theoretical challenges remain to be addressed, however, including: (i) identifying factors that favor self-association over copigmentation or vice versa; (ii) characterizing metal-mediated copigmentation, which has only been addressed by a few computational investigations[335] and which is poorly understood in many respects, it is not clear how flavylium deprotonation and metal binding (which itself induces proton loss) affect the thermodynamics of copigmentation and induce spectral change; and (iii) coming to a better understanding of band broadening in the UV−vis spectra of copigmentation complexes, which significantly influence their perceived color.

AUTHOR INFORMATION

Corresponding Authors

*E-mail: patrick.trouillas@unilim.fr.
*E-mail: michal.otyepka@upol.cz.

Notes

The authors declare no competing financial interest.

Biographies

Patrick Trouillas received his Ph.D. degree in solid-state physics (optoelectronic properties of fullerene) at the University of Limoges (France). He then joined CEA for a postdoctoral position dealing with thermal exchanges in thin solid films. In 2000, he reoriented his research toward natural compounds (e.g., polyphenols) and pharmaceutical/cosmetic applications. He is currently Assistant Professor at the University of Limoges, jointly affiliated to (i) INSERM-U850 (Limoges) and (ii) the Regional Centre of Advanced Technologies and Materials in Olomouc (Czech Republic). Within active EU networks, he has extensively worked on Molecular Modeling as a tool to rationalize: (i) drug-lipid bilayer interaction and membrane crossing; (ii) biological (antioxidant) properties of natural compounds; and (iii) pigments and dyes' molecular properties. This gave P.T. the opportunity to meet J-C.S-G, J.G., and M.O., with whom he has developed many research projects; he met V.F. and O.D. within the international polyphenol community.

Juan-Carlos Sancho-García completed a Ph.D. in Quantum and Computational Chemistry in 2001. During that period, he also held (1999) a Research Fellowship of the J. Heyrovský Institute of Physical Chemistry in Prague (Czech Republic). He later worked (2002−2004) as a Marie Curie Fellowship at the Laboratory for Chemistry of Novel Materials in Mons (Belgium). He obtained (2005) a tenured-track "Ramón y Cajal" Postdoctoral Senior Grant at the University of Alicante, becoming next (2010) an Associate Professor and Lecturer in Physical Chemistry. He has also recently served as an external scientific advisor for high-tech companies and research hubs, such as the Samsung Advanced Institute of Technology, and led as Principal Investigator research projects uninterruptedly from 2004. His main research interest has always been the development and application of DFT methods to challenging systems, in various fields of Chemistry and Materials Science. He met Patrick Trouillas in 2009 and started to work on pigmentation and copigmentation issues, after some preliminary theoretical studies on polyphenol compounds. This fruitful collaboration crystallized in joint publications and in the associated training of young researchers.

Victor De Freitas graduated in Chemistry from the Faculty of Science of the University of Porto (FCUP) in 1984. In 1995, he obtained his Ph.D. in Biological and Medical Sciences in the University of Bordeaux II (France), with a specialization in Oenology. After his Ph.D., he returned to the Department of Chemistry and Biochemistry (DQB) of FCUP, where he has been developing his teaching and research activities. He is currently Full Professor at the University of Porto and member of the REQUIMTE-LAQV Research Centre, where he has been developing an independent area of research on polyphenol compounds: (i) chemical transformations resulting from oxidation processes of polyphenolic pigments, including technological applications in the food industry; (ii) interaction of different classes of polyphenols with proteins in the sensory and nutritional context; and (iii) antioxidant and biological properties of polyphenolic compounds.

Johannes Gierschner received his Ph.D. in Physical Chemistry in Tübingen, Germany (2000). After stays in Tübingen, Mons, and Georgia Tech, Atlanta, GA, he joined IMDEA Nanoscience in 2008 as a senior researcher (Ramón y Cajal fellow, 2008−2013). From 2008−2010, he was a visiting researcher at the University of Valencia, and since 2009, he is regular visiting researcher at Seoul National University. In 2013, he completed his habilitation (Priv. Doz., University Tübingen). His work integrates optical spectroscopy and computational chemistry to elucidate structure−property relationships in conjugated organic materials.

Michal Otyepka received his Ph.D. degree in Physical Chemistry at the Palacký University, Olomouc, Czech Republic (2004). Currently, he is a head of the Department of Physical Chemistry and vice-director of the Regional Centre of Advanced Technologies and Materials, both at the Palacký University, Olomouc. His research is mostly focused on modeling of biomacromolecules, 2D materials and their interactions, and chemistry of graphene derivatives.

Olivier Dangles studied chemistry at the Ecole Normale Supérieure of Cachan, France (1981−1985), and he obtained a Ph.D. in organic chemistry at the University of Paris-Orsay (1989). He was an assistant professor at the University of Strasbourg (1989−1992), and then a researcher at the National Center of Scientific Research (CNRS, 1992−1995), where he devoted his research to the chemistry of anthocyanins in relation to the expression of natural colors (group of Prof. R. Brouillard). In 1995, he was appointed a Prof. of chemistry at the University of Lyon. Since 2000, he has been a Prof. of chemistry at the University of Avignon, and he works in a joint research unit of Avignon University and the National Institute for Agricultural Research (INRA). His main research topics deal with the chemistry of polyphenols and carotenoids in relation to their coloring properties and their effects on human health: (i) mechanisms of oxidation and antioxidant activity; (ii) interactions with proteins; and (iii) lipids and metal ions and chemical synthesis of metabolites.

ACKNOWLEDGMENTS

P.T. thanks the "Conseil Régional du Limousin" for financial support and CALI (CAlcul en LImousin). Financial support from the Czech Science Foundation (P208/12/G016), the Ministry of Education, Youth and Sports of the Czech Republic (project LO1305), and the Operational Program Education for Competitiveness-European Social Fund (project CZ.1.07/2.3.00/20.0058 of the Ministry of Education, Youth and Sports of the Czech Republic) is also gratefully acknowledged. The

DOI: 10.1021/acs.chemrev.5b00507
Chem. Rev. 2016, 116, 4937−4982

work at IMDEA was supported by the Spanish Ministerio de Economía y Competitividad (MINECO; project CTQ2014-58801). P.T. thanks F. Di Meo and G. Fabre for fruitful discussions on noncovalent interactions and B. Chantemargue for giving a last minute helping hand.

ABBREVIATIONS AND SYMBOLS

AH^+	flavylium cation
A	neutral quinonoid base
A^-	anionic neutral quinonoid base
B	hemiketal
BSSE	basis set superposition error
BJ	Becke-Johnson
C_{cis}	*cis*-chalcone
C_{trans}	*trans*-chalcone
CC2	second-order approximate coupled cluster singles and doubles
CBS	complete basis set
CCSD	coupled-cluster singles and doubles
CCSD(T)	coupled-cluster singles, doubles, and triples
CD	circular dichroism
CI	configuration interaction
CIE	commission international de l'éclairage
CASPT2	complete-active-space perturbation theory
COSMO	conductor-like solvation model
CP	copigment
CT	charge transfer
dDsC	density-dependent energy dispersion energy correction
DFT	density functional theory
DFTB	density functional tight binding
DLPNO	domain-based local pair-natural-orbitals
DSSC	dye-sensitized solar cells
ES	excited state
GB	generalized born
HCA	hydroxycinnamic acid
HF	Hartree−Fock
IEFPCM	integral equation formalism polarizable continuum model
LR	linear-response
MAD	mean absolute deviation
MD	molecular dynamics
MDQ	MD with quenching
MetaD	meta-dynamics
MM	molecular mechanics
MM-GBSA	molecular mechanics- Poisson−Boltzmann/surface area
MM-PBSA	molecular mechanics-generalized born/surface area
MO	molecular orbital
MP2	second order Møller−Plesset perturbation theory
NMR	nuclear magnetic resonance
NOE	nuclear Overhauser effect
NTO	natural transition orbital
PCM	polarizable continuum model
PB	Poisson−Boltzmann
QM	quantum mechanics
REMD	replica exchange MD (REMD)
RSH	range-separated hybrid functionals
SA	surface area
SCS	spin-component-scaled
SS-PCM	state-specific polarizable continuum model
SS	state-specific
TD-DFT	time-dependent density functional theory
TD-HF	time-dependent Hartree−Fock
vdW-TS	van der Waals Tkatchenko-Scheffler correction
VV10	Vydrov-Voorhis nonlocal correlation functional
XC	exchange-correlation
XDM	exchange-hole dipole moment
ZINDO	Zerner's intermediate neglect of differential overlap-ZINDO

REFERENCES

(1) Yoshida, K.; Mori, M.; Kondo, T. Blue Flower Color Development by Anthocyanins: From Chemical Structure to Cell Physiology. *Nat. Prod. Rep.* **2009**, *26* (7), 857−964.
(2) Boulton, R. The Copigmentation of Anthocyanins and Its Role in the Color of Red Wine: A Critical Review. *Am. J. Enol. Vitic.* **2001**, *52* (2), 67−87.
(3) Landrum, J. T. *Carotenoids: Physical, Chemical, and Biological Functions and Properties*; CRC Press: Boca Raton, 2010.
(4) Haslam, E. *Practical Polyphenolics*; Cambridge University Press, 1998.
(5) Lee, D. *Nature's Palette: The Science of Plant Color*, Reprint ed.; University Of Chicago Press: Chicago, 2010.
(6) Willstätter, R.; Everest, A. E. Untersuchungen Über Die Anthocyane. I. Über Den Farbstoff Der Kornblume. *Justus Liebigs Ann. Chem.* **1913**, *401* (2), 189−232.
(7) Asen, S.; Stewart, R. N.; Norris, K. H. Anthocyanin, Flavonol Copigments, and pH Responsible for Larkspur Flower Colour. *Phytochemistry* **1975**, *14* (12), 2677−2682.
(8) Castañeda-Ovando, A.; Pacheco-Hernández, M.; de, L.; Páez-Hernández, M. E.; Rodríguez, J. A.; Galán-Vidal, C. A. Chemical Studies of Anthocyanins: A Review. *Food Chem.* **2009**, *113* (4), 859−871.
(9) He, F.; Liang, N.-N.; Mu, L.; Pan, Q.-H.; Wang, J.; Reeves, M. J.; Duan, C.-Q. Anthocyanins and Their Variation in Red Wines I. Monomeric Anthocyanins and Their Color Expression. *Molecules* **2012**, *17* (12), 1571−1601.
(10) Andersen, O. M.; Markham, K. R. *Flavonoids: Chemistry, Biochemistry and Applications*; CRC Press, 2005.
(11) Fulcrand, H.; Dueñas, M.; Salas, E.; Cheynier, V. Phenolic Reactions during Winemaking and Aging. *Am. J. Enol. Vitic.* **2006**, *57* (3), 289−297.
(12) Cheynier, V.; Dueñas-Paton, M.; Salas, E.; Maury, C.; Souquet, J.-M.; Sarni-Manchado, P.; Fulcrand, H. Structure and Properties of Wine Pigments and Tannins. *Am. J. Enol. Vitic.* **2006**, *57* (3), 298−305.
(13) de Freitas, V.; Mateus, N. Formation of Pyranoanthocyanins in Red Wines: A New and Diverse Class of Anthocyanin Derivatives. *Anal. Bioanal. Chem.* **2011**, *401* (5), 1463−1473.
(14) Mateus, N.; Silva, A. M. S.; Santos-Buelga, C.; Rivas-Gonzalo, J. C.; de Freitas, V. Identification of Anthocyanin-Flavanol Pigments in Red Wines by NMR and Mass Spectrometry. *J. Agric. Food Chem.* **2002**, *50* (7), 2110−2116.
(15) Mateus, N.; Oliveira, J.; Haettich-Motta, M.; de Freitas, V. New Family of Bluish Pyranoanthocyanins. *J. Biomed. Biotechnol.* **2004**, *2004* (5), 299−305.
(16) He, J.; Carvalho, A. R. F.; Mateus, N.; De Freitas, V. Spectral Features and Stability of Oligomeric Pyranoanthocyanin-Flavanol Pigments Isolated from Red Wines. *J. Agric. Food Chem.* **2010**, *58* (16), 9249−9258.
(17) He, J.; Oliveira, J.; Silva, A. M. S.; Mateus, N.; De Freitas, V. Oxovitisins: A New Class of Neutral Pyranone-Anthocyanin Derivatives in Red Wines. *J. Agric. Food Chem.* **2010**, *58* (15), 8814−8819.
(18) Chassaing, S.; Isorez, G.; Kueny-Stotz, M.; Brouillard, R. En Route to Color-Stable Pyranoflavylium Pigments—a Systematic Study of the Reaction between 5-Hydroxy-4-Methylflavylium Salts and Aldehydes. *Tetrahedron Lett.* **2008**, *49* (49), 6999−7004.
(19) Oliveira, J.; Mateus, N.; Freitas, V. de. Synthesis of a New Bluish Pigment from the Reaction of a Methylpyranoanthocyanin with Sinapaldehyde. *Tetrahedron Lett.* **2011**, *52* (16), 1996−2000.

DOI: 10.1021/acs.chemrev.5b00507
Chem. Rev. 2016, 116, 4937−4982

(20) Brouillard, R.; Dubois, J.-E. Mechanism of the Structural Transformations of Anthocyanins in Acidic Media. *J. Am. Chem. Soc.* **1977**, *99* (5), 1359−1364.
(21) McClelland, R. A.; Gedge, S. Hydration of the Flavylium Ion. *J. Am. Chem. Soc.* **1980**, *102* (18), 5838−5848.
(22) Pina, F.; Melo, M. J.; Laia, C. A. T.; Parola, A. J.; Lima, J. C. Chemistry and Applications of Flavylium Compounds: A Handful of Colours. *Chem. Soc. Rev.* **2012**, *41* (2), 869−908.
(23) Pina, F. Chemical Applications of Anthocyanins and Related Compounds. A Source of Bioinspiration. *J. Agric. Food Chem.* **2014**, *62* (29), 6885−6897.
(24) Nave, F.; Petrov, V.; Pina, F.; Teixeira, N.; Mateus, N.; de Freitas, V. Thermodynamic and Kinetic Properties of a Red Wine Pigment: Catechin-(4,8)-Malvidin-3- *O* -Glucoside. *J. Phys. Chem. B* **2010**, *114* (42), 13487−13496.
(25) Mora-Soumille, N.; Al Bittar, S.; Rosa, M.; Dangles, O. Analogs of Anthocyanins with a 3′,4′-Dihydroxy Substitution: Synthesis and Investigation of Their Acid−base, Hydration, Metal Binding and Hydrogen-Donating Properties in Aqueous Solution. *Dyes Pigm.* **2013**, *96* (1), 7−15.
(26) Yan, Q.; Zhang, L.; Zhang, X.; Liu, X.; Yuan, F.; Hou, Z.; Gao, Y. Stabilization of Grape Skin Anthocyanins by Copigmentation with Enzymatically Modified Isoquercitrin (EMIQ) as a Copigment. *Food Res. Int.* **2013**, *50* (2), 603−609.
(27) Fanzone, M.; González-Manzano, S.; Pérez-Alonso, J.; Escribano-Bailón, M. T.; Jofré, V.; Assof, M.; Santos-Buelga, C. Evaluation of Dihydroquercetin-3-O-Glucoside from Malbec Grapes as Copigment of Malvidin-3-O-Glucoside. *Food Chem.* **2015**, *175*, 166−173.
(28) Baranac, J. M.; Petranovic, N. A.; Dimitric-Markovic, J. M. Spectrophotometric Study of Anthocyan Copigmentation Reactions. 2. Malvin and the Nonglycosidized Flavone Quercetin. *J. Agric. Food Chem.* **1997**, *45* (5), 1694−1697.
(29) Dimitrić-Marković, J. M.; Petranović, N. A.; Baranac, J. M. A Spectrophotometric Study of the Copigmentation of Malvin with Caffeic and Ferulic Acids. *J. Agric. Food Chem.* **2000**, *48* (11), 5530−5536.
(30) Dimitrić-Marković, J. M.; Baranac, J. M.; Brdaric, T. P. Electronic and Infrared Vibrational Analysis of Cyanidin-Quercetin Copigment Complex. *Spectrochim. Acta, Part A* **2005**, *62*, 673−680.
(31) Lambert, S. G.; Asenstorfer, R. E.; Williamson, N. M.; Iland, P. G.; Jones, G. P. Copigmentation between Malvidin-3-Glucoside and Some Wine Constituents and Its Importance to Colour Expression in Red Wine. *Food Chem.* **2011**, *125* (1), 106−115.
(32) Malaj, N.; De Simone, B. C.; Quartarolo, A. D.; Russo, N. Spectrophotometric Study of the Copigmentation of Malvidin 3-O-Glucoside with P-Coumaric, Vanillic and Syringic Acids. *Food Chem.* **2013**, *141* (4), 3614−3620.
(33) Willstätter, R.; Zollinger, E. H. XVI. Über Die Farbstoffe Der Weintraube Und Der Heidelbeere, II. *Justus Liebigs Ann. Chem.* **1917**, *412* (2), 195−216.
(34) Robinson, G. M.; Robinson, R. A Survey of Anthocyanins. I. *Biochem. J.* **1931**, *25* (5), 1687−1705.
(35) Asen, S.; Stewart, R. N.; Norris, K. H.; Massie, D. R. A Stable Blue Non-Metallic Co-Pigment Complex of Delphanin and C-Glycosyl-flavones in Prof. Blaauw Iris. *Phytochemistry* **1970**, *9* (3), 619−627.
(36) Asen, S.; Stewart, R. N.; Norris, K. H. Co-Pigmentation Effect of Quercetin Glycosides on Absorption Characteristics of Cyanidin Glycosides and Color of Red Wing Azalea. *Phytochemistry* **1971**, *10* (1), 171−175.
(37) Asen, S.; Stewart, R. N.; Norris, K. H. Co-Pigmentation of Anthocyanins in Plant Tissues and Its Effect on Color. *Phytochemistry* **1972**, *11* (3), 1139−1144.
(38) Asen, S.; Norris, K. H.; Stewart, R. N. Copigmentation of Aurone and Flavone from Petals of Antirrhinum Majus. *Phytochemistry* **1972**, *11* (9), 2739−2741.
(39) Hoshino, T.; Matsumoto, U.; Goto, T. Self-Association of Some Anthocyanins in Neutral Aqueous Solution. *Phytochemistry* **1981**, *20* (8), 1971−1976.
(40) Hoshino, T.; Matsumoto, U.; Harada, N.; Goto, T. Chiral Exciton Coupled Stacking of Anthocyanins: Interpretation of the Origin of Anomalous CD Induced by Anthocyanin Association. *Tetrahedron Lett.* **1981**, *22* (37), 3621−3624.
(41) Hoshino, T.; Matsumoto, U.; Goto, T. Evidences of the Self-Association of Anthocyanins I. Circular Dichroism of Cyanin Anhydrobase. *Tetrahedron Lett.* **1980**, *21* (18), 1751−1754.
(42) Hoshino, T.; Matsumoto, U.; Goto, T.; Harada, N. Evidence for the Self-Association of Anthocyanins IV. PMR Spectroscopic Evidence for the Vertical Stacking of Anthocyanin Molecules. *Tetrahedron Lett.* **1982**, *23* (4), 433−436.
(43) Hoshino, T.; Goto, T. Effects of pH and Concentration on the Self-Association of Malvin Quinonoidal Base: Electronic and Circular Dichroic Studies. *Tetrahedron Lett.* **1990**, *31* (11), 1593−1596.
(44) Hoshino, T. Self-Association of Flavylium Cations of Anthocyanidin 3,5-Diglucosides Studied by Circular Dichroism and 1H NMR. *Phytochemistry* **1992**, *31* (2), 647−653.
(45) Hoshino, T. An Approximate Estimate of Self-Association Constants and the Self-Stacking Conformation of Malvin Quinonoidal Bases Studied by 1H NMR. *Phytochemistry* **1991**, *30* (6), 2049−2055.
(46) Brouillard, R.; Mazza, G.; Saad, Z.; Albrecht-Gary, A. M.; Cheminat, A. The Co-Pigmentation Reaction of Anthocyanins: A Microprobe for the Structural Study of Aqueous Solutions. *J. Am. Chem. Soc.* **1989**, *111* (7), 2604−2610.
(47) Figueiredo, P.; Elhabiri, M.; Saito, N.; Brouillard, R. Anthocyanin Intramolecular Interactions. A New Mathematical Approach To Account for the Remarkable Colorant Properties of the Pigments Extracted from *Matthiola Incana*. *J. Am. Chem. Soc.* **1996**, *118* (20), 4788−4793.
(48) Figueiredo, P.; Elhabiri, M.; Toki, K.; Saito, N.; Dangles, O.; Brouillard, R. New Aspects of Anthocyanin Complexation. Intramolecular Copigmentation as a Means for Colour Loss? *Phytochemistry* **1996**, *41* (1), 301−308.
(49) Zhang, B.; Liu, R.; He, F.; Zhou, P.-P.; Duan, C.-Q. Copigmentation of Malvidin-3-O-Glucoside with Five Hydroxybenzoic Acids in Red Wine Model Solutions: Experimental and Theoretical Investigations. *Food Chem.* **2015**, *170*, 226−233.
(50) Teixeira, N.; Cruz, L.; Brás, N. F.; Mateus, N.; Ramos, M. J.; de Freitas, V. Structural Features of Copigmentation of Oenin with Different Polyphenol Copigments. *J. Agric. Food Chem.* **2013**, *61* (28), 6942−6948.
(51) Fossen, T.; Rayyan, S.; Holmberg, M. H.; Nimtz, M.; Andersen, Ø. M. Covalent Anthocyanin−flavone Dimer from Leaves of Oxalis Triangularis. *Phytochemistry* **2007**, *68* (5), 652−662.
(52) Saito, N.; Nakamura, M.; Shinoda, K.; Murata, N.; Kanazawa, T.; Kato, K.; Toki, K.; Kasai, H.; Honda, T.; Tatsuzawa, F. Covalent Anthocyanin−flavonol Complexes from the Violet-Blue Flowers of Allium "Blue Perfume. *Phytochemistry* **2012**, *80*, 99−108.
(53) Hayashi, K.; Abe, Y.; Mitsui, S. Blue Anthocyanin from the Flowers of Commelina, the Crystallisation and Some Properties Thereof. *Proc. Jpn. Acad.* **1958**, *34* (6), 373−378.
(54) Shibata, K.; Shibata, Y.; Kasiwagi, I. Studies on Anthocyanins: Color Variationin Anthocyanins. *J. Am. Chem. Soc.* **1919**, *41* (2), 208−220.
(55) Bloor, S. J. Blue Flower Colour Derived from Flavonol-Anthocyanin Co-Pigmentation in Ceanothus Papillosus. *Phytochemistry* **1997**, *45* (7), 1399−1405.
(56) Tamura, H.; Kondo, T.; Goto, T. The Composition of Commelinin, a Highly Associated Metalloanthocaynin Present in the Blue Flower Petals of Commelina Communis. *Tetrahedron Lett.* **1986**, *27* (16), 1801−1804.
(57) Kondo, T.; Ueda, M.; Isobe, M.; Goto, T. A New Molecular Mechanism of Blue Color Development with Protocyanin, a Supramolecular Pigment from Cornflower, Centaurea Cyanus. *Tetrahedron Lett.* **1998**, *39* (45), 8307−8310.
(58) Kondo, T.; Oyama, K.; Yoshida, K. Chiral Molecular Recognition on Formation of a Metalloanthocyanin: A Supramolecular Metal Complex Pigment from Blue Flowers of Salvia Patens. *Angew. Chem., Int. Ed.* **2001**, *40* (5), 894−897.

DOI: 10.1021/acs.chemrev.5b00507
Chem. Rev. 2016, 116, 4937−4982

(59) Mori, M.; Kondo, T.; Yoshida, K. Cyanosalvianin, a Supramolecular Blue Metalloanthocyanin, from Petals of Salvia Uliginosa. *Phytochemistry* **2008**, *69* (18), 3151−3158.
(60) Yoshida, K.; Toyama-Kato, Y.; Kameda, K.; Kondo, T. Sepal Color Variation of Hydrangea Macrophylla and Vacuolar pH Measured with a Proton-Selective Microelectrode. *Plant Cell Physiol.* **2003**, *44* (3), 262−268.
(61) Kondo, T.; Toyama-Kato, Y.; Yoshida, K. Essential Structure of Co-Pigment for Blue Sepal-Color Development of Hydrangea. *Tetrahedron Lett.* **2005**, *46* (39), 6645−6649.
(62) Tanaka, M.; Fujimori, T.; Uchida, I.; Yamaguchi, S.; Takeda, K. A Malonylated Anthocyanin and Flavonols in Blue Meconopsis Flowers. *Phytochemistry* **2001**, *56* (4), 373−376.
(63) Yoshida, K.; Kitahara, S.; Ito, D.; Kondo, T. Ferric Ions Involved in the Flower Color Development of the Himalayan Blue Poppy, Meconopsis Grandis. *Phytochemistry* **2006**, *67* (10), 992−998.
(64) Markham, K. R.; Mitchell, K. A.; Boase, M. R. Malvidin-3-O-Glucoside-5-O-(6-Acetylglucoside) and Its Colour Manifestation in "Johnson"s Blue' and Other "Blue" Geraniums. *Phytochemistry* **1997**, *45* (2), 417−423.
(65) Yabuya, T.; Nakamura, M.; Iwashina, T.; Yamaguchi, M.; Takehara, T. Anthocyanin-Flavone Copigmentation in Bluish Purple Flowers of Japanese Garden Iris (Iris Ensata Thunb.). *Euphytica* **1997**, *98* (3), 163−167.
(66) Bimpilas, A.; Tsimogiannis, D.; Balta-Brouma, K.; Lymperopoulou, T.; Oreopoulou, V. Evolution of Phenolic Compounds and Metal Content of Wine during Alcoholic Fermentation and Storage. *Food Chem.* **2015**, *178*, 164−171.
(67) Hermosín Gutiérrez, I. Influence of Ethanol Content on the Extent of Copigmentation in a Cencibel Young Red Wine. *J. Agric. Food Chem.* **2003**, *51* (14), 4079−4083.
(68) Monagas, M.; Bartolomé, B. Anthocyanins and Anthocyanin-Derived Compounds. In *Wine Chemistry and Biochemistry*; Moreno-Arribas, M. V., Polo, M. C., Eds.; Springer: New York, 2009; pp 439−462.
(69) Rustioni, L.; Bedgood, D. R.; Failla, O.; Prenzler, P. D.; Robards, K. Copigmentation and Anti-Copigmentation in Grape Extracts Studied by Spectrophotometry and Post-Column-Reaction HPLC. *Food Chem.* **2012**, *132* (4), 2194−2201.
(70) De Rosso, M.; Tonidandel, L.; Larcher, R.; Nicolini, G.; Dalla Vedova, A.; De Marchi, F.; Gardiman, M.; Giust, M.; Flamini, R. Identification of New Flavonols in Hybrid Grapes by Combined Liquid Chromatography−mass Spectrometry Approaches. *Food Chem.* **2014**, *163*, 244−251.
(71) Kelebek, H.; Canbas, A.; Selli, S. HPLC-DAD−MS Analysis of Anthocyanins in Rose Wine Made From Cv. Öküzgözü Grapes, and Effect of Maceration Time on Anthocyanin Content. *Chromatographia* **2007**, *66* (3−4), 207−212.
(72) Gordillo, B.; Rodríguez-Pulido, F. J.; González-Miret, M. L.; Quijada-Morín, N.; Rivas-Gonzalo, J. C.; García-Estévez, I.; Heredia, F. J.; Escribano-Bailón, M. T. Application of Differential Colorimetry To Evaluate Anthocyanin−Flavonol−Flavanol Ternary Copigmentation Interactions in Model Solutions. *J. Agric. Food Chem.* **2015**, *63* (35), 7645−7653.
(73) Somers, T. C.; Vérette, E. Phenolic Composition of Natural Wine Types. In *Wine Analysis*; Linskens, P. D. H.-F., Jackson, P. D. J. F., Eds.; Modern Methods of Plant Analysis; Springer: Berlin, 1988; pp 219−257.
(74) González-Manzano, S.; Dueñas, M.; Rivas-Gonzalo, J. C.; Escribano-Bailón, M. T.; Santos-Buelga, C. Studies on the Copigmentation between Anthocyanins and Flavan-3-Ols and Their Influence in the Colour Expression of Red Wine. *Food Chem.* **2009**, *114* (2), 649−656.
(75) Fernandes, A.; Brás, N. F.; Mateus, N.; Freitas, V. de. A Study of Anthocyanin Self-Association by NMR Spectroscopy. *New J. Chem.* **2015**, *39* (4), 2602−2611.
(76) Heras-Roger, J.; Pomposo-Medina, M.; Díaz-Romero, C.; Darias-Martín, J. Copigmentation, Colour and Antioxidant Activity of Single-Cultivar Red Wines. *Eur. Food Res. Technol.* **2014**, *239* (1), 13−19.
(77) García-Marino, M.; Escudero-Gilete, M. L.; Heredia, F. J.; Escribano-Bailón, M. T.; Rivas-Gonzalo, J. C. Color-Copigmentation Study by Tristimulus Colorimetry (CIELAB) in Red Wines Obtained from Tempranillo and Graciano Varieties. *Food Res. Int.* **2013**, *51* (1), 123−131.
(78) Schwarz, M.; Picazo-Bacete, J. J.; Winterhalter, P.; Hermosín-Gutiérrez, I. Effect of Copigments and Grape Cultivar on the Color of Red Wines Fermented after the Addition of Copigments. *J. Agric. Food Chem.* **2005**, *53* (21), 8372−8381.
(79) Aleixandre-Tudó, J. L.; Álvarez, I.; Lizama, V.; García, M. J.; Aleixandre, J. L.; Du Toit, W. J. Impact of Caffeic Acid Addition on Phenolic Composition of Tempranillo Wines from Different Wine-making Techniques. *J. Agric. Food Chem.* **2013**, *61* (49), 11900−11912.
(80) Gris, E. F.; Ferreira, E. A.; Falcão, L. D.; Bordignon-Luiz, M. T. Influence of Ferulic Acid on Stability of Anthocyanins from Cabernet Sauvignon Grapes in a Model System and a Yogurt System. *Int. J. Food Sci. Technol.* **2007**, *42* (8), 992−998.
(81) Talcott, S. T.; Peele, J. E.; Brenes, C. H. Red Clover Isoflavonoids as Anthocyanin Color Enhancing Agents in Muscadine Wine and Juice. *Food Res. Int.* **2005**, *38* (10), 1205−1212.
(82) Liu, S.; Fu, Y.; Nian, S. Buffering Colour Fluctuation of Purple Sweet Potato Anthocyanins to Acidity Variation by Surfactants. *Food Chem.* **2014**, *162*, 16−21.
(83) Kovac, V.; Alonso, E.; Bourzeix, M.; Revilla, E. Effect of Several Enological Practices on the Content of Catechins and Proanthocyanidins of Red Wines. *J. Agric. Food Chem.* **1992**, *40* (10), 1953−1957.
(84) Canals, R.; del Carmen Llaudy, M.; Canals, J. M.; Zamora, F. Influence of the Elimination and Addition of Seeds on the Colour, Phenolic Composition and Astringency of Red Wine. *Eur. Food Res. Technol.* **2008**, *226* (5), 1183−1190.
(85) Escribano-Bailon, M. T.; Santos-Buelga, C. Anthocyanin Copigmentation - Evaluation, Mechanisms and Implications for the Colour of Red Wines. *Curr. Org. Chem.* **2012**, *16* (6), 715−723.
(86) Quijada-Morín, N.; Dangles, O.; Rivas-Gonzalo, J. C.; Escribano-Bailón, M. T. Physico-Chemical and Chromatic Characterization of Malvidin 3-Glucoside-Vinylcatechol and Malvidin 3-Glucoside-Vinylguaiacol Wine Pigments. *J. Agric. Food Chem.* **2010**, *58* (17), 9744−9752.
(87) Oliveira, J.; Mateus, N.; Silva, A. M. S.; de Freitas, V. Equilibrium Forms of Vitisin B Pigments in an Aqueous System Studied by NMR and Visible Spectroscopy. *J. Phys. Chem. B* **2009**, *113* (32), 11352−11358.
(88) Brouillard, R.; Dangles, O. Anthocyanin Molecular Interactions: The First Step in the Formation of New Pigments during Wine Aging? *Food Chem.* **1994**, *51* (4), 365−371.
(89) Wrolstad, R. E.; Erlandson, J. A. Effect of Metal Ions on the Color of Strawberry Puree. *J. Food Sci.* **1973**, *38* (3), 460−463.
(90) Starr, M. S.; Francis, F. J. Effect of Metallic Ions on Color and Pigment Content of Cranberry Juice Cocktail. *J. Food Sci.* **1973**, *38* (6), 1043−1046.
(91) Kallio, H.; Pallasaho, S.; Kärppä, J.; Linko, R. R. Comparison of the Half-Lives of the Anthocyanins in the Juice of Crowberry, Empetrum Nigrum. *J. Food Sci.* **1986**, *51* (2), 408−410.
(92) Osawa, Y. Chapter 2 - Copigmentation of Anthocyanins. In *Anthocyanins As Food Colors*; Markakis, P., Ed.; Academic Press, 1982; pp 41−68.
(93) Rein, M. J.; Heinonen, M. Stability and Enhancement of Berry Juice Color. *J. Agric. Food Chem.* **2004**, *52* (10), 3106−3114.
(94) Maccarone, E.; Maccarrone, A.; Rapisarda, P. Stabilization of Anthocyanins of Blood Orange Fruit Juice. *J. Food Sci.* **1985**, *50* (4), 901−904.
(95) Wilska-Jeszka, J.; Korzuchowska, A. Anthocyanins and Chlorogenic Acid Copigmentation - Influence on the Colour of Strawberry and Chokeberry Juices. *Z. Lebensm.-Unters. Forsch.* **1996**, *203* (1), 38−42.
(96) Hernández-Herrero, J. A.; Frutos, M. J. Influence of Rutin and Ascorbic Acid in Colour, Plum Anthocyanins and Antioxidant Capacity Stability in Model Juices. *Food Chem.* **2015**, *173*, 495−500.
(97) Sari, P.; Wijaya, C. H.; Sajuthi, D.; Supratman, U. Colour Properties, Stability, and Free Radical Scavenging Activity of Jambolan

DOI: 10.1021/acs.chemrev.5b00507
Chem. Rev. 2016, 116, 4937−4982

(Syzygium Cumini) Fruit Anthocyanins in a Beverage Model System: Natural and Copigmented Anthocyanins. *Food Chem.* **2012**, *132* (4), 1908−1914.
(98) Fischer, U. A.; Carle, R.; Kammerer, D. R. Thermal Stability of Anthocyanins and Colourless Phenolics in Pomegranate (Punica Granatum L.) Juices and Model Solutions. *Food Chem.* **2013**, *138* (2−3), 1800−1809.
(99) Pan, Y.-Z.; Guan, Y.; Wei, Z.-F.; Peng, X.; Li, T.-T.; Qi, X.-L.; Zu, Y.-G.; Fu, Y.-J. Flavonoid C-Glycosides from Pigeon Pea Leaves as Color and Anthocyanin Stabilizing Agent in Blueberry Juice. *Ind. Crops Prod.* **2014**, *58*, 142−147.
(100) Goto, T.; Kondo, T. Struktur Und Molekulare Stapelung von Anthocyanen—Variation Der Blütenfarben. *Angew. Chem.* **1991**, *103* (1), 17−33.
(101) Liao, H.; Cai, Y.; Haslam, E. Polyphenol Interactions. Anthocyanins: Co-Pigmentation and Colour Changes in Red Wines. *J. Sci. Food Agric.* **1992**, *59* (3), 299−305.
(102) Brouillard, R.; Wigand, M.-C.; Dangles, O.; Cheminat, A. pH and Solvent Effects on the Copigmentation Reaction of Malvin with Polyphenols, Purine and Pyrimidine Derivatives. *J. Chem. Soc., Perkin Trans. 2* **1991**, No. 8, 1235−1241.
(103) Baranac, J. M.; Petranovic, N. A.; Dimitric-Markovic, J. M. Spectrophotometric Study of Anthocyan Copigmentation Reactions. *J. Agric. Food Chem.* **1996**, *44* (5), 1333−1336.
(104) Oszmiański, J.; Bakowska, A.; Piacente, S. Thermodynamic Characteristics of Copigmentation Reaction of Acylated Anthocyanin Isolated from Blue Flowers ofScutellaria Baicalensis Georgi with Copigments. *J. Sci. Food Agric.* **2004**, *84* (12), 1500−1506.
(105) Ferreira da Silva, P.; Lima, J. C.; Freitas, A. A.; Shimizu, K.; Maçanita, A. L.; Quina, F. H. Charge-Transfer Complexation as a General Phenomenon in the Copigmentation of Anthocyanins. *J. Phys. Chem. A* **2005**, *109* (32), 7329−7338.
(106) Galland, S.; Mora, N.; Abert-Vian, M.; Rakotomanomana, N.; Dangles, O. Chemical Synthesis of Hydroxycinnamic Acid Glucosides and Evaluation of Their Ability To Stabilize Natural Colors via Anthocyanin Copigmentation. *J. Agric. Food Chem.* **2007**, *55* (18), 7573−7579.
(107) Alluis, B.; Dangles, O. Quercetin (=2-(3,4-Dihydroxyphenyl)-3,5,7-Trihydroxy-4H-1-Benzopyran-4-One) Glycosides and Sulfates: Chemical Synthesis, Complexation, and Antioxidant Properties. *Helv. Chim. Acta* **2001**, *84* (5), 1133−1156.
(108) Nave, F.; Brás, N. F.; Cruz, L.; Teixeira, N.; Mateus, N.; Ramos, M. J.; Di Meo, F.; Trouillas, P.; Dangles, O.; De Freitas, V. Influence of a Flavan-3-Ol Substituent on the Affinity of Anthocyanins (Pigments) toward Vinylcatechin Dimers and Proanthocyanidins (Copigments). *J. Phys. Chem. B* **2012**, *116* (48), 14089−14099.
(109) Dangles, O.; Elhajji, H. Synthesis of 3-Methoxy-and 3-B-D-Glucopyranosy1oxy) Flavylium Ions. Influence of the Flavylium Substitution Pattern on the Reactivity of Anthocyanins in Aqueous Solution. *Helv. Chim. Acta* **1994**, *77* (6), 1595−1610.
(110) Cruz, L.; Brás, N. F.; Teixeira, N.; Mateus, N.; Ramos, M. J.; Dangles, O.; De Freitas, V. Vinylcatechin Dimers Are Much Better Copigments for Anthocyanins than Catechin Dimer Procyanidin B3. *J. Agric. Food Chem.* **2010**, *58* (5), 3159−3166.
(111) Malien-Aubert, C.; Dangles, O.; Amiot, M. J. Influence of Procyanidins on the Color Stability of Oenin Solutions. *J. Agric. Food Chem.* **2002**, *50* (11), 3299−3305.
(112) Benesi, H. A.; Hildebrand, J. H. A Spectrophotometric Investigation of the Interaction of Iodine with Aromatic Hydrocarbons. *J. Am. Chem. Soc.* **1949**, *71* (8), 2703−2707.
(113) Dangles, O.; Brouillard, R. Polyphenol Interactions. The Copigmentation Case: Thermodynamic Data from Temperature Variation and Relaxation Kinetics. Medium Effect. *Can. J. Chem.* **1992**, *70* (8), 2174−2189.
(114) Di Meo, F.; Sancho Garcia, J. C.; Dangles, O.; Trouillas, P. Highlights on Anthocyanin Pigmentation and Copigmentation: A Matter of Flavonoid Π-Stacking Complexation To Be Described by DFT-D. *J. Chem. Theory Comput.* **2012**, *8* (6), 2034−2043.
(115) Awika, J. M. Behavior of 3-Deoxyanthocyanidins in the Presence of Phenolic Copigments. *Food Res. Int.* **2008**, *41* (5), 532−538.
(116) El Hajji, H.; Dangles, O.; Figueiredo, P.; Brouillard, R. 3′-(β-D-Glycopyranosyloxy) Flavylium Ions: Synthesis and Investigation of Their Properties in Aqueous Solution. Hydrogen Bonding as a Mean of Colour Variation. *Helv. Chim. Acta* **1997**, *80* (2), 398−413.
(117) Limón, P. M.; Gavara, R.; Pina, F. Thermodynamics and Kinetics of Cyanidin 3-Glucoside and Caffeine Copigments. *J. Agric. Food Chem.* **2013**, *61* (22), 5245−5251.
(118) Melo, M. J.; Moncada, M. C.; Pina, F. On the Red Colour of Raspberry (Rubus Idaeus). *Tetrahedron Lett.* **2000**, *41* (12), 1987−1991.
(119) Gierschner, J.; Lüer, L.; Milián-Medina, B.; Oelkrug, D.; Egelhaaf, H.-J. Highly Emissive H-Aggregates or Aggregation-Induced Emission Quenching? The Photophysics of All-Trans Para-Distyrylbenzene. *J. Phys. Chem. Lett.* **2013**, *4* (16), 2686−2697.
(120) Gierschner, J.; Park, S. Y. Luminescent Distyrylbenzenes: Tailoring Molecular Structure and Crystalline Morphology. *J. Mater. Chem. C* **2013**, *1* (37), 5818−5832.
(121) Gonnet, J.-F. Colour Effects of Co-Pigmentation of Anthocyanins revisited—1. A Colorimetric Definition Using the CIELAB Scale. *Food Chem.* **1998**, *63* (3), 409−415.
(122) Gordillo, B.; Rodríguez-Pulido, F. J.; Escudero-Gilete, M. L.; González-Miret, M. L.; Heredia, F. J. Comprehensive Colorimetric Study of Anthocyanic Copigmentation in Model Solutions. Effects of pH and Molar Ratio. *J. Agric. Food Chem.* **2012**, *60* (11), 2896−2905.
(123) Gonnet, J.-F. Colour Effects of Co-Pigmentation of Anthocyanins revisited—2.A Colorimetric Look at the Solutions of Cyanin Co-Pigmented Byrutin Using the CIELAB Scale. *Food Chem.* **1999**, *66* (3), 387−394.
(124) Xu, H.; Liu, X.; Yan, Q.; Yuan, F.; Gao, Y. A Novel Copigment of Quercetagetin for Stabilization of Grape Skin Anthocyanins. *Food Chem.* **2015**, *166*, 50−55.
(125) Shao, P.; Zhang, J.; Fang, Z.; Sun, P. Complexing of Chlorogenic Acid with B-Cyclodextrins: Inclusion Effects, Antioxidative Properties and Potential Application in Grape Juice. *Food Hydrocolloids* **2014**, *41*, 132−139.
(126) Mistry, T. V.; Cai, Y.; Lilley, T. H.; Haslam, E. Polyphenol Interactions. Part 5. Anthocyanin Co-Pigmentation. *J. Chem. Soc., Perkin Trans. 2* **1991**, No. 8, 1287−1296.
(127) Son, T.-D.; Chachaty, C. Nucleoside Conformations: XIV. Conformation of Adenosine Monophosphates in Aqueous Solution by Proton Magnetic Resonance Spectroscopy. *Biochim. Biophys. Acta, Nucleic Acids Protein Synth.* **1974**, *335* (1), 1−13.
(128) Leydet, Y.; Gavara, R.; Petrov, V.; Diniz, A. M.; Jorge Parola, A.; Lima, J. C.; Pina, F. The Effect of Self-Aggregation on the Determination of the Kinetic and Thermodynamic Constants of the Network of Chemical Reactions in 3-Glucoside Anthocyanins. *Phytochemistry* **2012**, *83*, 125−135.
(129) Dimicoli, J. L.; Hélène, C. Complex Formation between Purine and Indole Derivatives in Aqueous Solutions. Proton Magnetic Resonance Studies. *J. Am. Chem. Soc.* **1973**, *95* (4), 1036−1044.
(130) Alluis, B.; Pérol, N.; El Hajji, H.; Dangles, O. Water-Soluble Flavonol (=3Hydroxy2-Phenyl-4H-1-Benzopyran-4-One) Derivatives: Chemical Synthesis, Colouring, and Antioxidant Properties. *Helv. Chim. Acta* **2000**, *83* (2), 428−443.
(131) Hondo, T.; Yoshida, K.; Nakagawa, A.; Kawai, T.; Tamura, H.; Goto, T. Structural Basis of Blue-Colour Development in Flower Petals from Commelina Communis. *Nature* **1992**, *358* (6386), 515−518.
(132) Shiono, M.; Matsugaki, N.; Takeda, K. Phytochemistry: Structure of the Blue Cornflower Pigment. *Nature* **2005**, *436* (7052), 791−791.
(133) Dufour, C.; Sauvaitre, I. Interactions between Anthocyanins and Aroma Substances in a Model System. Effect on the Flavor of Grape-Derived Beverages. *J. Agric. Food Chem.* **2000**, *48* (5), 1784−1788.
(134) Tuominen, A.; Sinkkonen, J.; Karonen, M.; Salminen, J.-P. Sylvatiins, Acetylglucosylated Hydrolysable Tannins from the Petals of Geranium Sylvaticum Show Co-Pigment Effect. *Phytochemistry* **2015**, *115*, 239−251.

DOI: 10.1021/acs.chemrev.5b00507
Chem. Rev. 2016, 116, 4937−4982

(135) Dangles, O.; Saito, N.; Brouillard, R. Kinetic and Thermodynamic Control of Flavylium Hydration in the Pelargonidin-Cinnamic Acid Complexation. Origin of the Extraordinary Flower Color Diversity of Pharbitis Nil. *J. Am. Chem. Soc.* **1993**, *115* (8), 3125−3132.
(136) Eiro, M. J.; Heinonen, M. Anthocyanin Color Behavior and Stability during Storage: Effect of Intermolecular Copigmentation. *J. Agric. Food Chem.* **2002**, *50* (25), 7461−7466.
(137) Houbiers, C.; Lima, J. C.; Maçanita, A. L.; Santos, H. Color Stabilization of Malvidin 3-Glucoside: Self-Aggregation of the Flavylium Cation and Copigmentation with the Z-Chalcone Form. *J. Phys. Chem. B* **1998**, *102* (18), 3578−3585.
(138) Elhabiri, M.; Figueiredo, P.; Toki, K.; Figueiredo, P.; Toki, K.; Saito, N.; Brouillard, R.; Figueiredo, P.; Toki, K.; et al. Anthocyanin−aluminium and − gallium Complexes in Aqueoussolution. *J. Chem. Soc., Perkin Trans. 2* **1997**, No. 2, 355−362.
(139) Al Bittar, S.; Mora, N.; Loonis, M.; Dangles, O. Chemically Synthesized Glycosides of Hydroxylated Flavylium Ions as Suitable Models of Anthocyanins: Binding to Iron Ions and Human Serum Albumin, Antioxidant Activity in Model Gastric Conditions. *Molecules* **2014**, *19* (12), 20709−20730.
(140) Kasha, M.; Rawls, H. R.; Ashraf El-Bayoumi, M. The Exciton Model in Molecular Spectroscopy. *Pure Appl. Chem.* **1965**, *11* (3−4), 371−392.
(141) Yoshida, K.; Toyama, Y.; Kameda, K.; Kondo, T. Contribution of Each Caffeoyl Residue of the Pigment Molecule of Gentiodelphin to Blue Color Development. *Phytochemistry* **2000**, *54* (1), 85−92.
(142) Yoshida, K.; Kondo, T.; Goto, T. Intramolecular Stacking Conformation of Gentiodelphin, a Diacylated Anthocyanin from Gentiana Makinoi. *Tetrahedron* **1992**, *48* (21), 4313−4326.
(143) Nerdal, W.; Andersen, Ø. M. Evidence for Self-Association of the Anthocyanin Petanin in Acidified, Methanolic Solution Using Two-Dimensional Nuclear Overhauser Enhancement NMR Experiments and Distance Geometry Calculations. *Phytochem. Anal.* **1991**, *2* (6), 263−270.
(144) Nerdal, W.; Andersen, Ø. M. Intermolecular Aromatic Acid Association of an Anthocyanin (petanin) Evidenced by Two-Dimensional Nuclear Overhauser Enhancement Nuclear Magnetic Resonance Experiments and Distance Geometry Calculations. *Phytochem. Anal.* **1992**, *3* (4), 182−189.
(145) Yoshida, K.; Kondo, T.; Goto, T. Unusually Stable Monoacylated Anthocyanin from Purple Yam Dioscorea Alata. *Tetrahedron Lett.* **1991**, *32* (40), 5579−5580.
(146) Mori, M.; Miki, N.; Ito, D.; Kondo, T.; Yoshida, K. Structure of Tecophilin, a Tri-Caffeoylanthocyanin from the Blue Petals of Tecophilaea Cyanocrocus, and the Mechanism of Blue Color Development. *Tetrahedron* **2014**, *70* (45), 8657−8664.
(147) Terahara, N.; Callebaut, A.; Ohba, R.; Nagata, T.; Ohnishi-Kameyama, M.; Suzuki, M. Triacylated Anthocyanins from Ajuga Reptans Flowers and Cell Cultures. *Phytochemistry* **1996**, *42* (1), 199−203.
(148) Terahara, N.; Toki, K.; Saito, N.; Honda, T.; Matsui, T.; Osajima, Y. Eight New Anthocyanins, Ternatins C1-C5 and D3 and Preternatins A3 and C4 from Young Clitoria Ternatea Flowers. *J. Nat. Prod.* **1998**, *61* (11), 1361−1367.
(149) Escribano-Bailón, T.; Dangles, O.; Brouillard, R. Coupling Reactions between Flavylium Ions and Catechin. *Phytochemistry* **1996**, *41* (6), 1583−1592.
(150) Dueñas, M.; Fulcrand, H.; Cheynier, V. Formation of Anthocyanin−flavanol Adducts in Model Solutions. *Anal. Chim. Acta* **2006**, *563* (1−2), 15−25.
(151) Dueñas, M.; Salas, E.; Cheynier, V.; Dangles, O.; Fulcrand, H. UV−Visible Spectroscopic Investigation of the 8,8-Methylmethine Catechin-Malvidin 3-Glucoside Pigments in Aqueous Solution: Structural Transformations and Molecular Complexation with Chlorogenic Acid. *J. Agric. Food Chem.* **2006**, *54* (1), 189−196.
(152) Chassaing, S.; Lefeuvre, D.; Jacquet, R.; Jourdes, M.; Ducasse, L.; Galland, S.; Grelard, A.; Saucier, C.; Teissedre, P.-L.; Dangles, O.; et al. Physicochemical Studies of New Anthocyano-Ellagitannin Hybrid Pigments: About the Origin of the Influence of Oak C-Glycosidic Ellagitannins on Wine Color. *Eur. J. Org. Chem.* **2010**, *2010* (1), 55−63.
(153) Bloor, S. J. Overview of Methods for Analysis and Identification of Flavonoids. *Methods Enzymol.* **2001**, *335*, 3−14.
(154) Dangles, O.; Saito, N.; Brouillard, R. Anthocyanin Intramolecular Copigment Effect. *Phytochemistry* **1993**, *34* (1), 119−124.
(155) Figueiredo, P.; George, F.; Tatsuzawa, F.; Toki, K.; Saito, N.; Brouillard, R. New Features of Intramolecular Copigmentation by Acylated Anthocyanins. *Phytochemistry* **1999**, *51*, 125−132.
(156) Fleschhut, J.; Kratzer, F.; Rechkemmer, G.; Kulling, S. E. Stability and Biotransformation of Various Dietary Anthocyanins in Vitro. *Eur. J. Nutr.* **2006**, *45* (1), 7−18.
(157) Lopes, P.; Richard, T.; Saucier, C.; Teissedre, P.-L.; Monti, J.-P.; Glories, Y. Anthocyanone A: A Quinone Methide Derivative Resulting from Malvidin 3- *O* -Glucoside Degradation. *J. Agric. Food Chem.* **2007**, *55* (7), 2698−2704.
(158) Sadilova, E.; Carle, R.; Stintzing, F. C. Thermal Degradation of Anthocyanins and Its Impact on Color Andin Vitro Antioxidant Capacity. *Mol. Nutr. Food Res.* **2007**, *51* (12), 1461−1471.
(159) Yang, J.; Hu, W.; Usvyat, D.; Matthews, D.; Schütz, M.; Chan, G. K.-L. Ab Initio Determination of the Crystalline Benzene Lattice Energy to Sub-Kilojoule/mol Accuracy. *Science* **2014**, *345* (6197), 640−643.
(160) Cavalcanti, R. N.; Santos, D. T.; Meireles, M. A. A. Non-Thermal Stabilization Mechanisms of Anthocyanins in Model and Food systems—An Overview. *Food Res. Int.* **2011**, *44* (2), 499−509.
(161) Rodrigues, R. F.; Ferreira da Silva, P.; Shimizu, K.; Freitas, A. A.; Kovalenko, S. A.; Ernsting, N. P.; Quina, F. H.; Maçanita, A. Ultrafast Internal Conversion in a Model Anthocyanin-Polyphenol Complex: Implications for the Biological Role of Anthocyanins in Vegetative Tissues of Plants. *Chem. - Eur. J.* **2009**, *15* (6), 1397−1402.
(162) Ferreira da Silva, P.; Paulo, L.; Barbafina, A.; Elisei, F.; Quina, F. H.; Maçanita, A. L. Photoprotection and the Photophysics of Acylated Anthocyanins. *Chem. - Eur. J.* **2012**, *18* (12), 3736−3744.
(163) Song, B. J.; Sapper, T. N.; Burtch, C. E.; Brimmer, K.; Goldschmidt, M.; Ferruzzi, M. G. Photo- and Thermodegradation of Anthocyanins from Grape and Purple Sweet Potato in Model Beverage Systems. *J. Agric. Food Chem.* **2013**, *61* (6), 1364−1372.
(164) Malien-Aubert, C.; Dangles, O.; Amiot, M. J. Color Stability of Commercial Anthocyanin-Based Extracts in Relation to the Phenolic Composition. Protective Effects by Intra- and Intermolecular Copigmentation. *J. Agric. Food Chem.* **2001**, *49* (1), 170−176.
(165) Cabrita, L.; Petrov, V.; Pina, F. On the Thermal Degradation of Anthocyanidins: Cyanidin. *RSC Adv.* **2014**, *4* (36), 18939.
(166) Schneider, H.-J. Dispersive Interactions in Solution Complexes. *Acc. Chem. Res.* **2015**, *48* (7), 1815−1822.
(167) Hunter, C. A.; Sanders, J. K. M. The Nature of.pi.-.pi. Interactions. *J. Am. Chem. Soc.* **1990**, *112* (14), 5525−5534.
(168) Hwang, J.; Li, P.; Carroll, W. R.; Smith, M. D.; Pellechia, P. J.; Shimizu, K. D. Additivity of Substituent Effects in Aromatic Stacking Interactions. *J. Am. Chem. Soc.* **2014**, *136* (40), 14060−14067.
(169) Cockroft, S. L.; Hunter, C. A.; Lawson, K. R.; Perkins, J.; Urch, C. J. Electrostatic Control of Aromatic Stacking Interactions. *J. Am. Chem. Soc.* **2005**, *127* (24), 8594−8595.
(170) Meyer, E. A.; Castellano, R. K.; Diederich, F. Interactions with Aromatic Rings in Chemical and Biological Recognition. *Angew. Chem., Int. Ed.* **2003**, *42* (11), 1210−1250.
(171) Salonen, L. M.; Ellermann, M.; Diederich, F. Aromatic Rings in Chemical and Biological Recognition: Energetics and Structures. *Angew. Chem., Int. Ed.* **2011**, *50* (21), 4808−4842.
(172) Hunter, C. A. Quantifying Intermolecular Interactions: Guidelines for the Molecular Recognition Toolbox. *Angew. Chem., Int. Ed.* **2004**, *43* (40), 5310−5324.
(173) Trouillas, P.; Di Meo, F.; Gierschner, J.; Linares, M.; Sancho-García, J. C.; Otyepka, M. Optical Properties of Wine Pigments: Theoretical Guidelines with New Methodological Perspectives. *Tetrahedron* **2015**, *71* (20), 3079−3088.
(174) London, F. The General Theory of Molecular Forces. *Trans. Faraday Soc.* **1937**, *33* (0), 8b−26.

DOI: 10.1021/acs.chemrev.5b00507
Chem. Rev. 2016, 116, 4937−4982

(175) Chandler, D. Interfaces and the Driving Force of Hydrophobic Assembly. *Nature* **2005**, *437* (7059), 640−647.
(176) Biedermann, F.; Nau, W. M.; Schneider, H.-J. The Hydrophobic Effect Revisited—Studies with Supramolecular Complexes Imply High-Energy Water as a Noncovalent Driving Force. *Angew. Chem., Int. Ed.* **2014**, *53* (42), 11158−11171.
(177) Waters, M. L. Aromatic Interactions. *Acc. Chem. Res.* **2013**, *46* (4), 873−873.
(178) Yang, L.; Adam, C.; Nichol, G. S.; Cockroft, S. L. How Much Do van Der Waals Dispersion Forces Contribute to Molecular Recognition in Solution? *Nat. Chem.* **2013**, *5* (12), 1006−1010.
(179) Mackerell, A. D. Empirical Force Fields for Biological Macromolecules: Overview and Issues. *J. Comput. Chem.* **2004**, *25* (13), 1584−1604.
(180) Wang, J.; Wolf, R. M.; Caldwell, J. W.; Kollman, P. A.; Case, D. A. Development and Testing of a General Amber Force Field. *J. Comput. Chem.* **2004**, *25* (9), 1157−1174.
(181) Cornell, W. D.; Cieplak, P.; Bayly, C. I.; Gould, I. R.; Merz, K. M.; Ferguson, D. M.; Spellmeyer, D. C.; Fox, T.; Caldwell, J. W.; Kollman, P. A. A Second Generation Force Field for the Simulation of Proteins, Nucleic Acids, and Organic Molecules. *J. Am. Chem. Soc.* **1996**, *118* (9), 2309−2309.
(182) Zgarbová, M.; Otyepka, M.; Sponer, J.; Hobza, P.; Jurecka, P. Large-Scale Compensation of Errors in Pairwise-Additive Empirical Force Fields: Comparison of AMBER Intermolecular Terms with Rigorous DFT-SAPT Calculations. *Phys. Chem. Chem. Phys.* **2010**, *12* (35), 10476−10493.
(183) Šponer, J.; Banáš, P.; Jurečka, P.; Zgarbová, M.; Kührová, P.; Havrila, M.; Krepl, M.; Stadlbauer, P.; Otyepka, M. Molecular Dynamics Simulations of Nucleic Acids. From Tetranucleotides to the Ribosome. *J. Phys. Chem. Lett.* **2014**, *5* (10), 1771−1782.
(184) Adcock, S. A.; McCammon, J. A. Molecular Dynamics: Survey of Methods for Simulating the Activity of Proteins. *Chem. Rev.* **2006**, *106* (5), 1589−1615.
(185) Case, D. A.; Cheatham, T. E.; Darden, T.; Gohlke, H.; Luo, R.; Merz, K. M.; Onufriev, A.; Simmerling, C.; Wang, B.; Woods, R. J. The Amber Biomolecular Simulation Programs. *J. Comput. Chem.* **2005**, *26* (16), 1668−1688.
(186) Brooks, B. R.; Brooks, C. L.; MacKerell, A. D.; Nilsson, L.; Petrella, R. J.; Roux, B.; Won, Y.; Archontis, G.; Bartels, C.; Boresch, S.; et al. CHARMM: The Biomolecular Simulation Program. *J. Comput. Chem.* **2009**, *30* (10), 1545−1614.
(187) Phillips, J. C.; Braun, R.; Wang, W.; Gumbart, J.; Tajkhorshid, E.; Villa, E.; Chipot, C.; Skeel, R. D.; Kalé, L.; Schulten, K. Scalable Molecular Dynamics with NAMD. *J. Comput. Chem.* **2005**, *26* (16), 1781−1802.
(188) Van Der Spoel, D.; Lindahl, E.; Hess, B.; Groenhof, G.; Mark, A. E.; Berendsen, H. J. C. GROMACS: Fast, Flexible, and Free. *J. Comput. Chem.* **2005**, *26* (16), 1701−1718.
(189) Leach, A. R. *Molecular Modelling: Principles and Applications*; Pearson, 2001.
(190) Vashisth, H.; Skiniotis, G.; Brooks, C. L. Collective Variable Approaches for Single Molecule Flexible Fitting and Enhanced Sampling. *Chem. Rev.* **2014**, *114* (6), 3353−3365.
(191) Bruccoleri, R. E.; Karplus, M. Conformational Sampling Using High-Temperature Molecular Dynamics. *Biopolymers* **1990**, *29* (14), 1847−1862.
(192) Chocholoušová, J.; Vacek, J.; Hobza, P. Acetic Acid Dimer in the Gas Phase, Nonpolar Solvent, Microhydrated Environment, and Dilute and Concentrated Acetic Acid: Ab Initio Quantum Chemical and Molecular Dynamics Simulations. *J. Phys. Chem. A* **2003**, *107* (17), 3086−3092.
(193) Zelený, T.; Hobza, P.; Kabelác, M. Microhydration of Guanine··· cytosine Base Pairs, a Theoretical Study on the Role of Water in Stability, Structure and Tautomeric Equilibrium. *Phys. Chem. Chem. Phys.* **2009**, *11* (18), 3430−3435.
(194) Sugita, Y.; Okamoto, Y. Replica-Exchange Molecular Dynamics Method for Protein Folding. *Chem. Phys. Lett.* **1999**, *314* (1−2), 141−151.
(195) Beck, D. A. C.; White, G. W. N.; Daggett, V. Exploring the Energy Landscape of Protein Folding Using Replica-Exchange and Conventional Molecular Dynamics Simulations. *J. Struct. Biol.* **2007**, *157* (3), 514−523.
(196) Laio, A.; Parrinello, M. Escaping Free-Energy Minima. *Proc. Natl. Acad. Sci. U. S. A.* **2002**, *99* (20), 12562−12566.
(197) Barducci, A.; Bonomi, M.; Parrinello, M. Metadynamics. *Wiley Interdiscip. Rev. Comput. Mol. Sci.* **2011**, *1* (5), 826−843.
(198) Brás, N. F.; Cruz, L.; Fernandes, P. A.; De Freitas, V.; Ramos, M. J. Conformational Study of Two Diasteroisomers of Vinylcatechin Dimers in a Methanol Solution. *Int. J. Quantum Chem.* **2011**, *111* (7−8), 1498−1510.
(199) Kollman, P. A.; Massova, I.; Reyes, C.; Kuhn, B.; Huo, S.; Chong, L.; Lee, M.; Lee, T.; Duan, Y.; Wang, W.; et al. Calculating Structures and Free Energies of Complex Molecules: Combining Molecular Mechanics and Continuum Models. *Acc. Chem. Res.* **2000**, *33* (12), 889−897.
(200) Bahar, I.; Lezon, T. R.; Bakan, A.; Shrivastava, I. H. Normal Mode Analysis of Biomolecular Structures: Functional Mechanisms of Membrane Proteins. *Chem. Rev.* **2010**, *110* (3), 1463−1497.
(201) Andricioaei, I.; Karplus, M. On the Calculation of Entropy from Covariance Matrices of the Atomic Fluctuations. *J. Chem. Phys.* **2001**, *115* (14), 6289−6292.
(202) Tsui, V.; Case, D. A. Theory and Applications of the Generalized Born Solvation Model in Macromolecular Simulations. *Biopolymers* **2000**, *56* (4), 275−291.
(203) Rocchia, W.; Alexov, E.; Honig, B. Extending the Applicability of the Nonlinear Poisson−Boltzmann Equation: Multiple Dielectric Constants and Multivalent Ions. *J. Phys. Chem. B* **2001**, *105* (28), 6507−6514.
(204) Baker, C. M.; Lopes, P. E. M.; Zhu, X.; Roux, B.; MacKerell, A. D. Accurate Calculation of Hydration Free Energies Using Pair-Specific Lennard-Jones Parameters in the CHARMM Drude Polarizable Force Field. *J. Chem. Theory Comput.* **2010**, *6* (4), 1181−1198.
(205) Allinger, N. L. Conformational Analysis. 130. MM2. A Hydrocarbon Force Field Utilizing V1 and V2 Torsional Terms. *J. Am. Chem. Soc.* **1977**, *99* (25), 8127−8134.
(206) Charlton, A. J.; Davis, A. L.; Jones, D. P.; Lewis, J. R.; Davies, A. P.; Haslam, E.; Williamson, M. P. The Self-Association of the Black Tea Polyphenol Theaflavin and Its Complexation with Caffeine. *J. Chem. Soc. Perkin Trans. 2* **2000**, No. 2, 317−322.
(207) Kunsági-Máté, S.; Szabó, K.; Nikfardjam, M. P.; Kollár, L. Determination of the Thermodynamic Parameters of the Complex Formation between Malvidin-3-O-Glucoside and Polyphenols. Copigmentation Effect in Red Wines. *J. Biochem. Biophys. Methods* **2006**, *69* (1−2), 113−119.
(208) Kalisz, S.; Oszmiański, J.; Hładyszowski, J.; Mitek, M. Stabilization of Anthocyanin and Skullcap Flavone Complexes − Investigations with Computer Simulation and Experimental Methods. *Food Chem.* **2013**, *138* (1), 491−500.
(209) Kunsági-Máté, S.; Ortmann, E.; Kollár, L.; Nikfardjam, M. P. Effect of the Solvatation Shell Exchange on the Formation of Malvidin-3- *O* -Glucoside−Ellagic Acid Complexes. *J. Phys. Chem. B* **2007**, *111* (40), 11750−11755.
(210) Sousa, A.; Araújo, P.; Cruz, L.; Brás, N. F.; Mateus, N.; De Freitas, V. Evidence for Copigmentation Interactions between Deoxyanthocyanidin Derivatives (Oaklins) and Common Copigments in Wine Model Solutions. *J. Agric. Food Chem.* **2014**, *62* (29), 6995−7001.
(211) Košinová, P.; Berka, K.; Wykes, M.; Otyepka, M.; Trouillas, P. Positioning of Antioxidant Quercetin and Its Metabolites in Lipid Bilayer Membranes: Implication for Their Lipid-Peroxidation Inhibition. *J. Phys. Chem. B* **2012**, *116* (4), 1309−1318.
(212) Sirk, T. W.; Brown, E. F.; Sum, A. K.; Friedman, M. Molecular Dynamics Study on the Biophysical Interactions of Seven Green Tea Catechins with Lipid Bilayers of Cell Membranes. *J. Agric. Food Chem.* **2008**, *56* (17), 7750−7758.
(213) Paloncýová, M.; Fabre, G.; DeVane, R. H.; Trouillas, P.; Berka, K.; Otyepka, M. Benchmarking of Force Fields for Molecule−

DOI: 10.1021/acs.chemrev.5b00507
Chem. Rev. 2016, 116, 4937−4982

Membrane Interactions. *J. Chem. Theory Comput.* **2014**, *10* (9), 4143−4151.
(214) Podloucká, P.; Berka, K.; Fabre, G.; Paloncýová, M.; Duroux, J.-L.; Otyepka, M.; Trouillas, P. Lipid Bilayer Membrane Affinity Rationalizes Inhibition of Lipid Peroxidation by a Natural Lignan Antioxidant. *J. Phys. Chem. B* **2013**, *117* (17), 5043−5049.
(215) Zhou, H.-X.; Gilson, M. K. Theory of Free Energy and Entropy in Noncovalent Binding. *Chem. Rev.* **2009**, *109* (9), 4092−4107.
(216) Černỳ, J.; Hobza, P. Non-Covalent Interactions in Biomacromolecules. *Phys. Chem. Chem. Phys.* **2007**, *9* (39), 5291−5303.
(217) Grimme, S.; Antony, J.; Schwabe, T.; Mück-Lichtenfeld, C. Density Functional Theory with Dispersion Corrections for Supramolecular Structures, Aggregates, and Complexes of (bio) Organic Molecules. *Org. Biomol. Chem.* **2007**, *5* (5), 741−758.
(218) Sherrill, C. D. Computations of Noncovalent N Interactions. *Rev. Comput. Chem.* **2008**, *26*, 1.
(219) Tschumper, G. S. Computations for Weak Noncovalent. *Rev. Comput. Chem.* **2008**, *26*, 39.
(220) Foster, M. E.; Sohlberg, K. Empirically Corrected DFT and Semi-Empirical Methods for Non-Bonding Interactions. *Phys. Chem. Chem. Phys.* **2010**, *12* (2), 307−322.
(221) Riley, K. E.; Pitoňák, M.; Jurečka, P.; Hobza, P. Stabilization and Structure Calculations for Noncovalent Interactions in Extended Molecular Systems Based on Wave Function and Density Functional Theories. *Chem. Rev.* **2010**, *110* (9), 5023−5063.
(222) Hobza, P. The Calculation of Intermolecular Interaction Energies. *Annu. Rep. Prog. Chem., Sect. C: Phys. Chem.* **2011**, *107*, 148−168.
(223) Grimme, S. Density Functional Theory with London Dispersion Corrections. *Wiley Interdiscip. Rev. Comput. Mol. Sci.* **2011**, *1* (2), 211−228.
(224) Klimeš, J.; Michaelides, A. Perspective: Advances and Challenges in Treating van Der Waals Dispersion Forces in Density Functional Theory. *J. Chem. Phys.* **2012**, *137* (12), 120901.
(225) Ehrlich, S.; Moellmann, J.; Grimme, S. Dispersion-Corrected Density Functional Theory for Aromatic Interactions in Complex Systems. *Acc. Chem. Res.* **2013**, *46* (4), 916−926.
(226) DiStasio, R. A., Jr.; Gobre, V. V.; Tkatchenko, A. Many-Body van Der Waals Interactions in Molecules and Condensed Matter. *J. Phys.: Condens. Matter* **2014**, *26* (21), 213202.
(227) Casimir, H.; Polder, D. The Influence of Retardation on the London-van Der Waals Forces. *Phys. Rev.* **1948**, *73* (4), 360.
(228) Starkschall, G.; Gordon, R. G. Calculation of Coefficients in the Power Series Expansion of the Long-Range Dispersion Force between Atoms. *J. Chem. Phys.* **1972**, *56* (6), 2801−2806.
(229) Tang, K.; Toennies, J. P. An Improved Simple Model for the van Der Waals Potential Based on Universal Damping Functions for the Dispersion Coefficients. *J. Chem. Phys.* **1984**, *80* (8), 3726−3741.
(230) Thakkar, A. J.; Hettema, H.; Wormer, P. E. Abinitio Dispersion Coefficients for Interactions Involving Rare-Gas Atoms. *J. Chem. Phys.* **1992**, *97* (5), 3252−3257.
(231) Lein, M.; Dobson, J. F.; Gross, E. K. Toward the Description of van Der Waals Interactions within Density Functional Theory. *J. Comput. Chem.* **1999**, *20* (1), 12−22.
(232) Kamal, C.; Ghanty, T.; Banerjee, A.; Chakrabarti, A. The van Der Waals Coefficients between Carbon Nanostructures and Small Molecules: A Time-Dependent Density Functional Theory Study. *J. Chem. Phys.* **2009**, *131* (16), 164708.
(233) Johnson, E. R.; Becke, A. D. A Post-Hartree−Fock Model of Intermolecular Interactions. *J. Chem. Phys.* **2005**, *123* (2), 024101.
(234) Becke, A. D.; Johnson, E. R. Exchange-Hole Dipole Moment and the Dispersion Interaction. *J. Chem. Phys.* **2005**, *122* (15), 154104.
(235) Johnson, E. R. Dependence of Dispersion Coefficients on Atomic Environment. *J. Chem. Phys.* **2011**, *135* (23), 234109.
(236) Misquitta, A. J. Intermolecular Interactions. In *Handbook of Computational Chemistry*; Springer, 2012; pp 157−193.
(237) Wen, S.; Nanda, K.; Huang, Y.; Beran, G. J. Practical Quantum Mechanics-Based Fragment Methods for Predicting Molecular Crystal Properties. *Phys. Chem. Chem. Phys.* **2012**, *14* (21), 7578−7590.
(238) Wu, Q.; Yang, W. Empirical Correction to Density Functional Theory for van Der Waals Interactions. *J. Chem. Phys.* **2002**, *116* (2), 515−524.
(239) Chai, J.-D.; Head-Gordon, M. Long-Range Corrected Hybrid Density Functionals with Damped Atom-Atom Dispersion Corrections. *Phys. Chem. Chem. Phys.* **2008**, *10* (44), 6615−6620.
(240) Liu, Y.; Goddard, W. A. I. A Universal Damping Function for Empirical Dispersion Correction on Density Functional Theory. *Mater. Trans.* **2009**, *50* (7), 1664−1670.
(241) Grimme, S.; Antony, J.; Ehrlich, S.; Krieg, H. A Consistent and Accurate Ab Initio Parametrization of Density Functional Dispersion Correction (DFT-D) for the 94 Elements H-Pu. *J. Chem. Phys.* **2010**, *132* (15), 154104.
(242) Grimme, S.; Ehrlich, S.; Goerigk, L. Effect of the Damping Function in Dispersion Corrected Density Functional Theory. *J. Comput. Chem.* **2011**, *32* (7), 1456−1465.
(243) Johnson, E. R.; Becke, A. D. A Post-Hartree-Fock Model of Intermolecular Interactions: Inclusion of Higher-Order Corrections. *J. Chem. Phys.* **2006**, *124* (17), 174104.
(244) Grimme, S. Accurate Description of van Der Waals Complexes by Density Functional Theory Including Empirical Corrections. *J. Comput. Chem.* **2004**, *25* (12), 1463−1473.
(245) Grimme, S. Semiempirical GGA-Type Density Functional Constructed with a Long-Range Dispersion Correction. *J. Comput. Chem.* **2006**, *27* (15), 1787−1799.
(246) Jurečka, P.; Černỳ, J.; Hobza, P.; Salahub, D. R. Density Functional Theory Augmented with an Empirical Dispersion Term. Interaction Energies and Geometries of 80 Noncovalent Complexes Compared with Ab Initio Quantum Mechanics Calculations. *J. Comput. Chem.* **2007**, *28* (2), 555−569.
(247) Tkatchenko, A.; Scheffler, M. Accurate Molecular van Der Waals Interactions from Ground-State Electron Density and Free-Atom Reference Data. *Phys. Rev. Lett.* **2009**, *102* (7), 073005.
(248) Steinmann, S. N.; Corminboeuf, C. A System-Dependent Density-Based Dispersion Correction. *J. Chem. Theory Comput.* **2010**, *6* (7), 1990−2001.
(249) Steinmann, S. N.; Corminboeuf, C. Comprehensive Benchmarking of a Density-Dependent Dispersion Correction. *J. Chem. Theory Comput.* **2011**, *7* (11), 3567−3577.
(250) Steinmann, S. N.; Corminboeuf, C. A Generalized-Gradient Approximation Exchange Hole Model for Dispersion Coefficients. *J. Chem. Phys.* **2011**, *134* (4), 044117.
(251) Liu, Y.; Goddard, W. A., III First-Principles-Based Dispersion Augmented Density Functional Theory: From Molecules to Crystals. *J. Phys. Chem. Lett.* **2010**, *1* (17), 2550−2555.
(252) Kim, H.; Choi, J.-M.; Goddard, W. A., III Universal Correction of Density Functional Theory to Include London Dispersion (up to Lr, Element 103). *J. Phys. Chem. Lett.* **2012**, *3* (3), 360−363.
(253) Román-Pérez, G.; Soler, J. M. Efficient Implementation of a van Der Waals Density Functional: Application to Double-Wall Carbon Nanotubes. *Phys. Rev. Lett.* **2009**, *103* (9), 096102.
(254) Andersson, Y.; Langreth, D. C.; Lundqvist, B. I. Van Der Waals Interactions in Density-Functional Theory. *Phys. Rev. Lett.* **1996**, *76* (1), 102−105.
(255) Dobson, J. F.; Dinte, B. P. Constraint Satisfaction in Local and Gradient Susceptibility Approximations: Application to a van Der Waals Density Functional. *Phys. Rev. Lett.* **1996**, *76* (11), 1780.
(256) Sato, T.; Tsuneda, T.; Hirao, K. Van Der Waals Interactions Studied by Density Functional Theory. *Mol. Phys.* **2005**, *103* (6−8), 1151−1164.
(257) Dion, M.; Rydberg, H.; Schröder, E.; Langreth, D. C.; Lundqvist, B. I. Van Der Waals Density Functional for General Geometries. *Phys. Rev. Lett.* **2004**, *92* (24), 246401.
(258) Pernal, K.; Podeszwa, R.; Patkowski, K.; Szalewicz, K. Dispersionless Density Functional Theory. *Phys. Rev. Lett.* **2009**, *103* (26), 263201.
(259) Klimeš, J.; Bowler, D. R.; Michaelides, A. Chemical Accuracy for the van Der Waals Density Functional. *J. Phys.: Condens. Matter* **2010**, *22* (2), 022201.

DOI: 10.1021/acs.chemrev.5b00507
Chem. Rev. 2016, 116, 4937−4982

(260) Lee, K.; Murray, É. D.; Kong, L.; Lundqvist, B. I.; Langreth, D. C. Higher-Accuracy van Der Waals Density Functional. *Phys. Rev. B: Condens. Matter Mater. Phys.* **2010**, *82* (8), 081101.
(261) Hamada, I. Van Der Waals Density Functional Made Accurate. *Phys. Rev. B: Condens. Matter Mater. Phys.* **2014**, *89* (12), 121103.
(262) Vydrov, O. A.; Van Voorhis, T. Nonlocal van Der Waals Density Functional Made Simple. *Phys. Rev. Lett.* **2009**, *103* (6), 063004.
(263) Vydrov, O. A.; Van Voorhis, T. Improving the Accuracy of the Nonlocal van Der Waals Density Functional with Minimal Empiricism. *J. Chem. Phys.* **2009**, *130* (10), 104105.
(264) Vydrov, O. A.; Van Voorhis, T. Implementation and Assessment of a Simple Nonlocal van Der Waals Density Functional. *J. Chem. Phys.* **2010**, *132* (16), 164113.
(265) Vydrov, O. A.; Van Voorhis, T. Nonlocal van Der Waals Density Functional: The Simpler the Better. *J. Chem. Phys.* **2010**, *133* (24), 244103.
(266) Sabatini, R.; Gorni, T.; de Gironcoli, S. Nonlocal van Der Waals Density Functional Made Simple and Efficient. *Phys. Rev. B: Condens. Matter Mater. Phys.* **2013**, *87* (4), 041108.
(267) Hujo, W.; Grimme, S. Performance of the van Der Waals Density Functional VV10 and (hybrid) GGA Variants for Thermochemistry and Noncovalent Interactions. *J. Chem. Theory Comput.* **2011**, *7* (12), 3866−3871.
(268) Aragó, J.; Ortí, E.; Sancho-García, J. C. Nonlocal van Der Waals Approach Merged with Double-Hybrid Density Functionals: Toward the Accurate Treatment of Noncovalent Interactions. *J. Chem. Theory Comput.* **2013**, *9* (8), 3437−3443.
(269) Cooper, V. R. Van Der Waals Density Functional: An Appropriate Exchange Functional. *Phys. Rev. B: Condens. Matter Mater. Phys.* **2010**, *81* (16), 161104.
(270) Vydrov, O. A.; Van Voorhis, T. Benchmark Assessment of the Accuracy of Several van Der Waals Density Functionals. *J. Chem. Theory Comput.* **2012**, *8* (6), 1929−1934.
(271) Hujo, W.; Grimme, S. Performance of Non-Local and Atom-Pairwise Dispersion Corrections to DFT for Structural Parameters of Molecules with Noncovalent Interactions. *J. Chem. Theory Comput.* **2013**, *9* (1), 308−315.
(272) Tran, F.; Hutter, J. Nonlocal van Der Waals Functionals: The Case of Rare-Gas Dimers and Solids. *J. Chem. Phys.* **2013**, *138* (20), 204103.
(273) Gobre, V. V.; Tkatchenko, A. Scaling Laws for van Der Waals Interactions in Nanostructured Materials. *Nat. Commun.* **2013**, *4*, 2341.
(274) Ambrosetti, A.; Alfè, D.; DiStasio, R. A., Jr.; Tkatchenko, A. Hard Numbers for Large Molecules: Toward Exact Energetics for Supramolecular Systems. *J. Phys. Chem. Lett.* **2014**, *5* (5), 849−855.
(275) Šimová, L.; Řezáč, J.; Hobza, P. Convergence of the Interaction Energies in Noncovalent Complexes in the Coupled-Cluster Methods Up to Full Configuration Interaction. *J. Chem. Theory Comput.* **2013**, *9* (8), 3420−3428.
(276) Řezáč, J.; Šimová, L.; Hobza, P. CCSD[T] Describes Noncovalent Interactions Better than the CCSD(T), CCSD(TQ), and CCSDT Methods. *J. Chem. Theory Comput.* **2013**, *9* (1), 364−369.
(277) Kong, L.; Bischoff, F. A.; Valeev, E. F. Explicitly Correlated R12/F12 Methods for Electronic Structure. *Chem. Rev.* **2012**, *112* (1), 75−107.
(278) Burns, L. A.; Marshall, M. S.; Sherrill, C. D. Appointing Silver and Bronze Standards for Noncovalent Interactions: A Comparison of Spin-Component-Scaled (SCS), Explicitly Correlated (F12), and Specialized Wavefunction Approaches. *J. Chem. Phys.* **2014**, *141* (23), 234111.
(279) Austin, B. M.; Zubarev, D. Y.; Lester, W. A., Jr. Quantum Monte Carlo and Related Approaches. *Chem. Rev.* **2012**, *112* (1), 263−288.
(280) Dubecký, M.; Jurečka, P.; Derian, R.; Hobza, P.; Otyepka, M.; Mitas, L. Quantum Monte Carlo Methods Describe Noncovalent Interactions with Subchemical Accuracy. *J. Chem. Theory Comput.* **2013**, *9* (10), 4287−4292.
(281) Dubecký, M.; Derian, R.; Jurečka, P.; Mitas, L.; Hobza, P.; Otyepka, M. Quantum Monte Carlo for Noncovalent Interactions: An Efficient Protocol Attaining Benchmark Accuracy. *Phys. Chem. Chem. Phys.* **2014**, *16* (38), 20915−20923.
(282) Neese, F.; Wennmohs, F.; Hansen, A. Efficient and Accurate Local Approximations to Coupled-Electron Pair Approaches: An Attempt to Revive the Pair Natural Orbital Method. *J. Chem. Phys.* **2009**, *130* (11), 114108.
(283) Neese, F.; Hansen, A.; Liakos, D. G. Efficient and Accurate Approximations to the Local Coupled Cluster Singles Doubles Method Using a Truncated Pair Natural Orbital Basis. *J. Chem. Phys.* **2009**, *131* (6), 064103.
(284) Huntington, L. M.; Nooijen, M. pCCSD: Parameterized Coupled-Cluster Theory with Single and Double Excitations. *J. Chem. Phys.* **2010**, *133* (18), 184109.
(285) Huntington, L. M. J.; Hansen, A.; Neese, F.; Nooijen, M. Accurate Thermochemistry from a Parameterized Coupled-Cluster Singles and Doubles Model and a Local Pair Natural Orbital Based Implementation for Applications to Larger Systems. *J. Chem. Phys.* **2012**, *136* (6), 064101.
(286) Hansen, A.; Liakos, D. G.; Neese, F. Efficient and Accurate Local Single Reference Correlation Methods for High-Spin Open-Shell Molecules Using Pair Natural Orbitals. *J. Chem. Phys.* **2011**, *135* (21), 214102.
(287) Riplinger, C.; Sandhoefer, B.; Hansen, A.; Neese, F. Natural Triple Excitations in Local Coupled Cluster Calculations with Pair Natural Orbitals. *J. Chem. Phys.* **2013**, *139* (13), 134101.
(288) Sparta, M.; Neese, F. Chemical Applications Carried out by Local Pair Natural Orbital Based Coupled-Cluster Methods. *Chem. Soc. Rev.* **2014**, *43* (14), 5032−5041.
(289) Liakos, D. G.; Hansen, A.; Neese, F. Weak Molecular Interactions Studied with Parallel Implementations of the Local Pair Natural Orbital Coupled Pair and Coupled Cluster Methods. *J. Chem. Theory Comput.* **2011**, *7* (1), 76−87.
(290) Liakos, D. G.; Neese, F. Improved Correlation Energy Extrapolation Schemes Based on Local Pair Natural Orbital Methods. *J. Phys. Chem. A* **2012**, *116* (19), 4801−4816.
(291) Schwabe, T. Accurate and Fast Treatment of Large Molecular Systems: Assessment of CEPA and pCCSD within the Local Pair Natural Orbital Approximation. *J. Comput. Chem.* **2012**, *33* (26), 2067−2072.
(292) Riplinger, C.; Neese, F. An Efficient and near Linear Scaling Pair Natural Orbital Based Local Coupled Cluster Method. *J. Chem. Phys.* **2013**, *138* (3), 034106.
(293) Sancho-García, J. C.; Aragó, J.; Ortí, E.; Olivier, Y. Obtaining the Lattice Energy of the Anthracene Crystal by Modern yet Affordable First-Principles Methods. *J. Chem. Phys.* **2013**, *138* (20), 204304.
(294) Grimme, S. Supramolecular Binding Thermodynamics by Dispersion-Corrected Density Functional Theory. *Chem. - Eur. J.* **2012**, *18* (32), 9955−9964.
(295) Calbo, J.; Ortí, E.; Sancho-García, J. C.; Aragó, J. Accurate Treatment of Large Supramolecular Complexes by Double-Hybrid Density Functionals Coupled with Nonlocal van Der Waals Corrections. *J. Chem. Theory Comput.* **2015**, *11* (3), 932−939.
(296) Pitoňák, M.; Řezáč, J.; Hobza, P. Spin-Component Scaled Coupled-Clusters Singles and Doubles Optimized towards Calculation of Noncovalent Interactions. *Phys. Chem. Chem. Phys.* **2010**, *12* (33), 9611−9614.
(297) Grimme, S. Improved Second-Order Møller−Plesset Perturbation Theory by Separate Scaling of Parallel-and Antiparallel-Spin Pair Correlation Energies. *J. Chem. Phys.* **2003**, *118* (20), 9095−9102.
(298) Szabados, Á. Theoretical Interpretation of Grimme's Spin-Component-Scaled Second Order Møller-Plesset Theory. *J. Chem. Phys.* **2006**, *125* (21), 214105.
(299) Fink, R. F. Spin-Component-Scaled Møller−Plesset (SCS-MP) Perturbation Theory: A Generalization of the MP Approach with Improved Properties. *J. Chem. Phys.* **2010**, *133* (17), 174113.
(300) Hill, J. G.; Platts, J. A. Spin-Component Scaling Methods for Weak and Stacking Interactions. *J. Chem. Theory Comput.* **2007**, *3* (1), 80−85.

DOI: 10.1021/acs.chemrev.5b00507
Chem. Rev. 2016, 116, 4937−4982

(301) Hill, J. G.; Platts, J. A. Calculating Stacking Interactions in Nucleic Acid Base-Pair Steps Using Spin-Component Scaling and Local Second Order Møller−Plesset Perturbation Theory. *Phys. Chem. Chem. Phys.* **2008**, *10* (19), 2785−2791.
(302) Karton, A.; Tarnopolsky, A.; Lamere, J.-F.; Schatz, G. C.; Martin, J. M. Highly Accurate First-Principles Benchmark Data Sets for the Parametrization and Validation of Density Functional and Other Approximate Methods. Derivation of a Robust, Generally Applicable, Double-Hybrid Functional for Thermochemistry and Thermochemical Kinetics. *J. Phys. Chem. A* **2008**, *112* (50), 12868−12886.
(303) Distasio, R. A., Jr.; Head-Gordon, M. Optimized Spin-Component Scaled Second-Order Møller-Plesset Perturbation Theory for Intermolecular Interaction Energies. *Mol. Phys.* **2007**, *105* (8), 1073−1083.
(304) Marchetti, O.; Werner, H.-J. Accurate Calculations of Intermolecular Interaction Energies Using Explicitly Correlated Coupled Cluster Wave Functions and a Dispersion-Weighted MP2 Method. *J. Phys. Chem. A* **2009**, *113* (43), 11580−11585.
(305) Riley, K. E.; Platts, J. A.; Řezáč, J.; Hobza, P.; Hill, J. G. Assessment of the Performance of MP2 and MP2 Variants for the Treatment of Noncovalent Interactions. *J. Phys. Chem. A* **2012**, *116* (16), 4159−4169.
(306) Takatani, T.; Hohenstein, E. G.; Sherrill, C. D. Improvement of the Coupled-Cluster Singles and Doubles Method via Scaling Same-and Opposite-Spin Components of the Double Excitation Correlation Energy. *J. Chem. Phys.* **2008**, *128* (12), 124111.
(307) Jung, Y.; Lochan, R. C.; Dutoi, A. D.; Head-Gordon, M. Scaled Opposite-Spin Second Order Møller−Plesset Correlation Energy: An Economical Electronic Structure Method. *J. Chem. Phys.* **2004**, *121* (20), 9793−9802.
(308) Lochan, R. C.; Jung, Y.; Head-Gordon, M. Scaled Opposite Spin Second Order Møller-Plesset Theory with Improved Physical Description of Long-Range Dispersion Interactions. *J. Phys. Chem. A* **2005**, *109* (33), 7598−7605.
(309) Takatani, T.; Sherrill, C. D. Performance of Spin-Component-Scaled Møller−Plesset Theory (SCS-MP2) for Potential Energy Curves of Noncovalent Interactions. *Phys. Chem. Chem. Phys.* **2007**, *9* (46), 6106−6114.
(310) Antony, J.; Grimme, S. Is Spin-Component Scaled Second-Order Møller-Plesset Perturbation Theory an Appropriate Method for the Study of Noncovalent Interactions in Molecules? *J. Phys. Chem. A* **2007**, *111* (22), 4862−4868.
(311) Bachorz, R. A.; Bischoff, F. A.; Höfener, S.; Klopper, W.; Ottiger, P.; Leist, R.; Frey, J. A.; Leutwyler, S. Scope and Limitations of the SCS-MP2 Method for Stacking and Hydrogen Bonding Interactions. *Phys. Chem. Chem. Phys.* **2008**, *10* (19), 2758−2766.
(312) King, R. A. On the Accuracy of Spin-Component-Scaled Perturbation Theory (SCS-MP2) for the Potential Energy Surface of the Ethylene Dimer. *Mol. Phys.* **2009**, *107* (8−12), 789−795.
(313) Grabowski, I.; Fabiano, E.; Sala, F. D. A Simple Non-Empirical Procedure for Spin-Component-Scaled MP2 Methods Applied to the Calculation of the Dissociation Energy Curve of Noncovalently-Interacting Systems. *Phys. Chem. Chem. Phys.* **2013**, *15* (37), 15485−15493.
(314) Jeziorski, B.; Moszynski, R.; Szalewicz, K. Perturbation Theory Approach to Intermolecular Potential Energy Surfaces of van Der Waals Complexes. *Chem. Rev.* **1994**, *94* (7), 1887−1930.
(315) Misquitta, A. J.; Podeszwa, R.; Jeziorski, B.; Szalewicz, K. Intermolecular Potentials Based on Symmetry-Adapted Perturbation Theory with Dispersion Energies from Time-Dependent Density-Functional Calculations. *J. Chem. Phys.* **2005**, *123* (21), 214103.
(316) Hesselmann, A.; Jansen, G.; Schütz, M. Interaction Energy Contributions of H-Bonded and Stacked Structures of the AT and GC DNA Base Pairs from the Combined Density Functional Theory and Intermolecular Perturbation Theory Approach. *J. Am. Chem. Soc.* **2006**, *128* (36), 11730−11731.
(317) Řezáč, J.; Riley, K. E.; Hobza, P. S66: A Well-Balanced Database of Benchmark Interaction Energies Relevant to Biomolecular Structures. *J. Chem. Theory Comput.* **2011**, *7* (8), 2427−2438.
(318) Sinnokrot, M. O.; Sherrill, C. D. Substituent Effects in Π−π Interactions: Sandwich and T-Shaped Configurations. *J. Am. Chem. Soc.* **2004**, *126* (24), 7690−7697.
(319) Sure, R.; Grimme, S. Corrected Small Basis Set Hartree-Fock Method for Large Systems. *J. Comput. Chem.* **2013**, *34* (19), 1672−1685.
(320) Goerigk, L.; Collyer, C. A.; Reimers, J. R. Recommending Hartree−Fock Theory with London-Dispersion and Basis-Set-Superposition Corrections for the Optimization or Quantum Refinement of Protein Structures. *J. Phys. Chem. B* **2014**, *118* (50), 14612−14626.
(321) Brandenburg, J.; Grimme, S. Dispersion Corrected Hartree-Fock and Density Functional Theory for Organic Crystal Structure Prediction. *Top. Curr. Chem.* **2013**, *345*, 1.
(322) Brandenburg, J. G.; Hochheim, M.; Bredow, T.; Grimme, S. Low-Cost Quantum Chemical Methods for Noncovalent Interactions. *J. Phys. Chem. Lett.* **2014**, *5* (24), 4275−4284.
(323) Grimme, S.; Brandenburg, J. G.; Bannwarth, C.; Hansen, A. Consistent Structures and Interactions by Density Functional Theory with Small Atomic Orbital Basis Sets. *J. Chem. Phys.* **2015**, *143* (5), 054107.
(324) Stewart, J. J. Optimization of Parameters for Semiempirical Methods I. Method. *J. Comput. Chem.* **1989**, *10* (2), 209−220.
(325) Weber, W.; Thiel, W. Orthogonalization Corrections for Semiempirical Methods. *Theor. Chem. Acc.* **2000**, *103* (6), 495−506.
(326) Stewart, J. J. Optimization of Parameters for Semiempirical Methods VI: More Modifications to the NDDO Approximations and Re-Optimization of Parameters. *J. Mol. Model.* **2013**, *19* (1), 1−32.
(327) Tuttle, T.; Thiel, W. OM X-D: Semiempirical Methods with Orthogonalization and Dispersion Corrections. Implementation and Biochemical Application. *Phys. Chem. Chem. Phys.* **2008**, *10* (16), 2159−2166.
(328) Thiel, W. Semiempirical Quantum−chemical Methods. *Wiley Interdiscip. Rev. Comput. Mol. Sci.* **2014**, *4* (2), 145−157.
(329) Řezáč, J.; Fanfrlík, J.; Salahub, D.; Hobza, P. Semiempirical Quantum Chemical PM6 Method Augmented by Dispersion and H-Bonding Correction Terms Reliably Describes Various Types of Noncovalent Complexes. *J. Chem. Theory Comput.* **2009**, *5* (7), 1749−1760.
(330) Korth, M.; Pitoňák, M.; Řezáč, J.; Hobza, P. A Transferable H-Bonding Correction for Semiempirical Quantum-Chemical Methods. *J. Chem. Theory Comput.* **2010**, *6* (1), 344−352.
(331) Porezag, D.; Frauenheim, T.; Köhler, T.; Seifert, G.; Kaschner, R. Construction of Tight-Binding-like Potentials on the Basis of Density-Functional Theory: Application to Carbon. *Phys. Rev. B: Condens. Matter Mater. Phys.* **1995**, *51* (19), 12947.
(332) Seifert, G.; Porezag, D.; Frauenheim, T. Calculations of Molecules, Clusters, and Solids with a Simplified LCAO-DFT-LDA Scheme. *Int. J. Quantum Chem.* **1996**, *58* (2), 185−192.
(333) Elstner, M.; Hobza, P.; Frauenheim, T.; Suhai, S.; Kaxiras, E. Hydrogen Bonding and Stacking Interactions of Nucleic Acid Base Pairs: A Density-Functional-Theory Based Treatment. *J. Chem. Phys.* **2001**, *114* (12), 5149−5155.
(334) Elstner, M.; Porezag, D.; Jungnickel, G.; Elsner, J.; Haugk, M.; Frauenheim, T.; Suhai, S.; Seifert, G. Self-Consistent-Charge Density-Functional Tight-Binding Method for Simulations of Complex Materials Properties. *Phys. Rev. B: Condens. Matter Mater. Phys.* **1998**, *58* (11), 7260.
(335) Kunsági-Máté, S.; Ortmann, E.; Kollár, L.; Szabó, K.; Nikfardjam, M. P. Effect of Ferrous and Ferric Ions on Copigmentation in Model Solutions. *J. Mol. Struct.* **2008**, *891* (1−3), 471−474.
(336) Bondi, A. J. Van Der Waals Volumes and Radii. *J. Phys. Chem.* **1964**, *68* (3), 441−451.
(337) As seen in previous sections, we are aware that in principle, CCSD(T), or other methods such as QMC, are more desirable. However, such methods are currently too computationally demanding to be applied to real-world copigmentation systems.
(338) Freitas, A. A.; Shimizu, K.; Dias, L. G.; Quina, F. H. A Computational Study of Substituted Flavylium Salts and Their Quinonoidal Conjugate-Bases: S0→S1 Electronic Transition, Absolute

DOI: 10.1021/acs.chemrev.5b00507
Chem. Rev. 2016, 116, 4937−4982

pKa and Reduction Potential Calculations by DFT and Semiempirical Methods. *J. Braz. Chem. Soc.* **2007**, *18* (8), 1537−1546.
(339) Sakata, K.; Saito, N.; Honda, T. Ab Initio Study of Molecular Structures and Excited States in Anthocyanidins. *Tetrahedron* **2006**, *62* (15), 3721−3731.
(340) Anouar, E. H.; Gierschner, J.; Duroux, J.-L.; Trouillas, P. UV/Visible Spectra of Natural Polyphenols: A Time-Dependent Density Functional Theory Study. *Food Chem.* **2012**, *131* (1), 79−89.
(341) Millot, M.; Di Meo, F.; Tomasi, S.; Boustie, J.; Trouillas, P. Photoprotective Capacities of Lichen Metabolites: A Joint Theoretical and Experimental Study. *J. Photochem. Photobiol., B 111*, 17−26.10.1016/j.jphotobiol.2012.03.005
(342) Carvalho, A. R. F.; Oliveira, J.; De Freitas, V.; Mateus, N.; Melo, A. Unusual Color Change of Vinylpyranoanthocyanin−Phenolic Pigments. *J. Agric. Food Chem.* **2010**, *58* (7), 4292−4297.
(343) Quartarolo, A. D.; Russo, N. A Computational Study (TDDFT and RICC2) of the Electronic Spectra of Pyranoanthocyanins in the Gas Phase and Solution. *J. Chem. Theory Comput.* **2011**, *7* (4), 1073−1081.
(344) Milián-Medina, B.; Gierschner, J. Computational Design of Low Singlet−triplet Gap All-Organic Molecules for OLED Application. *Org. Electron.* **2012**, *13* (6), 985−991.
(345) Dreuw, A.; Weisman, J. L.; Head-Gordon, M. Long-Range Charge-Transfer Excited States in Time-Dependent Density Functional Theory Require Non-Local Exchange. *J. Chem. Phys.* **2003**, *119* (6), 2943−2946.
(346) Dreuw, A.; Head-Gordon, M. Single-Reference Ab Initio Methods for the Calculation of Excited States of Large Molecules. *Chem. Rev.* **2005**, *105* (11), 4009−4037.
(347) Casida, M. E.; Gutierrez, F.; Guan, J.; Gadea, F.-X.; Salahub, D.; Daudey, J.-P. Charge-Transfer Correction for Improved Time-Dependent Local Density Approximation Excited-State Potential Energy Curves: Analysis within the Two-Level Model with Illustration for H2 and LiH. *J. Chem. Phys.* **2000**, *113* (17), 7062−7071.
(348) Yanai, T.; Tew, D. P.; Handy, N. C. A New Hybrid Exchange−correlation Functional Using the Coulomb-Attenuating Method (CAM-B3LYP). *Chem. Phys. Lett.* **2004**, *393* (1−3), 51−57.
(349) Chai, J.-D.; Head-Gordon, M. Long-Range Corrected Hybrid Density Functionals with Damped Atom−atom Dispersion Corrections. *Phys. Chem. Chem. Phys.* **2008**, *10* (44), 6615−6620.
(350) Chai, J.-D.; Head-Gordon, M. Long-Range Corrected Double-Hybrid Density Functionals. *J. Chem. Phys.* **2009**, *131* (17), 174105.
(351) Caricato, M.; Trucks, G. W.; Frisch, M. J.; Wiberg, K. B. Oscillator Strength: How Does TDDFT Compare to EOM-CCSD? *J. Chem. Theory Comput.* **2011**, *7* (2), 456−466.
(352) Beyhan, S. M.; Götz, A. W.; Ariese, F.; Visscher, L.; Gooijer, C. Computational Study on the Anomalous Fluorescence Behavior of Isoflavones. *J. Phys. Chem. A* **2011**, *115* (9), 1493−1499.
(353) Malcıoğlu, O. B.; Calzolari, A.; Gebauer, R.; Varsano, D.; Baroni, S. Dielectric and Thermal Effects on the Optical Properties of Natural Dyes: A Case Study on Solvated Cyanin. *J. Am. Chem. Soc.* **2011**, *133* (39), 15425−15433.
(354) Petrone, A.; Cerezo, J.; Ferrer, F. J. A.; Donati, G.; Improta, R.; Rega, N.; Santoro, F. Absorption and Emission Spectral Shapes of a Prototype Dye in Water by Combining Classical/Dynamical and Quantum/Static Approaches. *J. Phys. Chem. A* **2015**, *119* (21), 5426−5438.
(355) Sinnecker, S.; Rajendran, A.; Klamt, A.; Diedenhofen, M.; Neese, F. Calculation of Solvent Shifts on Electronic G-Tensors with the Conductor-Like Screening Model (COSMO) and Its Self-Consistent Generalization to Real Solvents (Direct COSMO-RS). *J. Phys. Chem. A* **2006**, *110*, 2235−2245.
(356) Tomasi, J.; Mennucci, B.; Cammi, R. Quantum Mechanical Continuum Solvation Models. *Chem. Rev.* **2005**, *105*, 2999−3093.
(357) Ge, X.; Timrov, I.; Binnie, S.; Biancardi, A.; Calzolari, A.; Baroni, S. Accurate and Inexpensive Prediction of the Color Optical Properties of Anthocyanins in Solution. *J. Phys. Chem. A* **2015**, *119* (16), 3816−3822.
(358) Pedersen, M. N.; Hedegård, E. D.; Olsen, J. M. H.; Kauczor, J.; Norman, P.; Kongsted, J. Damped Response Theory in Combination with Polarizable Environments: The Polarizable Embedding Complex Polarization Propagator Method. *J. Chem. Theory Comput.* **2014**, *10* (3), 1164−1171.
(359) Olsen, J. M.; Aidas, K.; Kongsted, J. Excited States in Solution through Polarizable Embedding. *J. Chem. Theory Comput.* **2010**, *6* (12), 3721−3734.
(360) Sjöqvist, J.; Linares, M.; Mikkelsen, K. V.; Norman, P. QM/MM-MD Simulations of Conjugated Polyelectrolytes: A Study on Luminescent Conjugated Oligothiophenes for Use as Bio-Physical Probes. *J. Phys. Chem. A* **2014**, *118* (19), 3419−3428.
(361) Avila Ferrer, F. J.; Cerezo, J.; Stendardo, E.; Improta, R.; Santoro, F. Insights for an Accurate Comparison of Computational Data to Experimental Absorption and Emission Spectra: Beyond the Vertical Transition Approximation. *J. Chem. Theory Comput.* **2013**, *9* (4), 2072−2082.
(362) Avila Ferrer, F. J.; Cerezo, J.; Soto, J.; Improta, R.; Santoro, F. First-Principle Computation of Absorption and Fluorescence Spectra in Solution Accounting for Vibronic Structure, Temperature Effects and Solvent Inhomogenous Broadening. *Comput. Theor. Chem.* **2014**, *1040−1041*, 328−337.

DOI: 10.1021/acs.chemrev.5b00507
Chem. Rev. 2016, 116, 4937−4982